Self-trapped optical beams in nonlocal nonlinear media

A thesis submitted for the degree
of Doctor of Philosophy of
the Australian National University

Daniel Buccoliero

April 2009

THE AUSTRALIAN NATIONAL UNIVERSITY

Declaration

This thesis is an account of research undertaken in the Nonlinear Physics Centre and the Laser Physics Centre within the Research School of Physics and Engineering at the Australian National University between April 2006 and April 2009 while I was enrolled for the Doctor of Philosophy degree.

The research has been conducted under the supervision of Dr. Anton S. Desyatnikov, Dr. Ole Bang, Prof. Wieslaw Krolikowski, and Prof. Yuri S. Kivshar. However, unless specifically stated otherwise, the material presented within this thesis is my own.

None of the work presented here has ever been submitted for any degree at this or any other institution of learning.

Daniel Buccoliero
April 15, 2009

Refereed journal publications

1. **D. Buccoliero**, A. S. Desyatnikov, W. Krolikowski, and Y. S. Kivshar, *"Laguerre and Hermite soliton clusters in nonlocal nonlinear media,"* Phys. Rev. Lett. **98**, 053901–4 (2007).

2. **D. Buccoliero**, S. Lopez-Aguayo, S. Skupin, A. S. Desyatnikov, O. Bang, W. Krolikowski, and Y. S. Kivshar, *"Spiraling solitons and multipole localized modes in nonlocal nonlinear media,"* Physica B **394**, 351–356 (2007).

3. **D. Buccoliero**, A. S. Desyatnikov, W. Krolikowski, and Y. S. Kivshar, *"Spiraling multivortex solitons in nonlocal nonlinear media,"* Opt. Lett. **33**, 198–200 (2008).

4. **D. Buccoliero**, A. S. Desyatnikov, W. Krolikowski, and Y. S. Kivshar, *"Boundary effects on the dynamics of higher-order optical spatial solitons in nonlocal thermal media,"* J. Opt. A: Pure Appl. Opt. **11**, accepted January 28, 303173 (2009).

5. A. Alberucci, G. Assanto, **D. Buccoliero**, A. S. Desyatnikov, T. R. Marchant, and N. F. Smyth, *"Modulation analysis of boundary-induced motion of optical solitary waves in a nematic liquid crystal,"* Phys. Rev. A **79**, accepted March 19, AB10353 (2009).

6. **D. Buccoliero** and A. S. Desyatnikov, *"Quasi-periodic transformations of nonlocal spatial solitons,"* submitted to Opt. Express, April (2009).

Other refereed publications

7. **D. Buccoliero**, A. S. Desyatnikov, W. Krolikowski, and Yu. S. Kivshar, *"Rotating multipole vortex solitons in nonlocal media,"* Proc. SPIE **6725**, 672507–6 (2007).

Acknowledgments

I would like to express my gratitude to my supervisors Dr. Anton S. Desyatnikov and Prof. Wieslaw Krolikowski as well as the other members of my supervisory panel Dr. Ole Bang and Prof. Yuri S. Kivshar. In particular I would like to give emphasis to the invaluable support and guidance provided by Dr. Anton S. Desyatnikov and Prof. Wieslaw Krolikowski throughout my time in the group. A huge thanks goes to Prof. Yuri S. Kivshar for his outstanding overview, encouragement and leadership and to Dr. Ole Bang for persuading me to pursue this fantastic career opportunity.

During my Ph.D. I have been privileged to have the opportunity to collaborate with research groups from overseas and in that regard I would like to warmly thank Dr. Stefan Skupin from the Max Planck Institute for the Physics of Complex Systems, Dresden, Germany for supporting my visit to the institute and for agreeing to engage in a joint collaboration. Moreover I would like to mention the highly inspiring meetings I have had with Dr. Mark R. Dennis from the University of Bristol, UK especially during his visit to the group, which has resulted in a most rewarding collaboration. I am very grateful that he willingly shared his impressing ideas with us and of course for agreeing to provide me with a letter of recommendation. Finally special thanks go out to all the contributing authors of a recently accepted journal paper, and in particular to Dr. Noel R. Smyth from The University of Edinburgh, UK and Prof. Gaetano Assanto from the University of Rome "Roma Tre", Italy for also showing the kindness of writing me a letter of reference, which is highly appreciated and no doubt will be of immense significance in my further pursuit of an academic career.

I gratefully acknowledge the support given to me by the departmental administrators, Wendy Quinn, her successor, Kathy Hicks, and Belinda Barbour as well as Prof. Neil Manson for sorting out all sorts of practical and administrative problems. In particular Kathy Hicks has been a remarkable help at the end of my time in the group and I can not stress enough the importance of her efforts to aid me whenever needed.

I acknowledge the financial support provided by the Australian Research Council and the Australian National University, without which I obviously would not have had the possibility to undertake the study presented in this thesis.

Last but not least I would like to mention my unconditional love and appreciation to my wonderful wife and family who willingly and enthusiastically embarked with me on this great journey, -they made my decision to pull up the roots and travel half way around the world very easy and I am for ever indebted to them for that.

Abstract

The self-trapping of light in the form of solitons represents one of the most interesting and rewarding phenomena offered by nonlinear optics. As a result, the field of optical solitons has been experiencing a substantial growth over the past years. Recent developments indicate that the field is by no means yet fully explored. In any realistic nonlinear media with a local response however, the only known stable two-dimensional solitonic structures in bulk media is the fundamental soliton.

Therefore, the optical nonlocality, which appears in a large variety of physical systems, has received an increasing interest due to the fact that it has a substantial effect on both stabilization and propagation dynamics of self-trapped optical beams. Recent developments in the study of optical solitons in nonlocal nonlinear media have paved the way for highly interesting novel physics e.g., formations of multi-soliton bound states, stabilization of both single- and multi-charged vortex solitons as well as more involved vortex carrying beams. Such complex solitons exhibit intricate propagation dynamics which make the study of higher-order nonlocal solitons an intriguing and worthwhile area of nonlinear optics.

It is the main purpose of this thesis to explore in detail the propagation dynamics exhibited by various higher-order solitons. Special emphasis is given to the different stability regions and scenarios, which in certain cases involve highly nontrivial features and these will be discussed thoroughly. Two distinct nonlocal models are employed and a direct comparison between the evolution of identical beam symmetries in the two different settings is demonstrated and commented.

In Chapter 1 a brief introduction to nonlinear optics is presented and a short historical account of several theoretical and experimental studies that led to the emergence of the field of optical solitons is provided. Particular attention is given to optical vortices and vortex solitons which appear naturally when studying wave propagation in nonlinear optical media. Different higher-order structures carrying optical vortices are introduced and both experimental and numerical investigations regarding their propagation and stability properties are discussed. In the last part of the chapter the optical nonlocality is presented and it is demonstrated how the inherent properties of nonlocality can lead to stabilization of several higher-order solitons.

Motivated by previous studies, in Chapter 2 the multihump nonlocal solitons are constructed by employing a well-known set of linear modes, namely Hermite- (HG) and Laguerre-Gaussian (LG) waveguide modes. These solitons are identified

as Hermite- (HN) and Laguerre-nonlocal (LN) solitons and, despite their disparate symmetries, the numerous examples demonstrate that some of these states coexist energetically, which has significant effects on their propagation dynamics. As a result, the mutual transformations between the two symmetries are demonstrated and intermediate states, resembling generalized Hermite-Laguerre-Gaussian (HLG) modes, are observed. By a similar approach the higher-order nonlocal solitons in the form of genralized nonlocal (GN) solitons are obtained. Studies reveal that such complicated beam structures with several vortices embedded in their phase distributions experience similar dynamics during propagation. In this chapter, as the simplest example of a GN beam, the nonrotating quadrupole-like soliton is considered in detail.

In continuation of the preceding chapter, in Chapter 3 the GN states with nonzero angular momentum are studied. First, the family of the tripole-like beam is introduced and extensive numerical simulations reveal that all members exhibit stable propagation accompanied by spiraling above a certain power threshold. In contrast, the more involved 3×2 matrix solitons undergo both transformations and spiraling as they propagate, with the only exception being the nonrotating "pure" 3×2 matrix which simply becomes stable. By tracing the spatial locations of the vortices, the complex nodal line structures appear, and particular focus is aimed at the intriguing topological distributions in the form of vortex links and knots. To fully appreciate the underlying physics of such vortex formations the evolution of a fundamental soliton in a local saturable medium is considered. It is revealed that small oscillations trigger the appearances of numerous vortex loops, which surround the beam at nearly equidistant intervals. By considering a perturbed elliptically shaped fundamental beam and imposing a complicated phase which makes the beam rotate, the neighboring distorted loops merge to form both vortex links and knots.

In the final chapter a realistic nonlocal thermal model is employed which serves two purposes. First, it allows to compare beam evolution in two distinct media, and to determine whether the observed dynamics in previous chapters constitute generic phenomena obtainable in other physical systems. Second, it gives an idea of the prospects of experimentally realizing for instance symmetry transformations which could be of great importance to all-optical photonic elements.

Contents

CHAPTER 1

Introduction to nonlocal nonlinear optics

1.1 Introduction

One of the fundamental properties of wave propagation is that finite-sized optical beams experience diffraction, i.e. broadening of their spatial profile with the rate of diffraction conversely proportional to the initial width of the beam. However the diffraction can be exactly counterbalanced by a strong nonlinear coupling to the medium in which the beam propagates. This occurs whenever the response of the material exhibits a self-focusing effect by increasing the refractive index in regions of high beam intensity and hence acts effectively like an optical lens. The transverse profile of the beam can become invariant during propagation and the result is a traveling wave trapped in its own self-induced waveguide, i.e., an *optical spatial soliton* [1]. These nonlinear entities are very robust and offer a wealth of novel and exciting physics which has been a subject of great interest over the past few decades [2, 3].

The electromagnetic response of a nonlinear optical medium, often represented by the induced polarization, can be expressed by the power series in the field amplitude E

$$P = \chi^{(1)}\vdots E + \chi^{(2)}\vdots E^2 + \chi^{(3)}\vdots E^3 + ..., \tag{1.1}$$

where tensors $\chi^{(2)}$, $\chi^{(3)}$, ... denote nonlinear responses of the medium [4–6]. In case of a centrosymmetric medium $\chi^{(2)}$ vanishes and the main effect of the nonlinear response is the induced change of the refractive index, which is proportional to $\chi^{(3)}E^3$. When $\chi^{(3)} > 0$ the medium behaves self-focusing and supports the formation of bright solitons. If, on the other hand, $\chi^{(3)} < 0$, the medium is self-defocusing and does not support formation of bright solitons. It does however support a somewhat different kind of solitons, namely the so-called dark solitons [7, 8].

Mathematically, solitons are obtained as solutions to the partial differential equation governing the system, in nonlinear optics described by the normalized paraxial nonlinear Schrödinger (NLS) equation [1]

$$\mathrm{i}\frac{\partial E}{\partial z} + \frac{1}{2}\left(\frac{\partial^2 E}{\partial x^2} + \frac{\partial^2 E}{\partial y^2}\right) + \mathcal{F}(I)E = 0, \tag{1.2}$$

where $\mathcal{F}$, assumed to depend on the total beam intensity I, denotes the induced refractive index change of the medium and the sign of the change determines whether

the medium is self-focusing ($\mathrm{d}\mathcal{F}/\mathrm{d}I > 0$) or self-defocusing ($\mathrm{d}\mathcal{F}/\mathrm{d}I < 0$). In the self-focusing case the solutions are obtained in the form of bright spatial solitons, i.e., radially symmetric beams, with a flat phase front [3]. When the nonlinearity is self-defocusing, the solutions in the 1-D case have been shown theoretically [7] to consist of a dark dip on a constant bright background with a phase shift of π across the zero of intensity. Similarly, in 2-D dark solitons are obtained as beams consisting of a uniform illuminated background centered around a circular symmetric dark hole [8].

In general a wealth of nonlinear processes support the formation of spatial solitons [3], and $\mathcal{F}$ can take several different forms depending on the system under consideration. In the simplest case of a Kerr medium the response is given by $\mathcal{F} = I$ where the refractive index change is linearly proportional to the intensity of the beam. Other examples include the so-called saturable nonlinearity, $\mathcal{F} = I(1+sI)^{-1}$ where s is a saturation parameter, and the more involved nonlocal nonlinear response, where $\mathcal{F}$ in many cases can be represented by a convolution integral [see Section 1.3].

Traditionally the term soliton has been reserved exclusively for solutions to the fully integrable Schrödinger equation, which is limited to the case when (1+1)-D wave propagation in a nonlinear Kerr medium is considered. In most systems of interest however, the governing propagation equation will be nonintegrable and although self-trapped solutions exist, certain properties of such "solitary waves" differ significantly from the properties of solitons. On the other hand a wide range of features, e.g., the particle-like behavior, are preserved and over the years the distinction between solitary waves and solitons has become less pronounced. As a result in most of today's literature covering the subject the solitary waves are loosely termed solitons, as will be the case in this dissertation.

1.1.1 Optical solitons

With the invention of the laser in the early 1960s the experimental observations of self-trapping of optical beams were made possible due to this new source of high optical power which allowed to access nonlinearities. In particular, some of the first observations of trapping of light in the form of optical filamentation induced by a highly intense laser beam in glass were reported in 1964 [9] and in liquids a year later [10], thus laying the foundations of the studies of optical spatial solitons.

A few years earlier, in 1962, it had in fact already been suggested that under the right circumstances the optical beams would induce a waveguide in which they would self-trap [11]. In support of this idea, the self-trapping was investigated theoretically in nonlinear Kerr media [12] thereby providing a key to the understanding of soliton properties and dynamics. By investigating soliton interactions numerically [13], in 1965 it was shown that solitons exhibit particle-like behavior, demonstrated by the observation that after numerous collisions solitons preserve their original shape and size apparently unaffected by the strong interactions. This rather distinct feature led to the introduction of the term soliton [13].

As previously mentioned however, solutions to the fully integrable system differ from solutions obtained in the case where the equation is nonintegrable. A fully ana-

lytical treatment of soliton interactions was performed using the "Inverse Scattering Technique" [14] where (1+1)-D wave propagation in a nonlinear Kerr medium was considered. Since the equation is integrable no energy is lost during the collisions, and the number of solitons was found to be a conserved quantity. On the contrary, this is not always the case for solitary waves, nevertheless in both integrable and nonintegrable systems, quite surprisingly the self-trapped beams behave like classical particles in the sense that they exert "forces" on one another, resulting in either mutual attraction or repulsion. In particular, the experiments performed in 1-D glass wave guides [15] showed that in-phase Kerr solitons always attract each other, whereas out-of-phase Kerr solitons repel. At different relative phases the interaction is more complicated and involves energy transfer between the beams.

1.1.2 Soliton stability

Instability dynamics in nonlinear wave propagation are well-known and have been studied extensively both theoretically and experimentally. Specifically, catastrophic collapse occurs when strong self-focusing of a beam leads to a blow-up in the intensity, and examples of such behavior have been reported in, e.g., plasma waves [16], laser beams [17] and Bose-Einstein condensates BECs [18]. In addition, modulational instabilities which involve the exponential growth of a small perturbation of the beam as it propagates eventually leads to the break-up of the wave and filamentation, in which case it can act as a precursor for the formation of bright solitons. Modulational instability therefore has been the subject of intense studies in several various physical systems such as fluids [19], plasmas [20] and nonlinear optics [21].

Stability of solitons quickly became a subject of interest and it was soon shown that in bulk 3-D Kerr media all bright solitons are unstable, more specifically (1+1)-D solitons suffer from transverse instability, or modulational instability [22], which causes them to break up into filaments while (2+1)-D solitons undergo catastrophic collapse [23].

This scenario changes dramatically when a medium with saturating nonlinearities or, as it is demonstrated later [see Section 1.3.3], a nonlocal nonlinear medium is considered. A distinct difference between Kerr and saturable media and key to the stabilization of 2-D optical solitons is the upper limit of the increase in refractive index. Numerical studies have demonstrated stable propagation of 2-D optical solitons in a saturable medium [24] in which the catastrophic collapse is prevented due to the saturating properties of the nonlinearity. A few years later the first experimental observation of optical solitons was reported [25] confirming the above mentioned theoretical predictions. By launching a circular symmetric optical beam in a sodium vapor with saturable nonlinearity, it was demonstrated that at low power the beam diffracted, however by increasing the power the beam would eventually self-trap and form a stable bright optical soliton.

Nearly two decades later the first experimental investigations demonstrating stable propagation of 1-D dark solitons were published and were actually conducted in various kinds of bulk media with saturable nonlinearities [26, 27]. Shortly thereafter

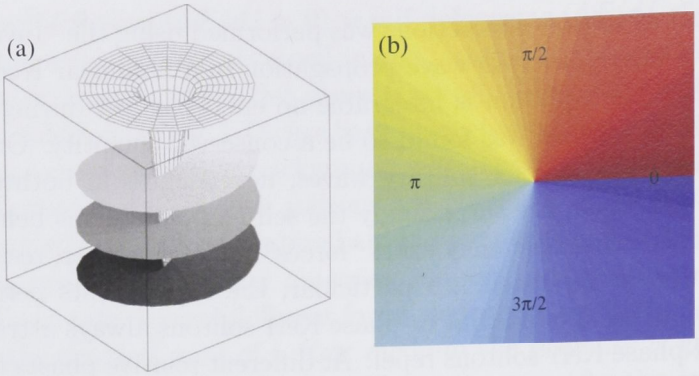

Figure 1.1: (a) Intensity distribution (mesh) and the characteristic helical wave front (surface) of an optical beam carrying a vortex (from Ref. [31]). (b) Phase distribution of a single charge optical vortex.

stable propagation of dark 2-D solitons in the form of dark optical vortex solitons, i.e., beams consisting of an optical vortex embedded in a uniform illuminated background, [see Section 1.2] was demonstrated experimentally in various types of media with defocusing nonlinearities [28–30].

Optical vortices represent generic phenomena and often appear when studying wave propagation in optical media. They originate from phase singularities in the solutions to the wave equation, and are characterized by an energy flow around the vortex core, and hence a zero of intensity at the center [31, 32].

The study of optical vortices and vortex solitons in particular has evolved into a field of great interest over the past years. Even so it still promises to uncover many new and exciting phenomena which makes it a worthwhile area of optics, both from a fundamental and applied physics point of view [32], and historically it has spawned an entirely new discipline termed *Singular Optics* [33–35].

1.2 Optical vortices and vortex solitons

When studying (2+1)-D wave propagation, the beams are usually represented by a scalar complex function ψ, and as a result phase singularities are points in the transverse plane where the field modulus vanishes, i.e., Re ψ = Im ψ = 0. As the wave propagates these points trace out lines in space, and, as it is shown in Section 3.5, given the right conditions such vortex lines may combine to form highly complex topological distributions in the form of vortex loops, links, and knots [36].

Optical vortices are formed by the phase singularities in a light wave, and they give rise to a rotation around the vortex core performed by the field itself. An optical beam carrying a vortex thus contains a helical wave front and around the vortex core, manifested by a zero of intensity, a phase gradient swirls, reminiscent

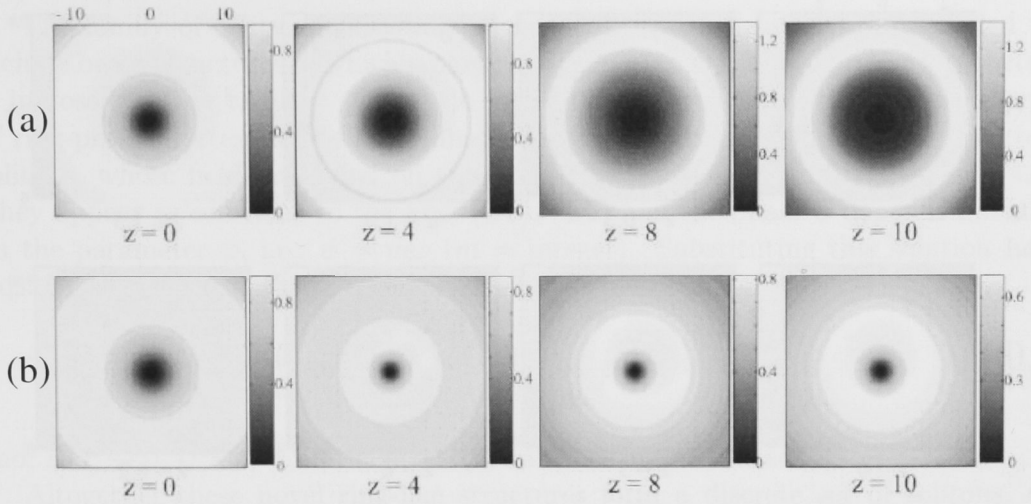

Figure 1.2: Evolution of a super-Gaussian beam carrying a phase dislocation in (a) linear medium, and (b) self-focusing Kerr medium (from Ref. [32]).

of a whirlpool in a liquid. More specifically, the phase in a given direction around the vortex core changes by a multiple of 2π [31, 32], [see Figure 1.1].

In other words, by letting $\psi(\mathbf{r},t) = \rho(\mathbf{r},t)\exp[i\chi(\mathbf{r},t)]$, with ρ being the real modulus and χ the phase, the change in phase around the vortex core, often termed the topological charge, is given by

$$S = (2\pi)^{-1} \oint \nabla\chi \mathrm{d}\mathbf{l}, \tag{1.3}$$

where $\mathrm{d}\mathbf{l}$ denotes a small increment on a counter-clockwise path around the vortex core. Note that the result is an integer.

As mentioned, light waves may carry optical vortices and the beams in a nonlinear medium make no exceptions. However, the dynamics of such topologically charged structures depend crucially on the properties of the medium under investigation. For example, the evolution of dark optical vortex solitons in de-focusing media involves stable propagation in which the dark vortex core self-traps and remains localized on a uniform constant intensity background during propagation, [see Figure 1.2]. Such stable propagation dynamics is in sharp contrast to vortex beam propagation in self-focusing media. As shown in Figure 1.3, the bright vortex beams with a topological charge embedded in their phase distribution have a doughnut-like structure. These structures are localized in the transverse plane and diffract if no nonlinearity is present.

In nonlinear Kerr-type focusing media they self-trap, nevertheless upon propagation they become unstable and experience azimuthal modulational instabilities, which eventually leads to beam filamentation into fundamental solitons. This is manifested by the decay of the original beam into several optical splinters that

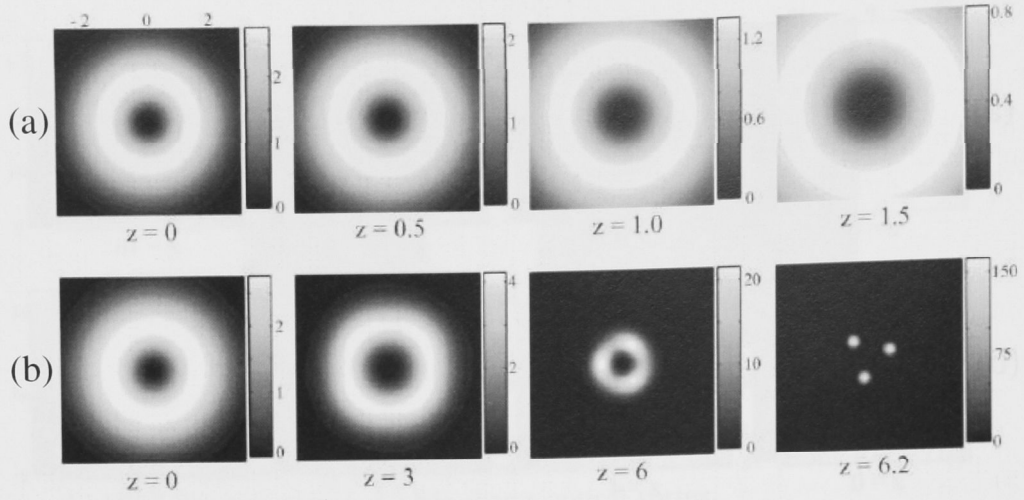

Figure 1.3: Evolution of a Gaussian beam carrying a single charge optical vortex in (a) linear medium, and (b) self-focusing Kerr medium (from Ref. [32]).

repel and twist around one another as they propagate, [see Figure 1.3]. The twisting of the splinters is due to conservation of angular momentum, which is being transferred to the filaments as the vortex beam breaks [32].

1.2.1 Radially symmetric beams in focusing Kerr-type media

Solutions to the generalized NLS equation [Eq. (1.2)] are obtained in the form,

$$E(x, y, z) = U(x, y) \exp[\mathrm{i}kz + \mathrm{i}\phi(x, y)], \tag{1.4}$$

where U and ϕ are real functions denoting amplitude and phase, respectively, and k is the propagation constant. By substituting Eq. (1.4) into Eq. (1.2) the following coupled system of equations for amplitude and phase is obtained,

$$\Delta_\perp U - kU - (\nabla\phi)^2 U + \mathcal{F}(U^2)U = 0, \tag{1.5}$$

$$\Delta_\perp \phi + 2\nabla\phi\nabla \ln U = 0, \tag{1.6}$$

in which $\Delta_\perp = \partial^2/\partial x^2 + \partial^2/\partial y^2$ is the transverse Laplacian.

In the particular case where ϕ is taken to be zero, the only possible solutions with the property of being localized in both transverse dimensions have been shown to consist of radially symmetric beams, i.e., with $U(x, y) = U(r)$, where $r = \sqrt{x^2 + y^2}$. Such modes include the fundamental soliton as well as higher order structures with one or more rings surrounding the central peak [37–40].

The modes U_n, with n being an integer denoting the number of rings in the intensity profile, form a discrete set of solitons, uniquely characterized by the corresponding soliton power $P_n(k)$,

$$P_n(k) = \int |E|^2 \mathrm{d}\mathbf{r} = \int U_n^2 \mathrm{d}\mathbf{r}. \tag{1.7}$$

The family of solitons consisting of the modes U_n can be further extended to include beam structures in which a phase dislocation in the form of an optical vortex is imposed on the radially symmetric intensity distribution. Indeed, the concept of ring-profile vortex beams in nonlinear media introduced a novel type of vortex solitons, whose field depended on the azimuthal parameter $\varphi = \tan^{-1}(y/x)$ [42]. They appear as solutions to the Eqs. (1.5), (1.6) and the phase ϕ depends linearly on the parameter φ, i.e., $\phi = m\varphi$ (m = integer). Substituting this solution into Eqs. (1.5), (1.6) then gives

$$\frac{\mathrm{d}^2U}{\mathrm{d}r^2} + \frac{1}{r}\frac{\mathrm{d}U}{\mathrm{d}r} - \frac{m^2}{r^2}U - kU + \mathcal{F}(U^2)U = 0, \tag{1.8}$$

and, as $r \to 0$, $U \sim r^{|m|}$ and hence $U(r)$ vanishes at the center.

Altogether these novel ring-like structures form a discrete set of solitons, or rather a family of radially symmetric solitons characterized by the power $P_{n,m}(k)$, which now depends on both the radial and the azimuthal numbers n and m. Being a subject of significant interest, following their introduction in 1985 [42], vortex solitons have been studied in a number of different cases [43–45].

In addition to the power $P_{n,m}(k)$, the beam orbital angular momentum (OAM) M represents another important integral of motion,

$$M = \mathrm{Im}\int E^*(\mathbf{r}\times\nabla E)\mathrm{d}\mathbf{r} = \int \frac{\partial\phi}{\partial\varphi}U^2\mathrm{d}\mathbf{r}, \tag{1.9}$$

with E^* being the complex conjugate of E. Although not directly connected, angular momentum and optical singularities are often found to appear simultaneously [46–48].

1.2.2 Instability dynamics in focusing media

As discussed previously, the bright 2-D solitons are unstable in Kerr media and experience catastrophic collapse during propagation. However, in saturable media such instability is eliminated and stable fundamental solitons have been found in both two and three spatial dimensions. In addition, an instability criterion has been established [49] and it states that solutions to the governing propagation equation [Eq. (1.2)] are stable if two conditions are simultaneously fulfilled. Specifically, the first one states that the power P of the soliton should increase with k, i.e., $\partial P/\partial k > 0$ while second the nonlinearity $\mathcal{F}$ must grow monotonically with intensity I. Vortex solitons in saturable media satisfy both of these conditions, but this, on the other hand, does not guarantee stable propagation. Indeed, as shown in Figure 1.3, vortex beams generally suffer from azimuthal instability and break up into filaments upon propagation.

So far no universal stability criterion regarding the azimuthal break-up of vortex solitons has been established, and the stability of these beams can only be investigated, by taking into account the various individual properties of the different media being considered.

The linear stability analysis is based on investigating the evolution of a small perturbation $|p| \ll E_0$ added to the solution E_0 of Eq. (1.2) [50–52], and by inserting this perturbed solution $E = E_0 + p$ into Eq. (1.2) one obtains

$$\mathrm{i}\frac{\partial p}{\partial z} + \Delta_\perp p + (\mathcal{F}_0 + |E_0|^2\mathcal{F}_0')p + E_0^2\mathcal{F}_0' p^* = 0, \tag{1.10}$$

where $\mathcal{F}_0 = \mathcal{F}(|E_0|^2)$ and $\mathcal{F}_0' = (\mathrm{d}\mathcal{F}/\mathrm{d}I)|_{I=|E_0|^2}$. This linear equation governs the evolution of the small perturbation p, and in the case where p does not grow during propagation, E_0 is linearly stable.

When investigating the stability of ring-profile vortices, the stationary solution $E_0 = U(r)\exp(\mathrm{i}kz + \mathrm{i}n\varphi)$ which solves Eq. (1.8), is radially symmetric. Hence p should be periodic in the azimuthal direction and it is therefore possible to express it as a Fourier series

$$p(r, \varphi, z) = \sum_{n=-\infty}^{\infty} p_n(r, z)\exp(\mathrm{i}n\varphi). \tag{1.11}$$

This expression is then substituted into Eq. (1.10) an the result is an infinite set of equations for the complex functions p_n obtained by comparing terms of equal angular dependence $n\varphi$.

Among all such modes p_n, only two modes are actually coupled, namely p_{n+s} and p_{n-s}, with s being any integer, and such two modes form a closed system with solutions given by

$$p_{n+s}(r, z) = u_s(r)\exp(\mathrm{i}kz + \gamma_s z) \tag{1.12}$$

$$p_{n-s}(r, z) = v_s^*(r)\exp(-\mathrm{i}kz - \gamma_s z). \tag{1.13}$$

The analysis thus involves solving an eigenvalue problem [32], with the eigenvalues being the so-called complex perturbation wave numbers γ_s and, if for some s the eigenvalue γ_s has a positive real part, the perturbations $p_{n\pm s}$ are instability modes and grow exponentially with grow rate Re γ_s, figure 1.4 shows the dependence of the growth rates on soliton power (a) and (b), and unstable propagation followed by break-up of the beams depicted in (c) and (d).

Cases shown are vortex solitons with topological charges $m = 1$ and $m = 2$ respectively in a saturable medium. The growth rate in each case vanishes for $k \to 0$ as well as in the opposite limit but, more importantly, at least one mode in each case has a nonzero value on the entire range of k-values, and thus all vortex solitons are linearly unstable in saturable media.

The mode with the highest growth rate determines how many splinters the vortex soliton decays into, and in case of the single charge beam, the fastest growing mode has $s = 2$, shown in Figure 1.4(a) and (c). Conversely for vortex beams of higher charge different instability modes dominate in different regimes of the soliton power, and the result is therefore a competition between instability modes, such as modes with $s = 3$, $s = 4$ and $s = 5$ in the case of the double charged vortex soliton, [see Figure 1.4(b)].

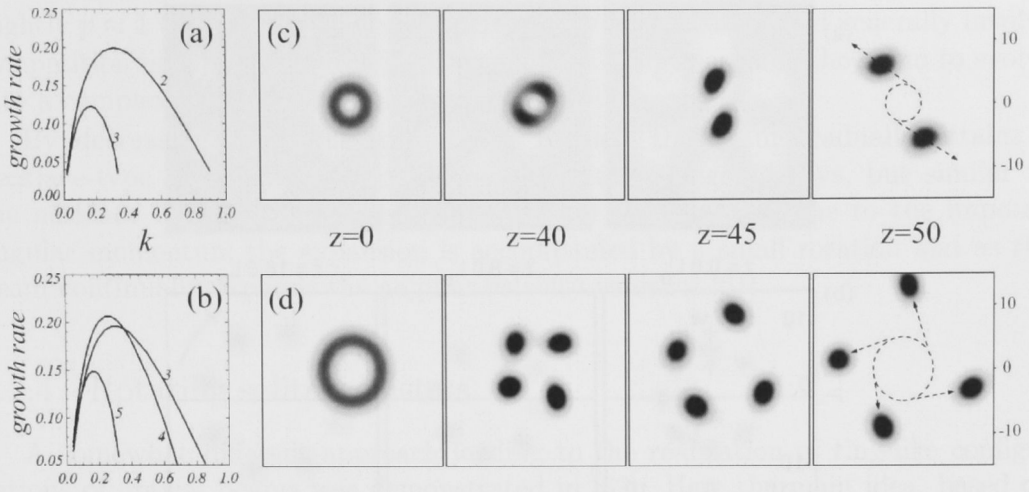

Figure 1.4: Growth rates Re γ_s of (a) single and (b) double charge vortex beam in a saturable medium, i.e., $\mathcal{F}(I) = I(I+1)^{-1}$. Corresponding index of the different instability modes are shown next to the curves (from Ref. [41]). Break-up dynamics of the vortex beams with topological charges (c) $m = 1$ and (d) $m = 2$ and corresponding fastest growing instability modes with indices $s = 2$ and $s = 4$ respectively (from Ref. [32]).

The dynamics shown in Figure 1.4 is obtained numerically and, by comparing the growth rates obtained by the linear stability analysis, it is evident that the analysis is in excellent agreement with the numerical solutions of the full system. In support of these findings the experiments have been conducted in saturable vapors and they all demonstrate symmetry breaking instabilities of the radially symmetric vortex beams [53–55].

The symmetry breaking dynamics of the ring-profile structure can be suppressed by applying azimuthal modulations to the initial structure. The resulting beam structures in effect take the form of optical necklaces, i.e., ring-like intensity distributions consisting of optical petals which are circularly distributed, [see Figure 1.5] and as such the beams are closely related to appropriate superpositions of Laguerre-Gaussian beams.

1.2.3 Ring-shaped optical necklaces

Experimental observation of self-trapping of an optical necklace-type beam in Kerr media has been reported [56] in which the propagation of a higher-order Laguerre-Gaussian mode was considered, [see Figure 1.5]. It was shown that at sufficient low powers, where the nonlinearity would be negligible, the beam as a whole would diffract, while the petal thickness remained roughly constant. Conversely, at high power the beam self-trapped and due to self-focusing the petal size decreased accordingly. Remarkably, the structure is very robust and allowed for sta-

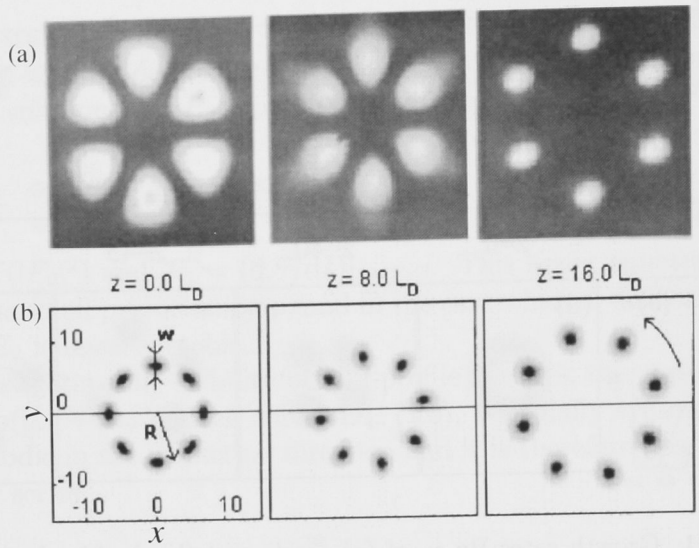

Figure 1.5: (a) Experimental demonstration of a necklace-type beam in the form of a higher-order Laguerre-Gaussian mode in a Kerr medium. At low power (middle) the beam diffracts, whereas at high power (left) the beam self-traps (from Ref. [56]). (b) Evolution of a necklace beam carrying an angular momentum (from Ref. [61]).

ble propagation at power levels several times higher than what would normally cause catastrophic collapse for a fundamental Gaussian beam. Further theoretical developments of optical necklaces [58], which investigated numerically the propagation of beam structures composed of several out-of-phase optical petals, demonstrated stable evolution of the necklaces which avoided catastrophic collapse. In contrast to previous studies, it was shown that during propagation the beams would expand self-similarly due to repulsion between neighboring petals, and preserve their original structure.

The beam structure itself can be approximated by an ansatz similar to,

$$E(x, y, z) = U(r)[\cos m\varphi + \mathrm{i}p \sin m\varphi] \exp(\mathrm{i}kz), \tag{1.14}$$

with the azimuthal modulation parameter $p = 0$.

Numerical and analytical studies [59] showed, that it is possible to effectively slow down the expansion of the ring, thus rendering it stable for several tens of diffraction lengths, by taking the radius of the ring to be sufficiently large, so that the radial profile $U(r)$ may be approximated to the well-known sech shape, found for exact 1-D solitons.

When $p \neq 0$ the beam obtains an additional phase modulation accompanied by a nonzero angular momentum. For $p = 1$ Eq. (1.14) represents a vortex beam with topological charge m and the propagation dynamics have been extensively studied [see Section 1.2.2]. However, by decreasing the modulation parameter only

slightly $p \approx 1$ the dynamics become increasingly complicated, and generally involve competition between several different instability modes, causing the beam to evolve into a complex structure of optical splinters [60].

By decreasing the parameter p even further, the beam gradually attains a necklace-type intensity distribution and in fact no longer decays, but similar to the necklace beams expands self-similarly, [see Figure 1.5]. Due to the imposed angular momentum the expansion is accompanied by a small rotation and as the beam continually expands the angular velocity vanishes [61].

1.2.4 Rotating soliton clusters

A somewhat different approach leading to the realization of ring-like configurations of optical beams was demonstrated in [62]. Here the main idea, based on mutual soliton interaction, i.e., attraction for in-phase solitons and repulsion for out-of-phase solitons, was to consider a superposition of N solitons with Gaussian envelopes $G_n(x, y, z)$, $n = 1, 2, ..., N$ propagating in bulk saturable nonlinear media.

Regardless of the character of the soliton interaction, such a configuration will be unstable due to an effective tension in the ring profile caused by either attractive or repulsive forces between the constituting solitons. This instability, however, can be eliminated simply by imposing a phase dislocation on the beam, which changes by $2\pi m$ around the ring. This induces an angular momentum which causes the beam to rotate during propagation and the resulting centrifugal force tends to compensate the tension in the ring.

The Gaussian envelopes in the field $E = \sum G_n$ take the form [62],

$$G_n = A \exp\left(-\frac{|\mathbf{r} - \mathbf{r}_n|^2}{2a^2} + \mathrm{i}\alpha_n \right), \tag{1.15}$$

where $\mathbf{r}_n$, a and α_n are the location, width and phase of the nth soliton respectively. By applying the constraint of zero linear momentum of the center of mass of the beam, the phase α_n was shown to be a linear function of n, or $\alpha_n = \theta n$, with the phase difference between two neighboring solitons θ given by,

$$\theta = \frac{2\pi m}{N} \quad (m = \text{integer}). \tag{1.16}$$

In order to look for stable solutions to the problem the effective particle approach was applied and interaction energies for various cluster constellations were obtained. In this approach, the appearance of a minimum point for a given configuration indicated that such a cluster represented a stable solution, and the stability was then later verified through extensive numerical simulations. In general, it was found that bound states of N solitons existed provided the phase step θ was less than or equal to $\pi/2$, and a cluster of topological charge m would be meta-stable only if $N \geq 4m$ [62]. One such stable configuration is shown in Figure 1.6 with $N = 4$ and $m = 1$, corresponding to a minimum of the effective interaction energy.

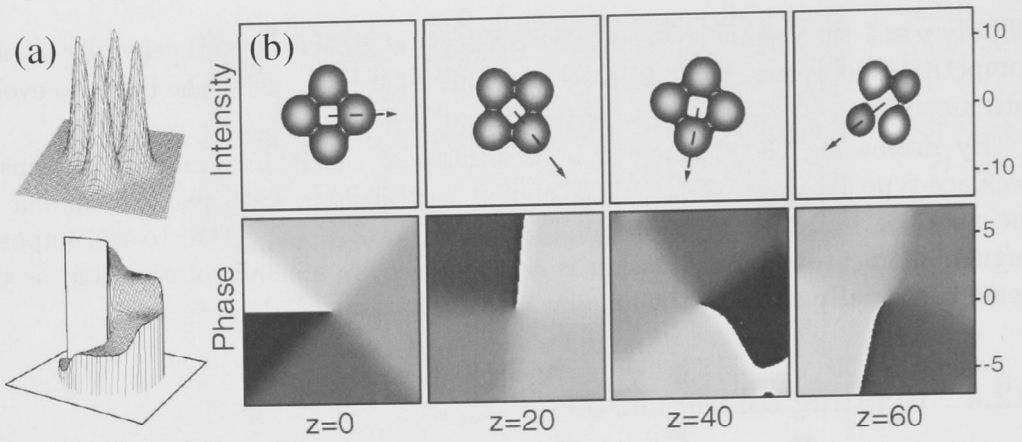

Figure 1.6: (a) Intensity and phase distribution of a rotating cluster of solitons with $N = 4$ and $m = 1$. Note that the vortex phase is a linear function of the azimuthal coordinate φ, while the staircase-like phase of the cluster is in fact a nonlinear phase configuration (from Ref. [63]). (b) Evolution of a rotating four-soliton cluster (from Ref. [62]).

1.2.5 Spatially modulated vortex beams: Azimuthons

Recently, a novel class of two-dimensional spatially localized optical beams in nonlinear media was introduced [64]. These so called azimuthons consist of a spatially modulated phase, and provide a link between the radially symmetric vortices and rotating soliton clusters. As with the rotating optical clusters and in contrast to the linear vortex phase, the phase of the azimuthon is a staircase-like nonlinear function of the polar angle.

The existence of the azimuthons was investigated in two different media [64], namely the Kerr medium and a saturable medium and through numerical simulations propagation of the structures was studied. In both cases, solutions to the governing equation were obtained by using an approximate (though rather accurate) variational approach and separation of variables. It was reported that the azimuthons are characterized by two azimuthal indices: the topological charge m and the number of the peaks N.

In contrast to the rotating soliton clusters which satisfy the existence condition $N \geq 4m$, rotating azimuthons were shown to exist for $N \geq 2m$ in saturable media, and truly stationary solutions, i.e., nonrotating beams with indices $N = 3$ and $m = 1$ were demonstrated.

It was furthermore reported that the angular momentum of the beams consisted of two significant contributions, which appeared to be the physical origin of the possibility of obtaining nonrotating structures with nonzero topological charges. Specifically, one contribution was attributed to the internal energy flow, while the second contribution stemmed from the modulation of the structure as a whole. Remarkably, the two contributions can be of opposite signs and as for the truly

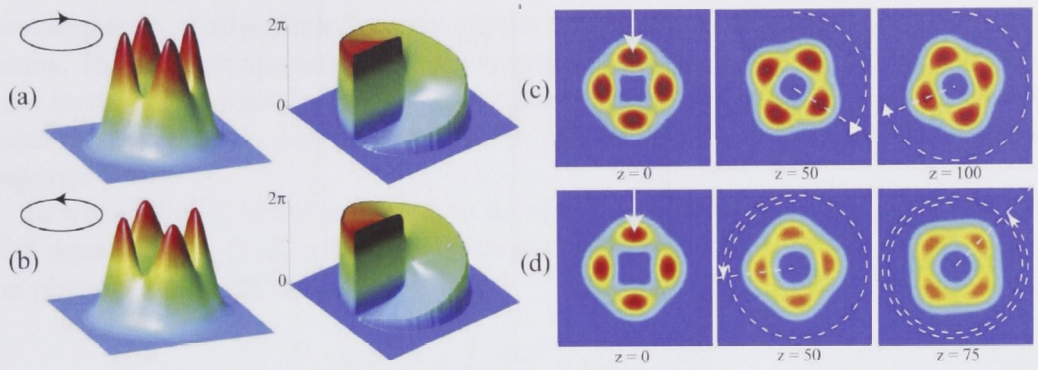

Figure 1.7: (a,b) Intensity and phase distribution of two similar azimuthons both with $N = 4$ and $m = 1$ but with opposite predicted angular velocities. (c,d) Propagation of the azimuthons, note the opposite angular velocities, indicated by arrows (from Ref. [64]).

stationary solution they exactly cancel each other, resulting in zero angular velocity. In other cases, as shown in Figure 1.7, the result is two similar solutions both with $N = 4$ and $m = 1$, but with opposite angular velocities [64].

As is well known, all optical beams, including azimuthons, are unstable in bulk Kerr media and eventually undergo catastrophic collapse, nevertheless in saturable media the azimuthons exhibit stable propagation for several diffraction lengths and even survive strong oscillations. However, as was pointed out in [64], similar to the dynamics exhibited by ring-like vortex beams, the azimuthons may also experience symmetry breaking instability and decay into several fundamental solitons.

In any known realistic nonlinear medium with a local response, higher-order optical solitons and vortices are known to be unstable. Consequently, much of the attention has been directed towards media with nonlocal nonlinear response which have attracted a significant interest recently. This has led to the discovery of certain highly intriguing properties of nonlocal solitons, which include arrest of catastrophic collapse [65] and significant suppression of modulational instability [66]. Nonlocality has thus proved to have a great impact on both stabilization and propagation dynamics of self-trapped optical beams and it follows that one of the most interesting and exciting properties of nonlocality is the ability to support a great variety of optical beams, e.g., multisoliton bound states, which are unstable in local media [32].

1.3 Nonlocal optical response and nonlocal solitons

Nonlocality is a generic feature of many different types of nonlinear systems. Nevertheless, in many cases the nonlocal properties of the nonlinear response being studied has been neglected [28, 67], which is justified when the nonlocal response exhibits a characteristic width much narrower than the propagating beam. When studying solitons however, nonlocality is of great importance for the beam

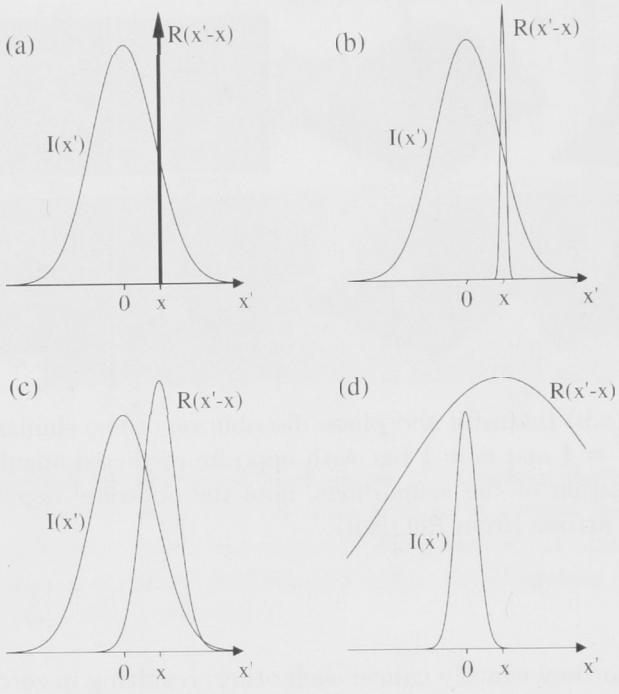

Figure 1.8: Schematic of four different regimes of the degree of nonlocality. The degree of nonlocality is given by the relative width between the spatial extent of the response function R and the width of the beam intensity I. (a) local nonlinear response function. In this case the response can be described by a delta function and hence $\mathcal{F}(I) = I$. (b) weakly nonlocal response, (c) general nonlocal response and (d) highly nonlocal response (from Ref. [68]).

propagation and stabilization, and therefore should be included in the governing equation [68].

In nonlocal optical media the nonlinear response at a particular point is not determined solely by the wave intensity at that point (as in local media), but depends also on the wave intensity in the vicinity of that point. It typically stems from certain transport processes responsible for the nonlinear response of the medium. These include, the charge drift in photorefractive crystals [69], atom diffusion in atomic vapors [70], or heat transfer in thermal nonlinear media [71]. It can also result from a long-range interaction of molecules or atoms as it occurs in nematic liquid crystals [72] or BECs [73, 74].

The stabilizing character of the nonlocal nonlinear response results from the fact that in nonlocal media a change of the nonlinear refractive index extends far beyond the physical extent of the wave itself, [see Figure 1.8]. This creates a broad waveguide-like structure which traps the beam. Even though the wave itself may exhibit strong spatial modulations, the nonlinearity-induced trapping "potential" is smooth because of the spatial "averaging" character of the nonlocality [75]. As

a consequence, nonlocal media may support stable propagation of complex optical beams. However, it appears that conjectures regarding stability of the complicated wave structures cannot be readily generalized to realistic nonlocal models. Certain stability properties do depend on the particular realization of the nonlocal nonlinear response [76].

In what follows, beam propagation in nonlocal media is governed by the general NLS equation Eq. (1.2), where the response $\mathcal{F}(I)$ is assumed to be represented by the phenomenological model

$$\mathcal{F}(I) = s \int R(\mathbf{r}' - \mathbf{r}) I(\mathbf{r}') \mathrm{d}\mathbf{r}', \tag{1.17}$$

where $s = 1$ ($s = -1$) denotes focusing (defocusing) nonlinearity and $\mathbf{r}$ covers transverse coordinates in D-dimensional space. It is further assumed that the response function is spatially localized, symmetric (i.e., $R(\mathbf{r}) = R(r)$ with $r = |\mathbf{r}|$), and normalized $\int R(\mathbf{r})\mathrm{d}\mathbf{r} = 1$.

Note that this model can not always be adequately applied to a given nonlocal nonlinear system. Indeed, in Chapter 4 a thermal system is investigated and a different approach to the problem must be exploited. However, most of the major properties exhibited by the nonlocal model in Eq. (1.17), are of a more or less generic character and therefore similar effects are expected to be detectable in more realistic nonlocal systems.

As can be seen in Figure 1.8, nonlocality is characterized by the spatial extent of the nonlinear response function, and the relative width of the response to the width of the beam intensity determines the "degree" of nonlocality [65]. It is often instructive to consider different regimes of the degree of nonlocality, and as presented in Figure 1.8(a), in the local limit the response function is given by a delta function $R(r) = \delta(|r|)$ in which case $\mathcal{F}(I) = I$, corresponding to the well-known local Kerr medium. In the weakly nonlocal limit, [see Figure 1.8(b)], where the spatial extent of the dependence of the nonlinear response on the beam intensity is nonzero, but the response still remains much narrower than the beam itself, it is possible to expand the intensity $I(\mathbf{r}')$ around the point $\mathbf{r}' = \mathbf{r}$ and obtain a simplified model

$$\mathcal{F}(I) = s(I + \gamma \nabla^2 I), \tag{1.18}$$

where

$$\gamma = \frac{1}{2} \int r^2 R(r) \mathrm{d}\mathbf{r}, \tag{1.19}$$

is positive definite and measures the relative width of the response [65]. This type of nonlinear response represents a model in its own right and governs nonlinear effects in plasma [77]. In addition, in 1-D it has been shown that this model supports the formation and stable propagation of both bright and dark solitons [78].

Conversely, when the characteristic width of the response function is much larger than the spatial extent of the beam, [see Figure 1.8(d)], an expansion of the response function $R(r)$ around the point $r' = r$ gives

$$\mathcal{F}(I) = -sr^2 P, \tag{1.20}$$

with

$$P = \int I \mathrm{d}\mathbf{r}. \tag{1.21}$$

In this highly nonlocal limit, the corresponding propagation equation becomes *linear*, with the response function thus reduced to the well-known linear harmonic potential [79].

The resulting linear model, introduced by Snyder and Mitchell in their seminal paper "*Accessible Solitons*" [79], constitutes a profound simplification of the problem and provides a relatively straightforward means of studying soliton propagation in various highly nonlocal media. As a consequence, numerous studies have been conducted and continue to be undertaken using this simplified linear model, and a large number of peer refereed journal papers on the subject have been published [80–90] clearly demonstrating that this is indeed a very vibrant and extremely popular area of nonlinear optics.

However, care must be taken since that in the general nonlocal case, [see Figure 1.8(c)], loosely defined as being neither weakly nor highly nonlocal, no such approximations are valid, and it is therefore usually necessary to resort to numerical and/or variational solutions to uncover the underlying physics of the system.

Therefore in this dissertation a more rigorous approach, involving variational techniques supplemented by sophisticated numerical simulations, will be adopted in order to study soliton propagation in nonlocal media considering the different degrees of nonlocality.

1.3.1 Suppression of modulational instability

With the nonlocal nonlinear response $\mathcal{F}(I)$ given by Eq. (1.17), the governing propagation equation takes the form

$$\mathrm{i}\frac{\partial E}{\partial z} + \frac{1}{2}\nabla_\perp^2 E + s\,E \int R(\mathbf{r}' - \mathbf{r}) I(\mathbf{r}') \mathrm{d}\mathbf{r}' = 0, \tag{1.22}$$

and plane wave solutions, in the form of stationary states, can be found with the generic form

$$E(\mathbf{r}, z) = \sqrt{\rho_0} \exp(\mathrm{i}\mathbf{k}_0 \cdot \mathbf{r} - \mathrm{i}\beta z), \tag{1.23}$$

where $\rho_0 > 0$ is the beam intensity and $\beta = k_0^2/2 - s\rho_0$ [68].

Analogous to the analysis in Section 1.2.2, stabilization of the stationary state against modulational instability is investigated by monitoring the evolution of a small perturbation $p(\mathbf{r}', z)$, which is added to the solution Eq. (1.23). The perturbed profile then reads,

$$E(\mathbf{r}, z) = [\sqrt{\rho_0} + p(\mathbf{r}', z)] \exp(\mathrm{i}\mathbf{k}_0 \cdot \mathbf{r} - \mathrm{i}\beta z), \tag{1.24}$$

with

$$p(\mathbf{r}', z) = \int \tilde{p}(\mathbf{k}) \exp(\mathrm{i}\mathbf{k} \cdot \mathbf{r}' + \lambda z) \mathrm{d}\mathbf{k}, \tag{1.25}$$

and $\mathbf{r}' = \mathbf{r} - \mathbf{k}_0 z$. Once more and similar to Section 1.2.2 the analysis involves solving an eigenvalue problem, and it has been shown [68] that the eigenvalues λ can be expressed through the relation

$$\lambda^2 = -k^2 \rho_0 \left(\frac{k^2}{4\rho_0} - s\tilde{R}(k) \right), \tag{1.26}$$

where $k = |\mathbf{k}|$ is the spatial frequency and $\tilde{R}(k)$ is the Fourier transform of $R(r)$.

In this particular case, if $\lambda^2 > 0$ the perturbation grows exponentially during propagation with the growth rate $\mathrm{Re}\lambda$, and the beam, as a result, suffers from modulational instability. From Eq. (1.26), it is evident that the sign of λ^2 depends crucially on the Fourier spectrum $\tilde{R}(k)$ of the response function, and a detailed analysis of all possible scenarios for several types of response functions has been reported in [91].

One major conclusion is that in the focusing case and provided the response function is localized and positive definite, the nonlocality suppresses modulational instability [68]. Note however that the modulational instability is never completely eliminated by the nonlocality. On the other hand, for a defocusing nonlinearity $\lambda^2 < 0$, and hence all solutions to Eq. (1.22) with $s = -1$ are stable [91].

1.3.2 Suppression of catastrophic collapse

Another truly intriguing aspect of nonlocality, in part responsible for its implementation in the NLS equation, is to have a profound effect on beam collapse. To some extent, this view was confirmed when it was proved analytically, that a specific type of nonlocal response allowed for the arrest of beam collapse [92]. A more general approach was explored in [65] and it provided a rigorous proof that for a symmetric response function with a positive definite Fourier spectrum, catastrophic collapse is completely prevented.

The analytical approach can be further extended to include much more general nonlocal response functions, with the only requirement being that the responses are symmetric and do not contain any singularities.

Now, in systems described by Eq. (1.22), both the power P and the Hamiltonian $\mathcal{H}$ represent important integrals of motion

$$P = \int I \mathrm{d}\mathbf{r} \tag{1.27}$$

and

$$\mathcal{H} = \frac{1}{2} ||\nabla_\perp E||_2^2 - \frac{1}{2} \int \mathcal{F}(I) I(\mathbf{r}) \mathrm{d}\mathbf{r}, \tag{1.28}$$

where $||\nabla_\perp E||_2^2 \equiv \int |\nabla_\perp E|^2 \mathrm{d}\mathbf{r}$. Moreover, for localized solutions to Eq. (1.22), P and $\mathcal{H}$ are conserved quantities.

Then, it is possible to show that the gradient norm $||\nabla_\perp E||_2^2$ is in fact bounded from above, and this is done by exploring the D-dimensional Fourier transform of the intensity $I(\mathbf{r})$,

$$\tilde{I}(\mathbf{k}) = \int I(\mathbf{r}) \exp(\mathrm{i}\mathbf{k} \cdot \mathbf{r}) \mathrm{d}\mathbf{r}, \tag{1.29}$$

and the inverse

$$\int I(\mathbf{r}) = \frac{1}{(2\pi)^D} \int \tilde{I}(\mathbf{k}) \exp(-\mathrm{i}\mathbf{k}\cdot\mathbf{r})\mathrm{d}\mathbf{k}. \tag{1.30}$$

When the nonlocal response $\mathcal{F}(I)$ is given by Eq. 1.17, the above relations Eq. (1.29) and Eq. (1.30) lead to the following relations

$$|\tilde{I}(\mathbf{k})| = \left| \int I(\mathbf{r}) \exp(\mathrm{i}\mathbf{k}\cdot\mathbf{r})\mathrm{d}\mathbf{r} \right| \leq P, \tag{1.31}$$

and

$$\int \mathcal{F}(I)I(\mathbf{r})\mathrm{d}\mathbf{r} = \frac{1}{(2\pi)^D} \int \tilde{R}(\mathbf{k})|\tilde{I}(\mathbf{k})|^2\mathrm{d}\mathbf{k}. \tag{1.32}$$

Consequently, for any response function with an absolute differentiable Fourier transform $\tilde{R}(\mathbf{k})$ it follows that

$$\left| \int \mathcal{F}(I)I(\mathbf{r})\mathrm{d}\mathbf{r} \right| \leq P^2 R_0, \tag{1.33}$$

where

$$R_0 \equiv \frac{1}{(2\pi)^D} \int \tilde{R}(\mathbf{k})\mathrm{d}\mathbf{k}. \tag{1.34}$$

By comparing Eq. (1.33) and Eq. (1.28) the resulting inequality then yields

$$|\mathcal{H}| \geq \frac{1}{2}||\nabla_\perp E||_2^2 - \frac{1}{2}P^2 R_0. \tag{1.35}$$

This result is of great importance to beam propagation in nonlocal media, since it basically provides a rigorous proof that, provided the Fourier spectrum of the response function under consideration is absolute differentiable, catastrophic collapse can not occur. This is due to the fact that the gradient norm, as previously mentioned, is bound from above by the conserved quantity $2|H| + P^2 R_0$ and hence a blow-up of the intensity, or identically the beam amplitude locally going to infinity, is prevented [68].

It should be stressed however, that depending of the spatial extent of the response, or rather the degree of nonlocality, collapse-like dynamics might still be exhibited by the propagating beam. Indeed, if the width of the beam is much larger than the characteristic width of the response, reminiscent of the weakly nonlocal case, the beam will initially experience contraction, similar to the dynamics found in local Kerr media. Nevertheless, by the time or distance the width of the beam becomes comparable to that of the nonlocality, the arrest of the beam collapse sets in and the beam will settle on a stationary phase with corresponding stable propagation, during which the two widths will remain comparable.

1.3.3 Nonlocal spatial solitons

Recent studies of self-trapped beams in nonlocal optical media have revealed many new and interesting phenomena e.g., the formation of higher-order solitons [93–95] and stabilization of so-called (3+1)-D spatiotemporal optical solitons [96] in media with nonlinearities similar to liquid crystals [97].

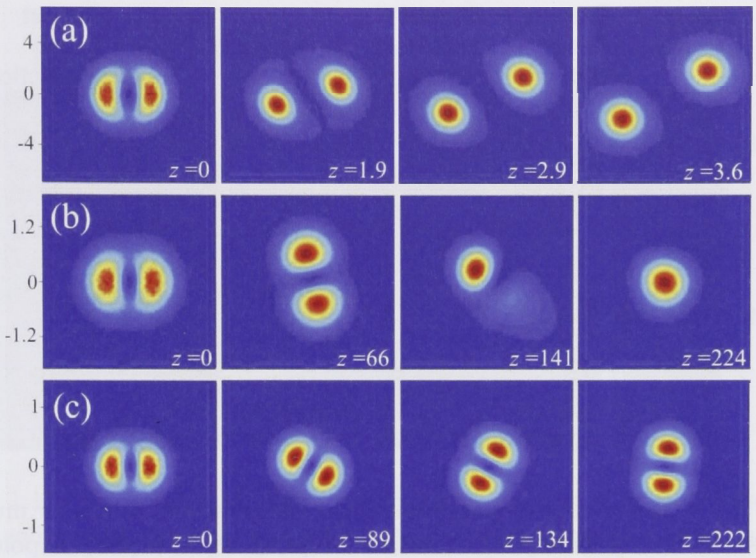

Figure 1.9: (a) Unstable propagation of rotating dipole, resulting in beam break-up into two filaments. (b) Evolution at a slightly higher power, here the initial filaments are forced to merge due to a stronger confinement from the increased nonlocality. (c) Stable propagation of the rotating dipole, for which the power exceeds the stability threshold (from Ref. [100]).

The existence of complex structures with nonzero angular momenta such as vortex solitons [75, 98, 99] and rotating azimuthons [64, 76, 100–102] suggested that nonlocality can even support higher-order spiraling solitons, [see Figure 1.9]. The figure depicts propagation of the simplest azimuthon, namely the rotating dipole in three different cases. In Figure 1.9(a) the evolution of the dipole in a weakly nonlocal medium is considered and it is evident that the beam eventually suffers from azimuthal instability and breaks up into two splinters, similarly to the behavior predicted in Section 1.2.2. The nonlocality is then slightly increased in Figure 1.9(b), nevertheless the dipole still displays unstable propagation, only this time the dynamics is different. As before the beam breaks up into two filaments, however due to the stronger nonlocality the splinters are forced together and eventually merge. Finally, in Figure 1.9(c), the degree of nonlocality exceeds a certain stability threshold, and the dipole exhibits stable propagation accompanied by spiraling of the structure as a whole [100].

Over the years many nonlocal effects have been investigated both theoretically and experimentally in studies involving nematic liquid crystals [103–114], materials with thermal nonlinearity [115–118], and photorefractive media [29, 119–123]. In particular, in [115] it was observed experimentally that a highly nonlocal nonlinear thermal medium could support formation of so-called scalar multipole solitons, [see Figure 1.10]. The observed structures geometrically resembled dipole, tripole, quadrupole, and necklace-type solitons, and they were organized as arrays of out-of-

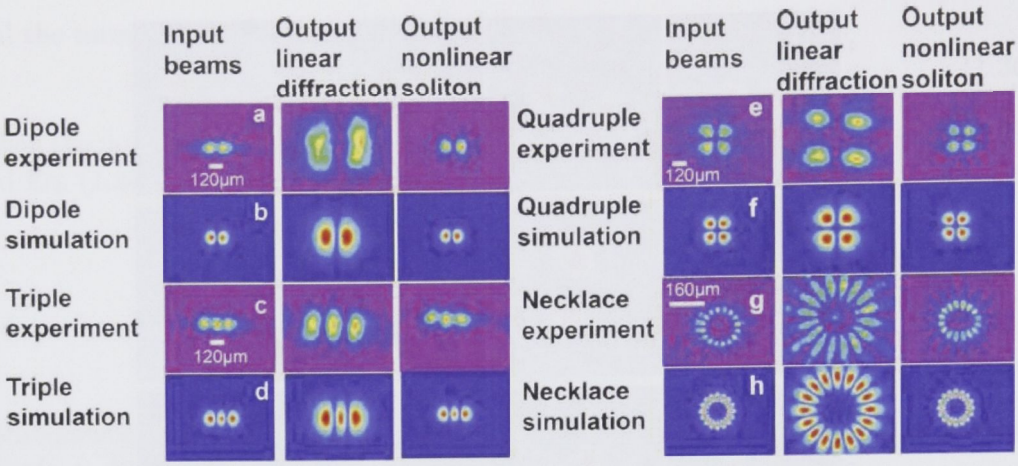

Figure 1.10: Experimental and theoretical observations of scalar multipole solitons. Pictures show the evolution of (a,b) dipole, (c,d) tripole, (e,f) quadrupole and (g,h) necklace solitons. Left-hand columns show input beams, columns in the middle depict diffracted beams at low powers and right-hand columns show self-trapped structures at high power (from Ref. [115]).

phase bright beams. Although such higher order solitons, except for the nonrotating dipole, are inherently unstable in a thermal medium [124, 125], the instability is rather weak in some ranges of the parameters and this allowed for their experimental observation [115].

1.3.4 Interaction of solitons

In local focusing nonlinear media, interaction of bright spatial solitons depends on the relative phase between the beams, [see Section 1.1.1]. Interestingly, the phase dependence is suppressed whenever the response is nonlocal in nature and the degree of nonlocality reaches a certain threshold.

Interactions of solitons in nonlocal media are in general long-range and in the case of two beams launched in parallel in a nonlocal medium, due to the nonlocality, each beam will induce a refractive index change which extends spatially far beyond the beam itself and reaches into the region of the other beam, thereby causing a mutual attraction between the beams.

Recently, experiments have demonstrated that in a highly nonlocal medium and with a spatial separation of the beams an order of magnitude larger than the respective beam widths, [see Figure 1.11], in spite of their large separation the solitons attract each other, and this manifests in an inwards bending of the soliton trajectories [117].

In addition, it has been observed that two out-of phase bright solitons, which repel in local media, also experience mutual attraction [126], and this paves the way of realizing bound states formed by out-of-phase solitons, e.g., similar to the case

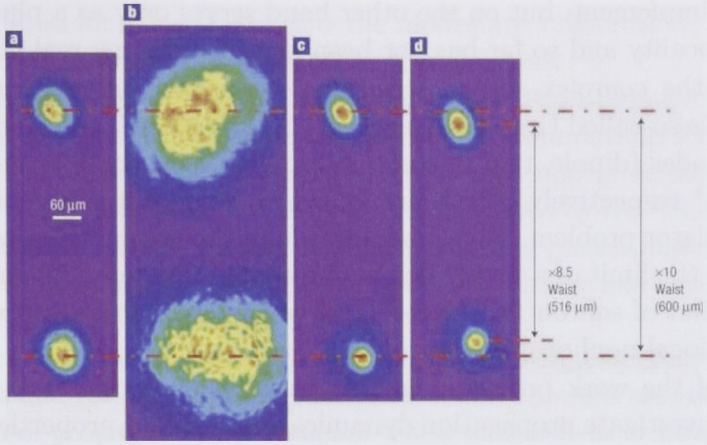

Figure 1.11: Experimental demonstration of long-range nonlocal interaction of two solitons launched in parallel. Note that the separation of the beams is approximately one order of magnitude larger than the characteristic widths of the beams. (a) Input profiles of the beams. (b) Diffracted beams at low power. (c) Individually launched beams (d) Beams launched simultaneously experiencing attraction from afar (from Ref. [117]).

of *soliton clusters* discussed in Section 1.2.4.

When the nonlocality is defocusing, it has been shown both theoretically [127] and experimentally [118], that it is possible to obtain bound states of dark solitons. Similar to the case of nonlocal bright solitons the formation of bound states of nonlocal dark solitons, is possible due to a long-range mutual attraction, mediated by the combined soliton induced waveguide structure stemming from the overlapping regions of refractive index changes.

Thus, nonlocality not only allows for stable propagation of multidimensional beams, through the substantial suppression of modulational instability and arrest of catastrophic collapse, it also supports formation and stable propagation of bound states of several interacting solitons regardless of the relative phases of the beams. This opens up the possibility of realizing even highly complex structures in nonlocal media, which promise to lead to a wealth of novel physics and as yet undiscovered phenomena in the realm of soliton propagation dynamics.

1.4 Outline of the thesis

The theoretical and experimental observations of the existence, stability, and interactions of spatial nonlocal optical solitons discussed above stimulate further theoretical studies of the properties of self-trapped optical beams in media with nonlocal nonlinear response.

In particular, the theoretical results regarding the rotating dipole were obtained using a Gaussian response function, which on one hand is very instructive and rela-

tively easy to implement, but on the other hand serves only as a phenomenological model of nonlocality and so far has not been identified in any real physical system.

Moreover, the complex soliton structures demonstrated in Figure 1.10 structurally resemble so-called Laguerre-Gaussian (LG) (necklace) and Hermite-Gaussian (HG) linear modes (dipole, tripole and quadrupole), henceforth termed "necklaces" and "matrices" respectively, which are known to represent solutions to the linear harmonic oscillator problem. This model was found to adequately describe a nonlocal medium in the limit of a highly nonlocal response function [79] and the question arises, what kind of soliton "necklaces" and "matrices" can be supported and stabilized by nonlocal nonlinear media.

The aim of the work presented in this dissertation is thus two-fold. First to theoretically investigate propagation dynamics and stability properties of a different family of higher-order solitons identified as Laguerre-nonlocal (LN) and Hermite-nonlocal (HN) solitons as well as the extended family of generalized nonlocal (GN) solitons which are obtained by employing a different set of linear waveguide modes, namely the generalized-Hermite-Laguerre-Gaussian (HLG) modes [128].

Secondly to investigate the stabilizing properties and boundary effects on beam propagation of a more realistic system, in form of a nonlocal nonlinear thermal medium.

In Chapter 2 a set of linear optical HG and LG waveguide modes are employed to construct higher-order spatial solitons in nonlocal nonlinear media in the form of soliton clusters, i.e., soliton necklaces and matrices. These higher-order modes consist of distinctly different symmetries and, more specifically, the multiple-ring soliton necklaces LN_{nm} are characterized by the number of radial nodes n, the topological index m as well as an additional modulation depth p, similar to the necklace beams in Section 1.2.3. The indices of the soliton matrices HN_{nm} determine the number of nodes in two orthogonal directions.

A variational approach is used to obtain solutions for all symmetries to the governing equation, and it turns out that distinctly different symmetries coexist, i.e., they share the same energy and power. This property has a profound effect on the propagation dynamics of the different beams, which in various cases involves intricate transformations between seemingly different beam structures of radial and rectangular symmetries. Therefore, depending on the profile of the soliton and the soliton power, the HN and LN modes can either experience stable propagation or quasiperiodic dynamics involving numerous transitions from one symmetry to the other, with subsequent revivals of the original input beam.

During the symmetry transformations intermediate states resembling the generalized Hermite–Laguerre–Gaussian (HLG) modes [128] are clearly distinguishable. This observation indicates that the higher-order self-trapped states may represent structurally stable localized solutions that belong to a general class of solitons with more complex structure and phase.

This motivates the construction of higher-order solitons that extend the HLG linear modes to the case of nonlinear media with the Gaussian nonlocal response and as expected for the $\mathrm{GN}_{nm}(\alpha = 0)$ the HN_{nm} modes are recovered, while for $\mathrm{GN}_{nm}(\alpha = \pi/4)$ the symmetry is that of the LN_{nm} modes, [see Section 2.3]. At

intermediate values for the parameter α the modes are substantially more complex and carry vortices embedded in their phase distributions.

A thorough investigation of the intriguing propagation dynamics displayed by the quadrupole-like beams is undertaken and extensive simulations for various values of α and different beam powers demonstrate that such multipole modes experience quasi-periodic dynamics similar to the dynamics displayed by the LN and HN modes. Despite the multiple vortices present in their pertaining phases however, the family of quadrupole solitons maintain a net zero topological charge and hence zero angular momentum M for all α [see Section 2.3].

In Chapter 3 therefore main focus is to explore the intriguing continuation $M > 0$ for HN solitons and to that end two generalized soliton families are considered which entail a wealth of propagation phenomena. These solitons either form bound states of self-trapped vortex beams or they can experience quasi-periodic transformations and, because the solitons attain a nonzero angular momentum, the propagation is accompanied by spiraling of the beams. By tracing the position of the vortices embedded in the phase distributions during propagation, complex vortex lines in the form of vortex loops, links and knots are demonstrated.

An elaborate approach is then employed to investigate in more detail the formation of these intriguing nodal line structures, and to that end the evolution of a fundamental soliton in a local nonlinear saturable medium is considered. It follows that due to relatively small oscillations in the beam profile several vortex loops surrounding the beam are formed. By perturbing the soliton further such that it attains both an elliptic symmetry as well as a nonzero angular momentum, several closely spaced loops merge to form both vortex links and knots.

The results concerning beam propagation in nonlocal media in the preceding chapters are obtained with the response function assumed to be Gaussian. In Chapter 4 a more realistic nonlocal medium is considered and therefore a different method must be applied, which involves solving simultaneously a coupled set of equations rather than just one governing equation, i.e., Eq. (1.22).

Initially the propagation of the rotating dipole and a necklace beam is studied and, similar to the results in [100], it is observed that above a certain power threshold the dipole solitons propagate stably for several tens of soliton periods. In addition, an example of a semi-stable rotating necklace-type soliton is demonstrated.

Due to the fact that the thermal response is determined by the details of heat transfer at the boundaries, the sample geometry has a profound effect on the structure of the formed solitons, their stability and mutual interaction. This is demonstrated by launching several beam symmetries in samples of different geometries and at different transverse positions in the sample. It is demonstrated that the beams undergo different transitions depending on the ratio of the sample, or in a different case experience a strong modulation of the input profile induced at an earlier stage of propagation due to a correspondingly stronger force resulting from the soliton being launched closer to the boundary.

CHAPTER 2

Necklaces and matrices of nonlocal solitons

2.1 Introduction

Historically, several attempts to realize higher-order solitons [58, 59], rotating soliton clusters [60, 62] as well as complex multipole soliton structures with nonzero angular momentum [64] in various local media have been put forward. In certain cases, the beams have been remarkably long-lived, however although clever in concept they have all, without exceptions, turned out to be inherently unstable.

As discussed in Section 1.3, nonlocality has a profound effect on soliton formation, stability and interaction, which, in part, is due to the fact that in nonlocal media the well-known beam collapse is arrested and the modulational instability is substantially suppressed [68]. Recent developments in the study of optical solitons in nonlocal nonlinear media have paved the way for interesting novel physics, which make higher-order nonlocal solitons an intriguing and worthwhile aspect of nonlinear optics. These include, e.g., formation of stable multi-soliton bound states [99, 129], stabilization of vortex solitons [98] and otherwise nonstationary structures, such as dipole solitons [100] as well as higher-order azimuthons [101].

Nonlocal solitons exhibit intricate dynamics, e.g., long-range attractive interactions [117], stable propagation accompanied by spiraling of the beam structure as a whole [100, 101], breather-like quasi-periodic oscillations [130], and anomalous refraction and reflection across interfaces [131].

Particular examples of nonlocal dipole, tripole, and quadrupole solitons, as well as necklace beams have been generated experimentally in lead glasses [115] with thermal nonlocal nonlinear responses. The nontrivial patterns composed of fundamental solitons become possible due to a balance between repulsion of out-of-phase individual solitons and a force from a broad effective potential induced by the beam.

Another approach to understand these structures is to employ an analogy with linear modes: "soliton necklaces" can be related to the linear optical Laguerre-Gaussian (LG) modes, while "soliton matrices" resemble the Hermite-Gaussian (HG) waveguide modes. The next logical step using this analogy then, is to ex-

plore exactly what kind of soliton "necklaces" and "matrices" can be supported and stabilized by nonlocal nonlinear medium.

In the first part of this chapter, a set of linear optical HG and LG waveguide modes are employed to construct higher-order spatial solitons in nonlocal nonlinear media in the form of soliton clusters: necklaces and matrices. Those novel types of solitons are identified as Hermite-nonlocal (HN_{nm}) and Laguerre-nonlocal (LN_{nm}) spatial solitons with distinct differences in their symmetry. In general the HN_{nm} consist of arrays of out-of-phase solitons arranged in matrix-like structures which can be both square and rectangular depending on the two indices n and m. Conversely, the LN_{nm} consist of radially symmetric intensity distributions, with a varying number of rings and topological index. In addition the modulation parameter p, $0 \leq p \leq 1$, determines the structure of the intensity distribution which varies from structurally resembling a necklace consisting of individual "petals" at $p = 0$ through intermediate geometries to consisting of one or more concentric rings $p = 1$, [see Figure 2.3]. Moreover, in several cases the two modes HN and LN in fact coincide, and one such example is the rather obvious case of the fundamental beam, obtained by HN_{00} and LN_{00}. Other examples include the "pure" nonrotating dipole given by HN_{10} and $\mathrm{LN}_{01}(p = 0)$ and the quadrupole obtained by HN_{11} and $\mathrm{LN}_{02}(p = 0)$.

Using the variational approach [132] and numerical minimization of the error functional [133], broad classes of higher-order localized states are obtained both analytically and numerically and it is further demonstrated that only a few of them are energetically separated from each other. In general, localized states with different symmetries coexist, i.e., they share the same power and energy. Indeed, in several cases, [see Figure 2.6], even more than two different states occupy the Hamiltonian $\mathcal{H}$ vs. power P bands.

Next, the variational solutions are used as input profiles for direct simulation of the beam propagation and because the variational profiles differ from the stationary solutions, at the initial stage, the beams oscillate slightly [99]. As expected, depending on the degree of nonlocality, several propagation dynamics are revealed. In the local regime the solitons are unstable, and different scenarios of soliton evolution are observed, depending on their power. At low power the beams either break up into several optical splinters as fundamental solitons or they exhibit irregular dynamics while remaining largely localized. A remarkably different instability scenario however, is also possible. Indeed, in cases when distinct beam symmetries coexist energetically and occupy the same energy band it can cause the disparate states to perform mutual transitions from one symmetry into another during propagation. Depending on the particular structure of the initially launched beam, at substantially higher powers or in the highly nonlocal limit, some solitons become stable, while others continue to undergo quasi-periodic transitions and revivals.

In order to fully appreciate the underlying physics of this coexistence of different states, in the second part of the chapter, a more general approach of constructing nonlocal solitons is considered by adopting the linear generalized Hermite-Laguerre-Gaussian (HLG) modes [128]. By adding an additional modulation parameter α, in particular $0 \leq \alpha \leq \pi/4$, a novel class of high-order nonlocal solitons is constructed

which allows for a simple continuous transition between the HN and LN self-trapped modes through α and thus it becomes evident that the HN and LN states belong to the same general family of solitons. Note that, although the HN, LN and GN beams share many common features, they display one important distinct difference. In particular, both HN and LN have zero lines, whereas all zeros in the GN are isolated points, i.e., points of intersection of real and imaginary parts of these functions [128]. In fact, except for a few trivial cases, all GN modes carry several phase singularities or vortices in their phase distributions.

As an example the family of generalized quadrupole solitons is presented, and simulations demonstrate that for certain values of α these solitons exhibit quasi-periodic behavior. This is manifested by a series of nontrivial transformations over several hundreds of soliton periods $\sim \pi/k$.

In general, theoretical studies of beam propagation in optical nonlocal nonlinear media often present highly complicated problems and in several cases the nonlocal response of the medium of interest can not be described by a response function. One such instance is when propagation in thermal media is considered [see Chapter 4].

Numerical modeling therefore involves solving simultaneously a coupled set of equations governing the propagation of optical beams and the physical effect responsible for the nonlocal properties of the medium such as charge drift [69], thermal diffusion [71], transport of atoms in atomic vapors [102], or long-range molecular re-orientational interactions [107].

In this chapter, the nonlinear response, i.e., the nonlocal change of the refractive index $\mathcal{F}(I)$, is described by a phenomenological model [Eq. (1.17)]. This greatly simplifies the problem and direct simulation of the beam propagation is performed with the fast-Fourier-transform splitstep algorithm, using the various variational solutions as input profiles.

As mentioned in Section 1.3, the degree of nonlocality is often characterized by different regimes, namely the weakly-, the general-, and the highly nonlocal limit. In the first and latter cases various technics can be employed in order to further simplify the problem significantly [see Section 1.3]. However in this chapter focus is mainly on the general nonlocal limit, and the following analysis therefore involves both numerical and variational solutions to demonstrate the various propagation and evolution dynamics.

In the following and throughout this chapter, the system under consideration is assumed to be governed by the nonlinear Schrödinger equation [Eq. (1.22)], with a Gaussian nonlocal response function

$$R(\mathbf{r}) = \exp(-\mathbf{r}^2/\sigma^2)/\pi\sigma^2, \tag{2.1}$$

where σ denotes the degree of nonlocality.

Stationary states, parameterized with propagation constant k, can be found in a generic form as $E(x, y, z) = U(x, y)\exp(ikz)$ with the Lagrangian $\mathcal{L} = -kP - \mathcal{H}$, where the corresponding integrals of motion are the beam power, $P = \int |U|^2 \mathrm{d}\mathbf{r}$, and Hamiltonian,

$$\mathcal{H} = \int \left(|\nabla U|^2 - \frac{1}{2}|U|^2 \int e^{-|\mathbf{r}-\mathbf{r}'|^2} |U'|^2 \mathrm{d}\mathbf{r}' \right) \mathrm{d}\mathbf{r}. \tag{2.2}$$

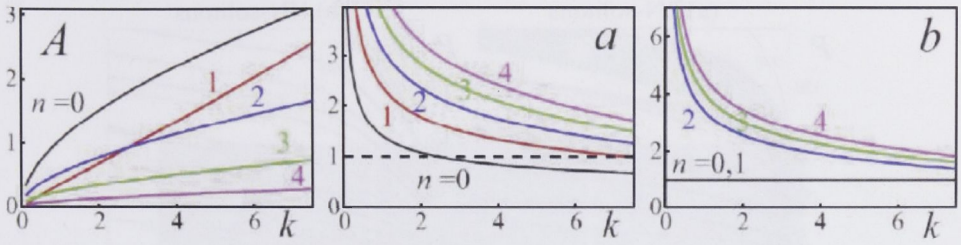

Figure 2.1: Variational parameters of the one-dimensional HN_n solitons, Eq. (2.3). The index n is shown next to the curves.

Physical variables absorb the transverse scale of nonlocality σ as follows, $\tilde{z} = z\sigma^2$, $\tilde{\mathbf{r}} = \mathbf{r}\sigma$, and $\tilde{E} = \sqrt{\pi}E/\sigma$. Note that the power, $\tilde{P} = \pi P$, and the orbital angular momentum, $\tilde{M} = \pi M$, do not depend on σ, here $M = \mathrm{Im}\int U^*|\mathbf{r}\times\nabla U|\mathrm{d}\mathbf{r}$. However, the soliton constant and the Hamiltonian scale as $\tilde{k} = k/\sigma^2$ and $\tilde{\mathcal{H}} = \pi\mathcal{H}/\sigma^2$. Note also that with this scaling the degree of nonlocality increases with propagation constant k and consequently beam power P.

2.2 Hermite- and Laguerre-Gaussian nonlocal solitons

In local media, it is well known that the only stable scalar solution is a fundamental soliton, however, as was discussed in Section 1.3.4, nonlocality enables a compensation for the soliton repulsion thereby stabilizing multihump solitons [94], similar to nonlinear modes in a confining potential [134].

In the linear limit, i.e., when $U \to 0$, such modes correspond to the diffracting linear HG modes

$$U_n(x) = A\exp(-x^2/2a^2)H_n(x/b), \tag{2.3}$$

where the integer index n determines the number of nodes across the Gaussian envelope and $H_n(t)$ is the Hermite polynomial

$$H_n(t) = (-1^n)e^{t^2}\frac{\mathrm{d}^n e^{-t^2}}{\mathrm{d}t^n}. \tag{2.4}$$

Separation of variables $U(x,y) = X(x)Y(y)$ in Eq. (2.2) leads to two coupled one-dimensional subsystems for the envelopes X and Y which can be, in general, complex. Indeed, the more general family of the HN solitons includes singular solutions with nontrivial phase and nonzero angular momentum, similar to the LN solitons. However, their structure is expected to contain multiple phase dislocations [see Section 2.3], and here only real envelopes $X(x) = U_n(x)$ and $Y(y) = U_m(y)$ given by Eq. (2.3) with independent parameters are considered. Deriving variational equations, the relations between the parameters of one-dimensional envelopes which give the final parameters of two-dimensional "soliton matrices" are established.

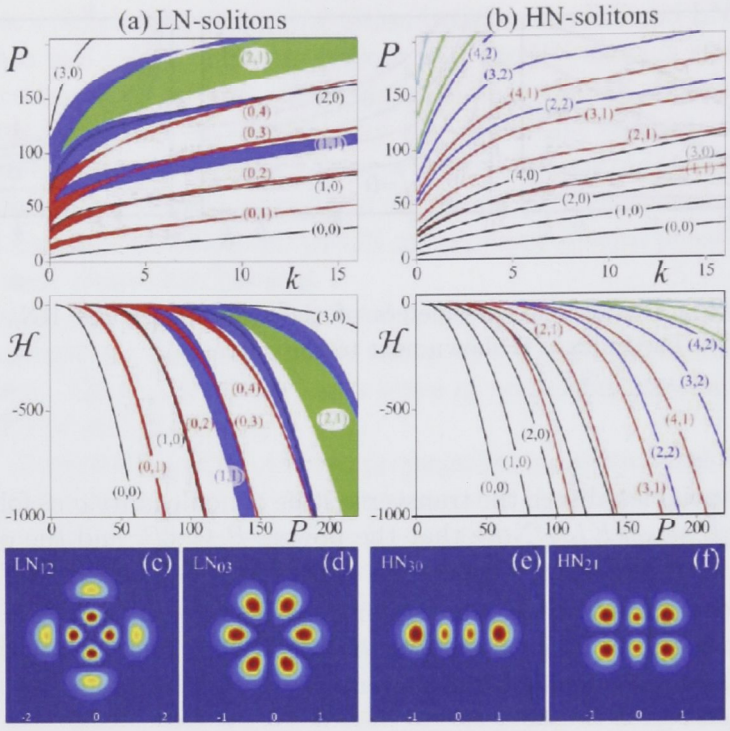

Figure 2.2: (a,b) Variational diagrams and (c–f) exact profiles for (a, c, d) Laguerre- and (b, e, f) Hermite-nonlocal solitons. Solitons in (c–f) have the power $P \simeq 200$.

Variational solutions corresponding to the HN_{nm} modes are derived using Eq. (2.3) as the ansatz in the nonlinear problem. The standard Ritz minimization procedure [132] is employed with the variational parameters A, a, and b ($b \equiv 1$ for $n = 0, 1$) and the obtained numerical solutions for different n are shown in Figure 2.1.

In order to establish the validity of the variational solutions they serve as a good guess for further use in numerical relaxation method by which an exact solution can be obtained. Thus two examples of exact HN_{nm} solitons are presented in Figure 2.2(e) and Figure 2.2(f). The exact envelopes $U(x, y)$ are obtained with relaxation procedure [133] which consist of numerical minimization of the error functional, $\int |f|^2 \mathrm{d}\mathbf{r}$, generated at the right hand side of the stationary NLS equation, $kU_{tr} + \delta\mathcal{H}/\delta U_{tr} = f$, so that $f \to 0$ when the trial function approaches the exact solution $U_{tr} \to U$.

Next, with the family of different HN modes established, a similar approach is adopted to obtain several solutions corresponding to the LN solitons. Due to their ring-like structure, the variational ansatz for the LN_{nm} solitons can be constructed using the separation of variables in the cylindrical coordinates

$$U(x, y) = R_{nm}(r)(\cos m\varphi + \mathrm{i}p \sin m\varphi), \tag{2.5}$$

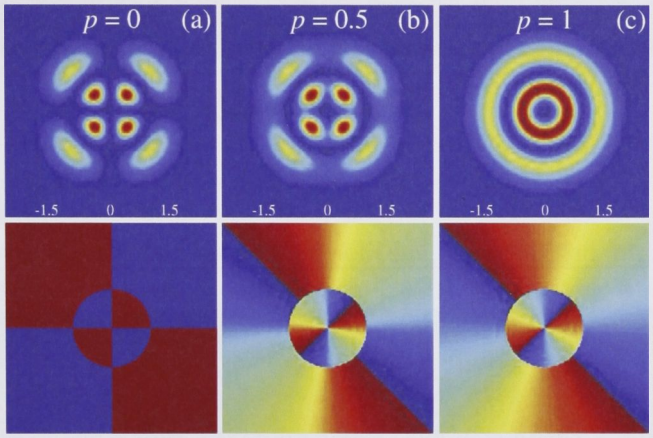

Figure 2.3: Intensity (top row) and phase (bottom row) distributions for the LN_{12} modes with three different values of the modulation parameter p, i.e., (a) $p = 0$, (b) $p = 0.5$ and (c) $p = 1$. Note that the phase distributions change noticeably from $p = 0 \rightarrow p > 0$, whereas they change only slightly for $0 < p \leq 1$. The colors for intensity (top row) are mapped from zero (blue) to maximal value (red), while phase (bottom row) is scaled from $-\pi$ to π.

where the radial envelope R_{nm} with n nodes solves the nonlinear ordinary differential equation [100]. Parameter $p \in [0, 1]$ determines the depth of azimuthal modulation ($p \equiv 1$ for $m = 0$) as well as the angular momentum, $M = 2mpP/(1 + p^2)$. Further simplification of this method was implemented in Refs. [124, 135] for the radially symmetric vortices with $p = 1$, however here it is extended to the general case $p \leq 1$.

Radial envelopes are sought in the form

$$R_{nm}(x, y) = Ar^m \exp(-r^2/2a^2) L_n^m(r^2/b^2) \tag{2.6}$$

with the generalized Laguerre polynomial

$$L_n^m(t) = \frac{1}{n!} t^{-m} e^t \frac{\mathrm{d}^n(t^{n+m} e^{-t})}{\mathrm{d}t^n}. \tag{2.7}$$

The results in terms of the soliton power P vs. propagation constant k and Hamiltonian $\mathcal{H}$ vs. P are plotted in Figure 2.2(a) for several different LN_{nm} solitons. The singular LN_{nm} solitons with $m \neq 0$ occupy the continuous bands in the diagrams in Figure 2.2(a) which are obtained by varying the modulation parameter p. Thus, soliton necklaces with $p = 0$ and vortex solitons with $p = 1$ form the lower and the upper-energy edges of the bands. For the lowest-order single-ring LN_{0m} necklaces

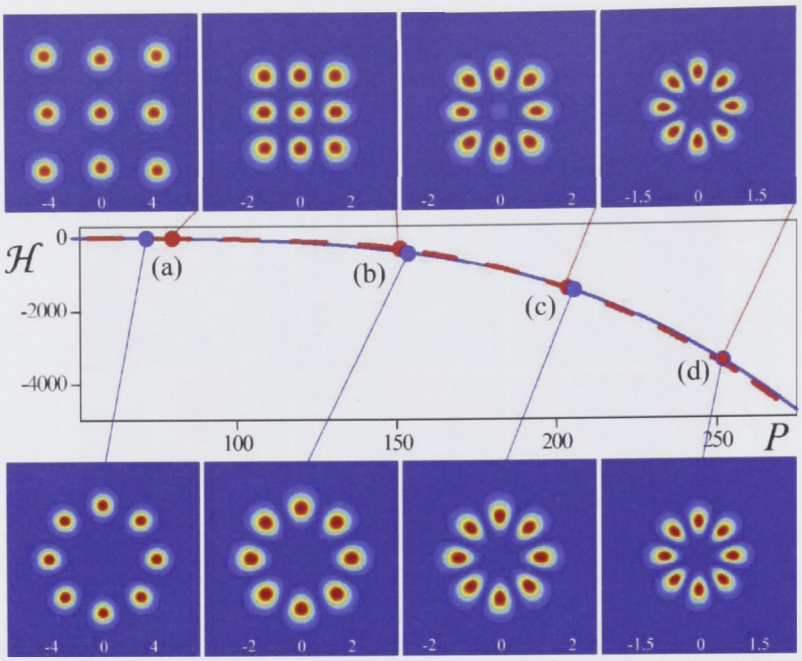

Figure 2.4: Coexistence of HN_{22} matrix (top row, dashed line) and $LN_{04}(p = 0)$ necklace (bottom row, solid line). Variational (lines) and exact (dots and profiles) solutions are shown for $k = 2.12$ (a), 11.5 (b), 30.34 (c), and 54.45 (d).

the bands are quite narrow, while their width diverges quickly with the number of rings. Note that solitons with different values of p are physically separated within the band by the conservation of the angular momentum M. In Figure 2.2(c) and Figure 2.2(d) two examples of exact LN_{nm} solitons are depicted.

To illustrate the effect of modulation parameter p on the various beam structures, in Figure 2.3 three distinct symmetries for the LN_{12} are depicted. At zero modulation, i.e., $p = 0$, the beam consists of individual out-of-phase "petals" arranged in a circular symmetric necklace-type distribution, similar to the necklace beams discussed in Section 1.2.3. When the modulation is increased the beam becomes more complex, and the petals are no longer well separated, which is particularly evident from the phase distribution resembling the phase structure of a double charged vortex beam. Note however, the zero ring splitting the phase distribution into two separate parts, which is due to the double ring structure of the beam. At maximum modulation, $p = 1$ the beam structure is that of a double ring double charged vortex beam, with the phase remaining more or less unchanged.

Above two distinct families of solutions have been introduced, but the comparison of two $\mathcal{H}(P)$ diagrams in Figures 2.2(a) and 2.2(b), or even more evident in Figures 2.6(a) and 2.6(b), suggests that it is not always possible to separate them energetically and to distinguish between "lower-" and "higher-order" solitons.

For the radially symmetric LN-solitons with $p = 1$, the variational solutions provide a very good approximation of the integral characteristics [135] (power and Hamiltonian), and here this result is confirmed for soliton necklaces $\mathrm{LN}_{nm}(p = 0)$ and low-order soliton matrices HN_{nm}. Indeed, for a given value of k, the power of exact solutions in Figure 2.2(c)–2.2(f) differs from variationally predicted values in Figures 2.2(a) and 2.2(b) within a remarkable 1% of accuracy, while differences in Hamiltonian values are within 10%.

However, for higher-order HN solitons, such as HN_{22} soliton matrix in Figure 2.4 (top), the profiles of exact solutions deviate considerably from the ansatz [Eq. (2.3)]. For low power in Figure 2.4(a), the HN_{22} soliton attains a shape of a square array of 9 out-of-phase spatially well-separated solitons, the square being stretched by its corners. At intermediate powers, [see Figure 2.4(b)], the shape is fairly close to the HG ansatz. With further increase of the power, the square geometry is gradually lost (there is still a nonzero peak at the origin of the "matrix" HN_{22} in (c)), and at approximately $P \geq 250$, the soliton matrix HN_{22} disappears by "fusion" with 8-soliton necklace $\mathrm{LN}_{04}(p = 0)$ [see Figure 2.4(d)]. The change of the geometry of the HN_{22} solutions slows down the relaxation procedure; in contrast to the $\mathrm{LN}_{04}(p = 0)$ solitons in Figure 2.4 (bottom), for which the variational ansatz [Eq. 2.5] provides an excellent approximation.

Two major conclusions can be drawn from Figure 2.4. First, the high-order HN_{nm} solitons can exist in a limited domain ($P \leq P_{max}$ and $k \leq k_{max}$). This implies that there should be an upper limit for the number of solitons in the matrix, $N \leq N_{max}$, where $N \equiv (n + 1)(m + 1)$. Second, despite distinct differences in their geometry, the soliton matrix HN_{22} and soliton necklace $\mathrm{LN}_{04}(p = 0)$ coexist energetically.

2.2.1 Instability dynamics

Variational solutions are used as input profiles for the direct simulation of the beam propagation and because the variational profiles differ from the stationary solutions, at the initial stage, the beams oscillate slightly [99]. As expected, power levels corresponding to different degrees of nonlocality, prompt various propagation dynamics. When the solitons are stable, the oscillations (internal modes) slowly decay with propagation [100] and stable propagation over several hundred soliton periods has been observed for a large number of various beam structures including both HN and LN solitons.

On the contrary, in Figure 2.5 an example of unstable dynamics displayed by two LN_{02} modes with different modulation depth p is depicted. At low power higher-order modes are unstable and in particular in Figure 2.5 it is evident that instabilities here involve a breakup of the beams which then evolve into several splinters that fly off in a spiraling motion due to a nonzero angular momentum of the initial state [see Section 1.2.2]. Note that at some intermediate propagation distance in Figure 2.5(a), the beam attains the symmetry of a tripole-like beam which is in excellent agreement with the fact that these two distinct structures actually belong to the same general family of solitons, [see Section 2.3, and in particular Figure 3.1]. Interestingly, the

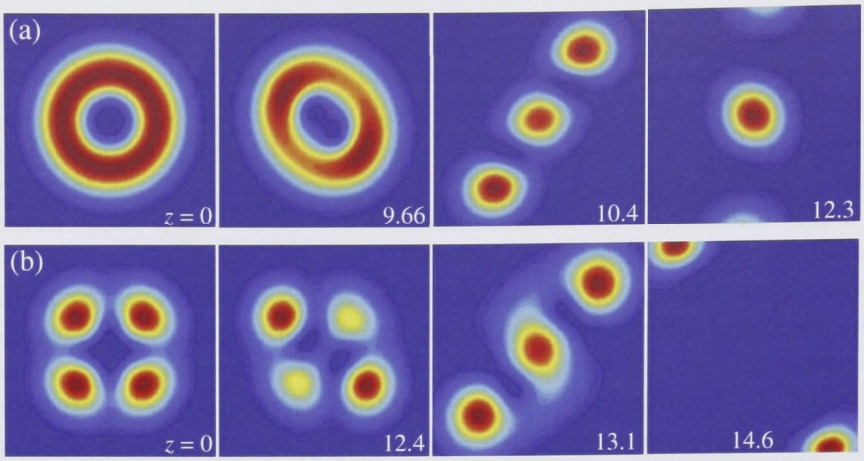

Figure 2.5: (a) Instability dynamics of the LN_{02} mode with modulation parameter $p = 1$. (b) Same mode, i.e., LN_{02} only this time with $p = 0.5$. Beam power $P = 75$ in both cases.

dynamics in Figure 2.5(b) depicting the breakup of the $LN_{02}(p = 0.5)$, are in fact quite similar to the dynamics in Figure 2.5(a).

In the case of the $LN_{02}(p = 0)$ (similar to HN_{11}) and at the same power, i.e., $P = 75$ the dynamics are remarkably different as shown in Figure 2.6(d). As will be shown in Section 2.3 this particular beam structure is obtained for $\alpha = 0$ in the family of the general quadrupole beams [see Figure 2.8(a)] and through complex transitions the beam evolves into the single-ring fundamental soliton $LN_{10}(p = 1)$ accompanied by several revivals of the original symmetry. As is evident from Figure 2.8(a), the $LN_{10}(p = 1)$ mode is furthermore part of the same general family of quadrupole solitons and realized for $\alpha = \pi/4$. The beam undergoes irregular dynamics in which neither of the disparate symmetries is distinguishable. It should be noted that at lower beam powers this particular structure, i.e., the $LN_{02}(p = 0)$ (or HN_{11}) evolves into four optical splinters which fly off diagonally due to a mutual repulsion of the out-of-phase petals [see Figure 2.8(a)].

In the following the intriguing quasi-periodic dynamics with soliton revivals and mode transformations are described in more detail. First, the transformation of the radially symmetric $LN_{10}(p = 1)$ soliton into the structure resembling $LN_{02}(p = 0)$ (or HN_{11}) quadrupole [see column (c) of Figure 2.6] is considered.

The corresponding $(\mathcal{H}, P)$ diagram in Figure 2.6(a) features crossing of these two modes, and also indicates that the single-ring fundamental soliton $LN_{10}(p = 1)$ exists always within the band of the quadrupole mode $LN_{02}(p = 0)$. This strongly points to the fact that energy crossing of the two states is responsible for the mutual transformation of these two modes observed in Ref. [135].

As the next step, the propagation of the quadrupole soliton in Figure 2.6(d) is simulated and subsequently remarkable similarities between the two are observed; the latter includes periodic transformations to the $LN_{10}(p = 1)$ as well as revivals.

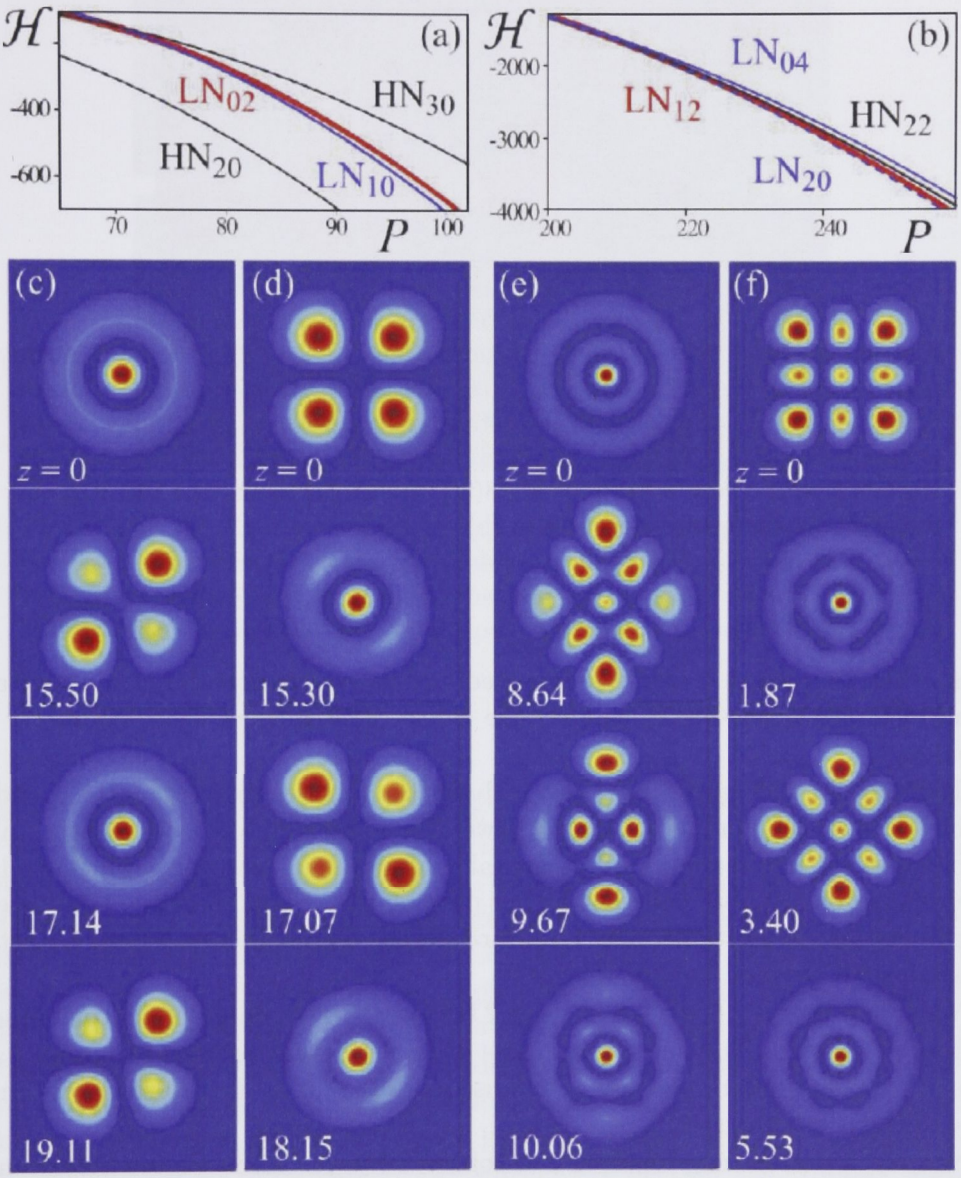

Figure 2.6: (a,b) Energy crossings chosen from the overlapping of two $(\mathcal{H}, P)$ diagrams in Figures 2.2(a) and 2.2 (b). Examples of the propagation dynamics of (c) $\mathrm{LN}_{10}(p = 1)$ soliton with $P = 100$, (d) HN_{11} (quadrupole, same as $\mathrm{LN}_{02}(p = 0)$) with $P = 75$, (e) $\mathrm{LN}_{20}(p = 1)$ with $P = 250$, and (f) HN_{22} with $P = 210$.

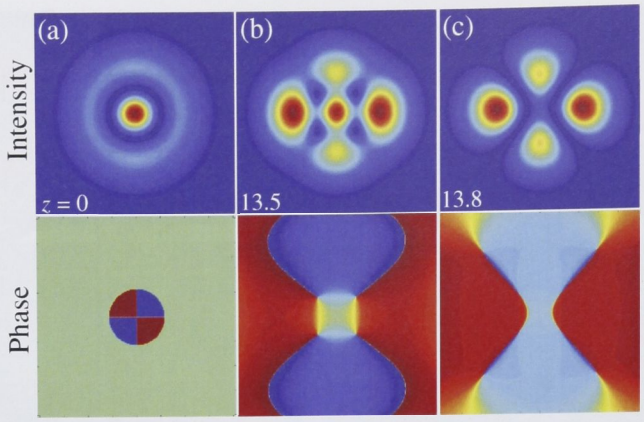

Figure 2.7: Evolution of the LN_{10} mode when $p = 1$. Propagation yields nontrivial transformations into the structure resembling the $LN_{02}(p = 0)$ (or HN_{11}) mode through intermediate states forming the entire family of the generalized GN_{11} mode. Depicted here is the intermediate state resembling the GN_{11} with $\alpha = \pi/8$ [see Figure 2.8(a)], note in particular the four vortices embedded in the phase structure in (b).

Thus, when two states cross, it is expected and indeed observed that mutual transformations of solitons occur, despite the sharp differences of their symmetry and stability.

The diagram in Figure 2.6(a) also includes the four-soliton matrix HN_{30} and the tripole HN_{20} [115]. In the region of powers in Figure 2.6(a), both soliton matrices disintegrate into repelling fundamental solitons; thus, transformations involving other states are not observed. For higher powers, the soliton matrices become energetically isolated and stable; note however that the tripole was shown to be unstable in media with thermal nonlinearity [124].

Next, in Figures 2.6(b), 2.6(e), and 2.6(f) another example of soliton transformations are shown. The energy diagrams of four different solitons in Figure 2.6(b) remain very close after crossing, and consequently, mutual transformations among three of them are observed.

Namely, a double-ring fundamental soliton $LN_{20}(p = 1)$ in Figure 2.6(e) undergoes complex dynamics where periodic appearance of $LN_{12}(p = 0)$ and HN_{22} states were clearly identified, followed by soliton revival. Similarly, the 3×3 soliton matrix HN_{22} in Figure 2.6(f) transforms quasi-periodically to $LN_{20}(p = 1)$ mode. Note that similarly to the $LN_{02}(p = 0)$ (or HN_{11}) and $LN_{10}(p = 1)$ which were particular realizations of the limiting values of parameter α within a general family of solitons, the modes $LN_{20}(p = 1)$ and HN_{22} also belong to the same general family of solitons [see Figure 2.8(b)].

Interestingly, the appearance of the eight-soliton necklace $LN_{04}(p = 0)$ was never observed, while its transformation to the matrix HN_{22} takes place (e.g., for $P = 220$, not shown), before it became stable at $P = 250$ [see Figure 2.4(b)]. Note also that

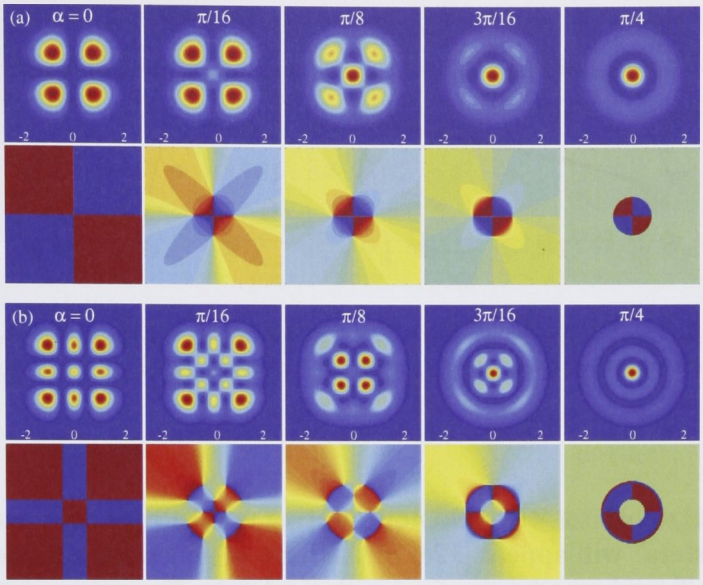

Figure 2.8: (a) Family of the quadrupole-like solitons for power $P = 200$ versus α. The colors for intensity (middle row) are mapped from zero (blue) to maximal value (red), while phase (bottom row) is scaled from $-\pi$ to π. (b) Family of the generalized 3×3 multipole solitons for power $P = 200$ versus α.

crossed states appear largely distorted by their internal vibrations. This observation suggests that overlapping of soliton internal modes, in addition to crossing of stationary states, must determine mutual soliton transformations.

The intriguing soliton coexistence can be better understood in terms of the so-called generalized Hermite-Laguerre-Gaussian $\mathrm{HLG}_{nm}(x, y; \alpha)$ modes in linear media [128]. Similar to column (a) in Figure 2.6, in Figure 2.7 the evolution of the fundamental single-ring soliton $\mathrm{LN}_{10}(p = 1)$ is shown, only this time showing an intermediate state resembling a HLG mode and it is immediately evident that such states consist of highly complicated structures with several vortices embedded in their phase structures, although keeping the net topological index constant, i.e., a zero charge and hence zero angular momentum [see Section 2.3]. Indeed, above in Figure 2.6 for all cases the transformations between states with zero vorticity and zero angular momentum were considered as the simplest examples.

It should be expected that, similar to the LN and HN solitons, there is a greater variety of nonlinear states parameterized by some structural parameter, such as the modulational parameter p for the LN-solitons. Indeed, while the ansatz $\sim \cos m\varphi + \mathrm{i}p \sin m\varphi$ [100] represents exactly the HLG_{nm} modal beam for $n = 0$ and $m = 1$ [128], it is no longer the case for higher-order HLG modes. Such higher-order modes promise to yield a wealth of interesting phenomena, e.g., through the important continuation $M > 0$ for HN solitons, which is offered by HLG modes with astigmatic transformations through the parameter α.

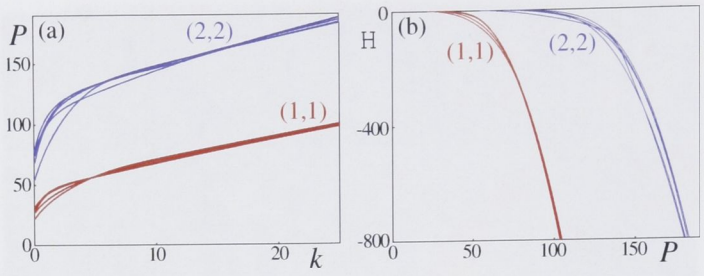

Figure 2.9: (a) Power vs. k for $\alpha = 0$; $\pi/16$; $\pi/8$; $3\pi/16$ and $\pi/4$, different families are denoted by indices next to the curves. (b) Hamiltonian vs. P.

Consequently both rotating and non-rotating novel states with multiple vortices, or "vortex clusters" will appear [128] in the form of generalized higher order beams [see Section 2.3] and quasi-periodic topological transformations within such self-localized beams bring many novel exciting phenomena.

Two sets of modes, namely the LG and HG beams, appear as two particular realizations of the HLG family, attained for the limiting values of the parameter α. Then, the idea of such generalization is that for the intermediate values of α, $0 \leq \alpha \leq \pi/4$ [128], any HLG beam also represents a self-similar and structurally stable solution.

2.3 Generalized nonlocal solitons

In this section the generalized family of HLG modes are employed, which realize, in a simple way, a continuous transformation between the HG and LG self-trapped modes through a single parameter α. More specifically, the two symmetries are recovered for the limiting values of this parameter, namely $\alpha = 0$ and $\alpha = \pi/4$ [128], i.e.,

$$\mathrm{HLG}_n(x, y; \alpha = 0) = (-\mathrm{i})^m \mathrm{HG}_{nm} \tag{2.8}$$

and

$$\mathrm{HLG}_{nm}(x, y; \alpha = \pi/4) = \begin{cases} (-1)^m 2^n m! \mathrm{LG}_{m(n-m)}(x, y) & (n \geq m) \\ (-1)^n 2^m n! \mathrm{LG}_{n(m-n)}(x, -y) & (n \leq m) \end{cases} \tag{2.9}$$

with all intermediate states remaining structurally stable.

Similarly to the variational approach in Section 2.2, higher-order solitons are constructed, that extend the HLG linear modes to the case of nonlinear media with the Gaussian nonlocal response. By introducing variational parameters in the form of soliton amplitude A, and soliton widths $a_{x,y}$ and $b_{x,y}$ respectively and varying α, rather complex beam profiles with several vortices embedded in their phase structure can be obtained, which in continuation of Section 2.3 enables the formation of soliton "matrices" with nonzero angular momentum.

Specifically, by considering stationary states of the form $E(x,y,z;\alpha) = U(x,y;\alpha)\exp(ikz)$, the envelopes $U_{nm}(x,y;\alpha)$ corresponding to the $\mathrm{HLG}_{nm}(x,y;\alpha)$ modes take the form,

$$\begin{aligned} U_{nm}(x,y;\alpha) = \; & A\exp(-x^2/2a_x^2 - y^2/2a_y^2) \\ & \times \sum_{j=0}^{n+m} C_{nm}^{j}(\alpha)\; H_{n+m-j}(x/b_x)\; H_j(y/b_y) \end{aligned} \tag{2.10}$$

where A is the soliton amplitude, H_j are Hermite polynomials and the coefficients $C_{nm}^{j}(a)$ are expressed in terms of Jacobi polynomials $P_j^{\mu,\nu}$ [128]:

$$C_{nm}^{j}(a) = \mathrm{i}^j \cos^{n-j}\alpha \sin^{m-j}\alpha P_j^{(n-j,m-j)}(-\cos 2\alpha). \tag{2.11}$$

Approximate stationary solutions are obtained using a standard variational derivation with the ansatz given by Eq. (2.10).

As the simplest example of nonrotating generalized beams the families of the generalized quadrupole and 3×3 matrix solitons are shown in Figure 2.8. According to Eq. (2.10) varying α allows for the continuous deformation from the pure quadrupole through intermediate states to a radially symmetric soliton,

$$\begin{aligned} U_{11}(x,y;\alpha) = \; & A\exp(-(x^2+y^2)/2a^2) \\ & \times \left[\left(x^2+y^2-b^2\right)\sin 2\alpha - 2\mathrm{i}xy\cos 2\alpha\right]/b^2, \end{aligned} \tag{2.12}$$

where $a \equiv a_{x,y}$ and $b \equiv b_{x,y}$.

Variational solutions for various values of a and k are obtained numerically to construct the family of the generalized quadrupole. At $\alpha = 0$ the structure of the beam takes the form of a 2×2 soliton matrix i.e. a square geometry formed by 4 peaks separated by zeros of intensity and a relatively simple phase structure, [see Figure 2.8(a)]. At intermediate values of α the profiles become more complex, note in particular in the figure the appearance of 4 separate vortices embedded in the phase distributions. The total topological index, and hence the angular momentum, however remains zero for all $0 \le \alpha \le \pi/4$ due to exact canceling of the topological indices of the individual vortices. At $\alpha = \pi/4$ a radially symmetric necklace mode emerges.

The family of the generalized 3×3 matrix GN_{22} is presented in Figure 2.8(b). The expressions for the GN_{22} are too cumbersome to be shown here, nevertheless by numerically deriving variational solutions, in Figure 2.8(b) beam profiles and their pertaining phase distributions are depicted.

Here the beam profiles range from a pure 3×3 matrix, i.e., the HN_{22} mode with zero topological charge consisting of 9 out-of-phase spots, through complex profiles with no less than 12 separate vortices embedded in the phase distributions and zero net topological charge. Finally, at $\alpha = \pi/4$ a triple ring beam appears corresponding to the $\mathrm{LN}_{20}(p=1)$ mode.

As with the HN and LN states, in Figure 2.9 several energy bands of $P(k)$ and $\mathcal{H}(P)$ formed by the two soliton families are shown and it clearly demonstrates how

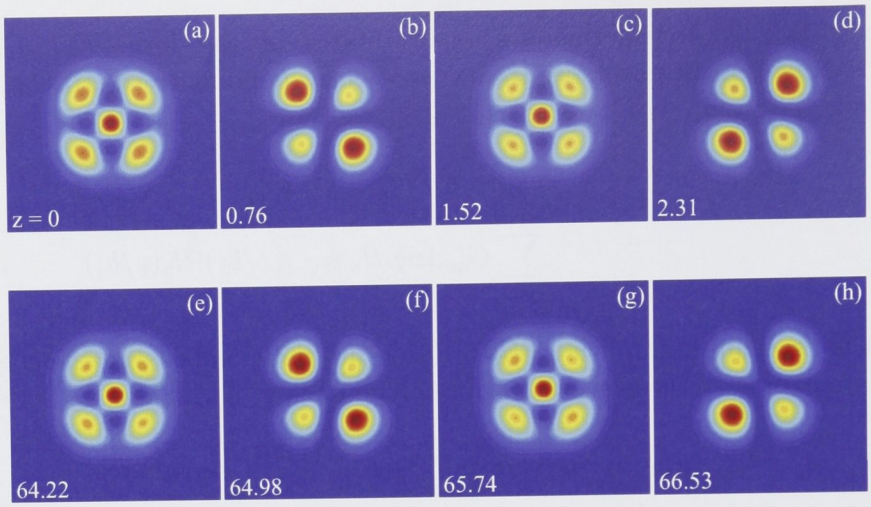

Figure 2.10: Quasi-periodic breather-like propagation of the $GN_{11}(x, y; \pi/8)$ mode with power $P = 200$. Note the large propagation distances in (e)–(h).

the energies for various values of α within the families GN_{11} and GN_{22} apparently cross and even coincide. Since propagation of both $GN_{11}(\alpha > 0)$ and $GN_{22}(\alpha > 0)$ (the latter not shown) involve transitions between disparate symmetries it strongly suggests that this coexistence determines the evolution of the solitons, and occupancy of different modes and the density of states can be directly related to the propagation dynamics displayed by the beams occupying the various energy bands.

2.4 Transformation dynamics

In the following, the propagation of the generalized quadrupole solitons GN_{11} is studied in detail. As before direct simulation of the beam propagation is performed with the fast-Fourier-transform splitstep algorithm, using the variational solutions from Section 2.3 as input profiles. Varying both α and power P numerous simulations are executed to investigate the dynamics and stability properties of these higher-order generalized beams.

As expected, at low P corresponding to the local limit, it is observed that the solitons become unstable and eventually they break. At higher power this scenario changes dramatically and the beams are found to evolve in various distinctive ways depending on α. In sharp contrast to the $GN_{11}(x, y; 0)$ mode which simply becomes stable at a certain power threshold, [see Figure 2.11] at all other values of α the beam dynamics become quasi-periodic and breather-like i.e., the solitons continuously experience nontrivial transformations and revivals over large propagation distances. Note the theoretical results regarding breather-like behavior in nonlocal thermal media [130] and in nonlinear media with a nonlocal Gaussian response [89, 136].

Quasi-periodic behavior of the intermediate states (i.e., $\alpha = \pi/16, \pi/8$, and

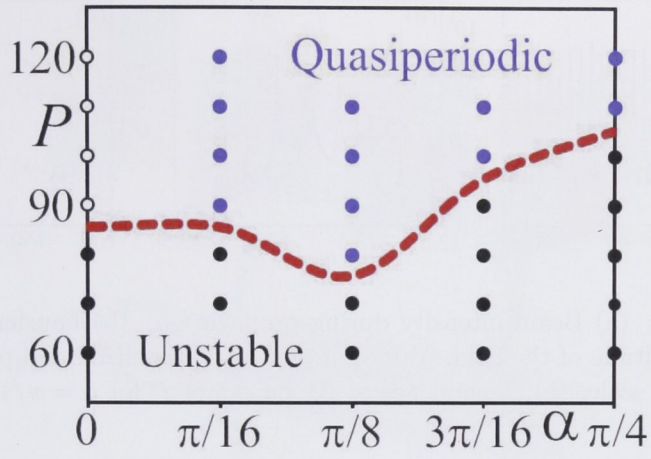

Figure 2.11: Stability domain in the parameter plane (α, P). Circles denote stable propagation while black and blue dots signify unstable and quasi-periodic propagation respectively.

$3\pi/16$) deviate significantly from the dynamics displayed by the $\mathrm{GN}_{11}(x, y; \pi/4)$ mode. This is manifested by the fact that the intermediate modes initiate the transformations immediately upon launching, in clear contrast to the $\mathrm{GN}_{11}(x, y; \pi/4)$ mode which appears to be structurally stable before undergoing any transformations. An example of quasi-periodic propagation is shown in Figure 2.10. Note the large propagation distances in Figures 2.10(e)– 2.10(h), it should be stressed here that the dynamics at intermediate distances, i.e., $2.31 < z < 64.22$ are identical to those displayed in the figure.

Depicted here is the evolution of the $\mathrm{GN}_{11}(x, y; \pi/8)$ at power $P = 200$ over several hundred soliton periods $\sim \pi/k$, and from the figure emphasis is given to two major observations. It should be noted here that the dynamics mentioned below are generic and indeed observed for all intermediate values of α. First, the propagation includes periodic transformations into the structure resembling the quadrupole $\mathrm{GN}_{11}(x, y; 0)$ followed by revivals of the initial structure. Interestingly however, transformations "the other way" i.e., into the radially symmetric $\mathrm{GN}_{11}(x, y; \pi/4)$ are never observed. Second, although the transformations seem reasonably regular at first sight, by closer inspection it becomes evident that the reappearances of identical quadrupole structures occur only at every other transformation due to the beating of two similar internal modes.

In Figure 2.11 the stability domain for the GN_{11} mode is shown in the plane (α, P), and here blue dots denote quasi-periodic behavior whereas circles mean stable propagation. Note that here the power threshold attains its maximum for $\alpha = \pi/4$.

The periodicity with which identical quadrupoles appear becomes important when the dynamics of the beams is further studied in detail. This is done by obtaining values of the field amplitude at each propagation step and in Figure 2.12(a)

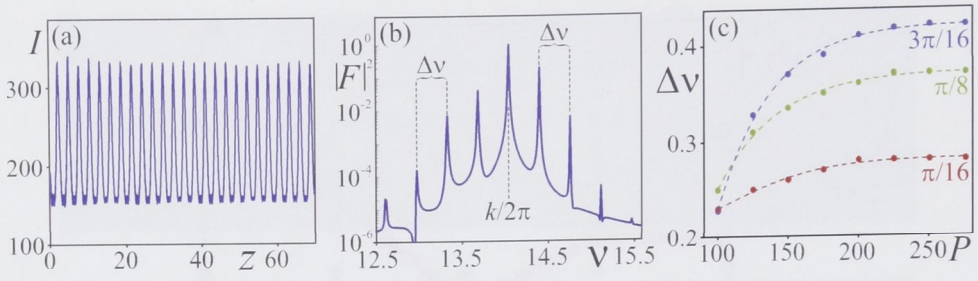

Figure 2.12: (a) Beam intensity during propagation. (b) Fourier transform of the amplitude of the field. Values of $|F|^2$ are normalized and plotted on a logarithmic scale. (c) Dependence of $\Delta\nu$ on power P for $\alpha = \pi/16, \pi/8$, and $3\pi/16$.

the resulting intensity I vs. propagation distance z is plotted.

This clearly shows how the intensity of the beam strongly oscillates during propagation and it should be stressed here that each of these oscillations corresponds to a transformation between different states. More specifically it is observed that minima and maxima correspond to the occurrences of the two different quadrupole structures respectively.

In the following, a Fourier transform of the field amplitude is performed which enables to obtain the frequency spectrum shown in Figure 2.12(b). Here the central frequency corresponds to the propagation constant k or rather $k/2\pi$ and neighboring peaks are shifted equidistantly on either side of $k/2\pi$. This shift denoted by $\Delta\nu$, is exactly the frequency with which the mutual transformations between the initial state and similar quadrupole structures occur.

Performing extensive numerical simulations of the beam propagation at various powers allows to examine the dependence of $\Delta\nu$ on P for the different values of α. The results are shown in Figure 2.12(c) in the parameter domain (P, α). Interestingly it is thus demonstrated that the shift $\Delta\nu$ increases monotonically with P, however at higher powers, the increase slows down significantly, indicating that at sufficiently high power it will eventually saturate and reach a certain maximum. Moreover, note that $\Delta\nu$ increases with α so it follows that stronger modulations of the quadrupole structure i.e. increasing α effectively slow down the transformations.

Describing and subsequently predicting analytically the dependence of $\Delta\nu$ on power presents an intriguing problem and promises to bring exciting novel physics, however for the time being the question remains unchallenged. Intriguingly, complex deformations of the $\mathrm{GN}_{11}(x, y; 0 < \alpha \leq \pi/4)$ beams involve intricate topological reactions within the beams in which pairs of vortices with opposite topological indices are created and annihilated. As a result the total topological index and hence zero angular momentum is conserved during propagation. In Figure 2.13 the phase distributions corresponding to the intensity profiles at the various propagation distances in Figures 2.10(a)– 2.10(d) are shown.

The spatial locations of the vortices have been traced and the resulting nodal

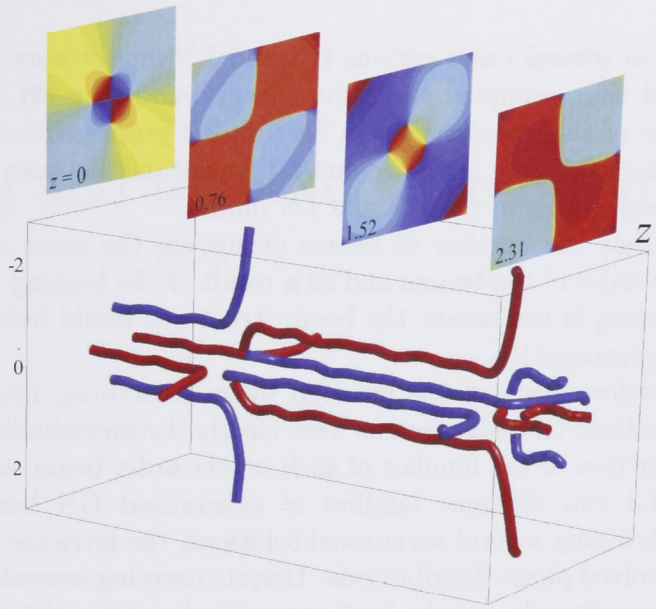

Figure 2.13: (top) Phase distributions at various propagation distances. (bottom) Trajectories of the four vortices embedded in the phase distribution. Blue line carry topological index -1, while red line has index 1.

lines (blue and red) of opposite topological index, i.e., -1 and 1 respectively, thus depict the vortex trajectories during propagation. From the respective phase structures it becomes even more evident that the transformations indeed involve beating of two distinct quadrupole-like modes, which in addition give rise to the continuous shift in topological indices of the four nodal lines.

2.5 Summary

In summary, by employing a set of linear optical HG, LG and HLG waveguide modes several higher-order spatial solitons in nonlocal nonlinear media have been constructed in the form of soliton necklaces, matrices as well as more complex structures.

In the first part of the chapter various beam structures were identified as Hermite-nonlocal HN and Laguerre-nonlocal LN beams, reminiscent of their linear counterparts, however with the additional variational parameters, namely soliton amplitude A and width a. For the LN modes an additional parameter was necessary to completely characterize the full soliton family consisting of various beam structures and in particular a so-called modulation parameter p defined the depth of the azimuthal modulation of the necklace-type LN modes. In a few cases the variational solutions have served as input for further use in numerical relaxation method, which revealed that the variational solutions in general provided a reasonable good

approximation.

Surprisingly, in several cases various HN and LN modes were found to coexist energetically and they occupied the same energy band in a $(\mathcal{H}, \mathcal{P})$ diagram and as a consequence of this coexistence, in Section 2.2 propagation dynamics in numerous cases entailed highly complex mutual transitions between disparate beam symmetries corresponding to the HN and LN modes.

It appeared that the number of beams occupying the same energy-bands increased with the order of the beams and as a result of the beating of various different modes coexisting in the bands, the beam structures would become increasingly distorted during propagation.

Despite the deformation of the involved beam structures, intermediate states resembling generalized Gaussian beams were clearly distinguishable and that motivated the introduction of the families of such higher-order beam structures.

In Section 2.3 two different families of generalized GN beams were introduced and, by obtaining several variational solutions, the intricate beam structures emerged with involved phase distributions. Despite carrying several vortices in their phases both the quadrupole and the 3×3 generalized matrix solitons exhibited zero net topological charge for all values of α.

As the simplest nonrotating case the propagation dynamics of the generalized quadrupole solitons was studied. It was demonstrated that members of the quadrupole family exhibited quasi-periodic dynamics in which the periodicity of the breather-like behavior resulted in a frequency shift $\Delta\nu$ which matched the frequency with which identical symmetries emerged and that $\Delta\nu$ increased monotonically with P.

Especially important now will be to investigate cases where $M > 0$ and the dynamics are expected to involve both beam transformations [100, 135, 137] as well as beam spiraling [101] depending on both the particular beam topology as well as beam power. Therefore, as the next step, in Chapter 3, the various variational solutions corresponding to the generalized tripole GN_{20} and the 3×2 matrix GN_{21} will be considered.

CHAPTER 3

Spiraling and topological transformations

3.1 Introduction

Nonlocal optical media and nonlocal optical solitons have received and continue to receive a great deal of attention, which is partly due to their large potential applications in photonic switches [79], all-optical switching and logic gating [138], and all-optical signal processing [139]. In addition, complex transformations between disparate higher-order beam structures [100, 135, 137] represent dynamics which, on one hand, are restricted to nonlocal media and, on the other hand, are of broad interest as they are similar to the astigmatic transformations [128] and may be useful for optical mode converters.

The importance of implementing nonlocal nonlinear media is further emphasized by the fact that such media have paved the way for interesting physics e.g., formations of multi-soliton bound states and stabilization of both single- and multi-charged vortex solitons as well as the more involved vortex carrying beams, e.g., azimuthons [64, 100, 101] and generalized Hermite-Laguerre-Gaussian (HLG) beams [see Section 2.3].

Evidently, nonlocal nonlinear optics possesses a wealth of possibilities of profound interest both from a practical and a more fundamental point of view. Practical because recent studies point to the applicability in desirable all-optical components and fundamental due to the great variety of intriguing physics yet to be uncovered. The aim of this chapter is mainly stimulated by the latter, namely to explore novel propagation dynamics which furthermore promise to lead to the observation and demonstration of highly exciting new aspects of nonlocal optical soliton phenomena.

In continuation of the preceding chapter the following study, which is based on a set of higher-order GN solitons with nonzero angular momentum, involves direct simulations of the governing equation and by varying different beam parameters such as power P and modulation variable α different stability scenarios can be thoroughly investigated by considering beam propagation over hundreds of soliton

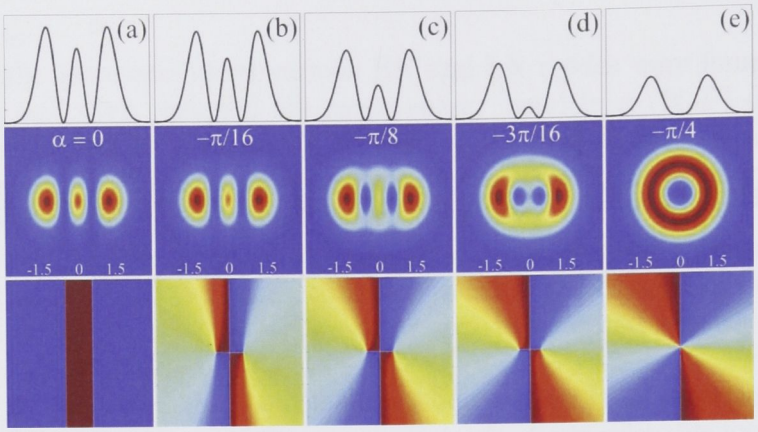

Figure 3.1: Family of the tripole-like solitons for power $P = 200$ versus α. The cross sections of the beam profiles are shown in the top row. The colors for intensity (middle row) are mapped from zero (blue) to maximal value (red), while phase (bottom row) is scaled from $-\pi$ to π.

periods $\sim \pi/k$.

Specifically, the numerical studies involve the generalized tripole and 3×2 matrix solitons and since both the tripole-like beams as well as the 3×2 matrices have a net nonzero topological charge and therefore a nonzero angular momentum the beams rotate during propagation.

Several types of propagation dynamics depending on the beam power are uncovered. At low power all solitons are unstable but at some power threshold the beams either exhibit stable rotation of the beam as a whole or undergo rather complex transformation dynamics accompanied by spiraling of the beam structure.

Indeed, above a certain power or equivalent degree of nonlocality, the generalized tripole soliton exhibits stable propagation accompanied by spiraling of the beam for all $0 < \alpha \leq \pi/4$, and intricate topological reactions leading to the formation of vortex links are observed.

Finally, recall in [100] the evolution of the double ring single charge soliton which was found to include both rotation and mutual transformations into a 3×2 matrix soliton. Hence the family of the generalized 3×2 matrix soliton is introduced, which give rise to nontrivial transformations accompanied by spiraling of the beams as well as formations of complex topological distributions such as vortex knots.

In order to fully appreciate the underlying physics of these intriguing phenomena of nodal line formations, in the last section the propagation of the fundamental soliton in a local nonlinear saturable medium is considered. It is revealed that small oscillations of the beam during propagation give rise to vortex loops surrounding the beam waist at nearly equidistant intervals. In addition, the intervals decrease with beam power, i.e., the number of loops increases and in some cases, the regularity and smoothness of the vortex loops increase with the amplitude of the oscillations.

By perturbing the fundamental soliton and imposing a more complicated phase

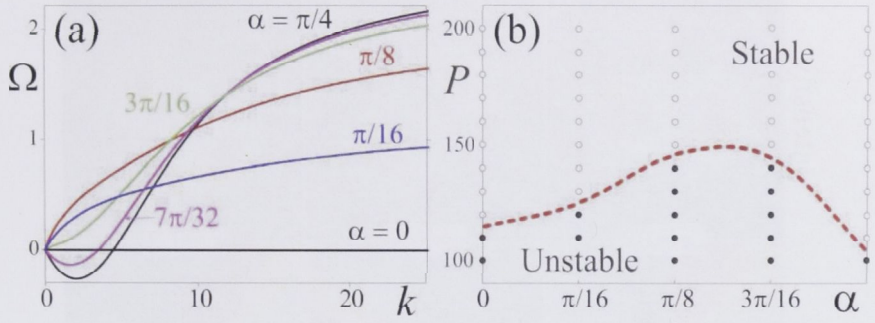

Figure 3.2: (a) Rotation velocity Eq. (3.2) of the tripole solitons. (b) Stability domain in the parameter plane (α, P).

structure as compared to the flat phase front of the fundamental, the beam attains an asymmetric shape and an angular momentum, and these two attributes combined can then trigger the formations of both vortex links and knots.

3.2 Spiraling of self-trapped optical vortices

As the first specific example, in this section a tripole-like mode soliton GN_{20} with nonzero angular momentum is considered. Through numerous simulations involving different beam powers as well as values of α, stable spatial rotation (spiraling) of the tripole soliton carrying two optical vortices of the same charge is observed.

The tripole soliton, i.e., a structure consisting of 3 in-line peaks separated by the zeros of intensity [see Figure 3.1(a)], corresponds to the mode $U_{20}(x, y; \alpha = 0)$ and, according to Eq. (2.10), it can be deformed continuously to a double-charge vortex beam

$$\begin{aligned} U_{20}(x, y; \alpha) = \; & A \exp(-(x^2 + y^2)/2a^2) \\ & \times [4(x \cos\alpha + iy \sin\alpha)^2/b^2 - \cos 2\alpha]. \end{aligned} \tag{3.1}$$

Note that a complex conjugation or, alternatively, reflection $\alpha \to -\alpha$, simply produces a vortex of the opposite charge.

Varying α is equivalent to the astigmatic transformation from the HN_{20} to $LN_{02}(p = 1)$ mode [128] and by numerically obtaining variational parameters for different values of α and k, soliton families as shown in the example of Figure 3.1 are constructed. For $\alpha = 0$ the solution has a relatively simple phase structure of the HN_{20}, i.e., a 3×1 matrix soliton of zero vorticity. More general tripole-like structures appear at the intermediate values of α and for all values the topological index remains constant. Here Figures 3.1(b)– 3.1(d) clearly show two separate vortices with the same topological charge embedded into the beam, which give rise to a nonzero angular momentum M. At $\alpha = \pi/4$ these vortices merge to form a double-charge vortex ring $LN_{02}(p = 1)$.

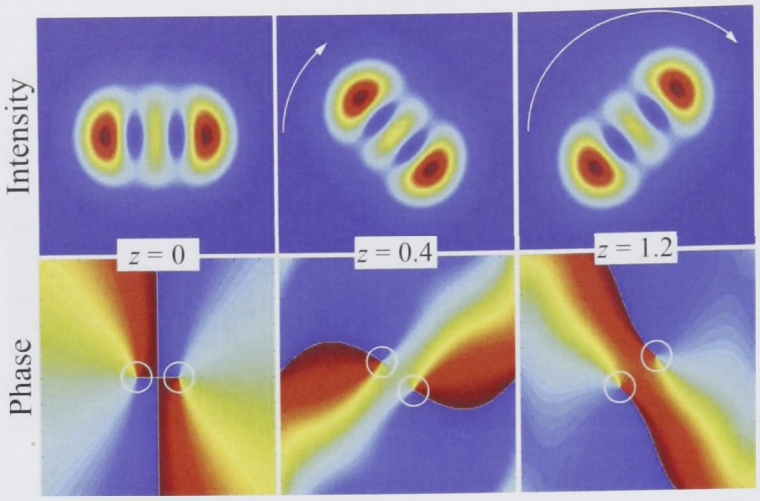

Figure 3.3: Propagation dynamics of the tripole with $\alpha = -\pi/8$, $k = 89.4$, and $P = 200$. The corresponding variational solution predicts $\Omega = 1.89$, which corresponds to the period of rotation (pitch) $\simeq 3.33$; the numerically obtained values are very close, pitch 3.03 and $\Omega \simeq 2.07$.

As the next step, the variational solutions act as an input for direct simulations of Eq. (1.22) using the fast-Fourier-transform split-step beam propagation algorithm. By performing extensive numerical simulations to study the dynamics and stability properties of the tripole soliton family, spiraling of tripole beams with nonzero angular momentum $\alpha \neq 0$ is observed. Surprisingly, this behavior is in sharp contrast with the dynamics of the corresponding linear modes, which do not rotate [128].

To resolve this controversy, an approach developed by Rozanov [140] is employed, which enables finding the rotation velocity Ω of localized beams, provided the solutions of the original propagation equation are known. So in the following, theoretical analysis allows for an estimation of the rotation velocity, i.e., the pitch of a helix formed by the braided vortex lines, and to reveal the underlying physical mechanism responsible for this spiraling effect.

By using the variational solutions, Ω can be represented as a sum of the linear Ω_{ln} and nonlinear Ω_{nln} parts,

$$\Omega = \Omega_{ln} + A^2 \Omega_{nln}, \tag{3.2}$$

where $\Omega_{ln} = \gamma \sin 2\alpha (8a^4 - 6a^2b^2 + b^4)$ and A is soliton amplitude. The expressions for $\Omega_{nln}(a, b; \alpha)$ and $\gamma(a, b; \alpha) > 0$ are too cumbersome to be shown here; note that inverting the sign of α reflects $\Omega \to -\Omega$. Importantly, in the limit $b \to a\sqrt{2}$, i.e., when $\mathrm{GN}(x, y; \alpha)$ is exactly an eigenmode of the linear equation, Ω_{ln} vanishes, as expected in accordance with [128]. Hence, it is precisely the deformation $b \neq a\sqrt{2}$ that initiates the rotation of the beam even in free propagation. Indeed, such deformed beams can be seen as a superposition of several GN modes, and the rotation appears as a beating between the modes. However, such beams always

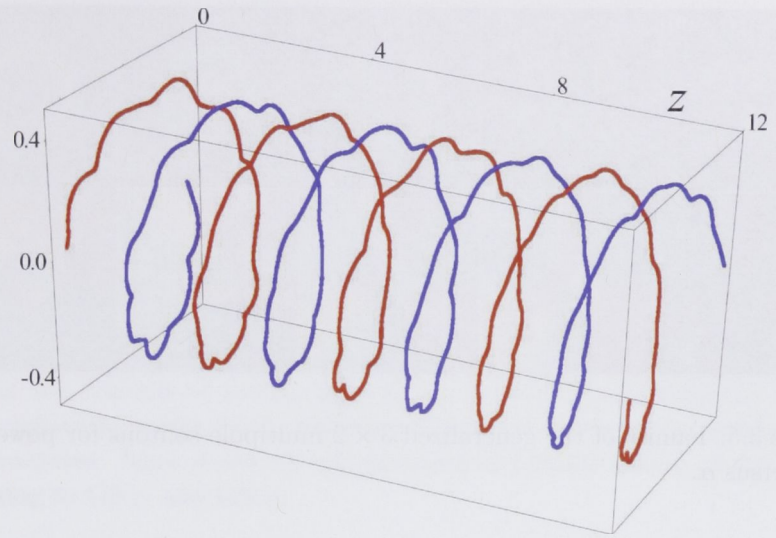

Figure 3.4: Double helix formed by the braided nodal lines obtained by tracing the spatial locations of the vortex cores during propagation in Figure 3.3.

rotate in nonlinear media because the nonlinear component Ω_{nln} does not vanish even for the linear modes with $b = a\sqrt{2}$. Note the similar effect of the enhanced rotation of two dark vortices in defocusing media [141] with respect to their spiraling in free propagation [142].

Using Eq. (3.2) and the variational solutions for A, a, and b, Ω can be calculated for different tripole solitons in the parameter domain (k, α) [see Figure 3.2(a)].

Surprisingly, for positive angular momentum $\alpha \geq 0$, negative angular velocity for small k and $\alpha > \pi/5$ is obtained. However, at such small values of k (and low power $P = \int |E|^2 \mathrm{d}\mathbf{r}$) the tripole beams are unstable and, similar to the case of local media, they break up into several fundamental solitons [see Figure 2.5(a) corresponding to the case where $\alpha = \pi/4$].

Since the approximate soliton profiles differ from the exact stationary solutions, the beams oscillate during their propagation, facilitating their break up at low powers. In contrast, for the powers above a certain threshold the tripole beams become stable, surviving strong oscillations over several hundreds of the soliton periods π/k. In Figure 3.2(b) the stability domain in the plane (α, P) is shown. In contrast with the case of rotating nonlocal dipole [100], where the stability threshold monotonically increases with angular intensity modulation, here the threshold attains its maximum for $\pi/8 < \alpha < 3\pi/8$. In both cases (dipole and tripole), the power threshold attains its minimum for the radially symmetric vortex ring, $\alpha = \pi/4$.

Increasing power in the scaled system is equivalent to the transition to highly nonlocal regime, $\sigma \to \infty$, where, as discussed in Section 1.3, the nonlinear term in Eq. (1.22) can be reduced to an effective harmonic potential:

$$\int R(|\mathbf{r}' - \mathbf{r}|)|E(\mathbf{r}')|^2 \mathrm{d}\mathbf{r}' \to (1 - r^2/\sigma^2)P/\pi\sigma^2. \tag{3.3}$$

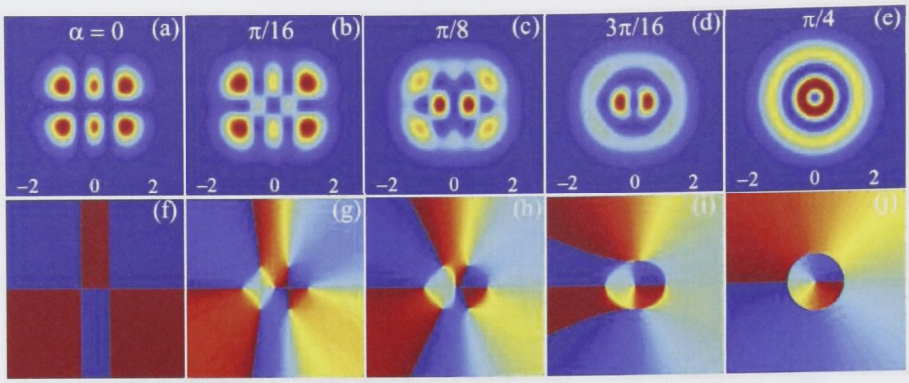

Figure 3.5: Family of the generalized 3×2 multipole solitons for power $P = 200$ versus α.

The governing equation [Eq. (1.22)] then becomes linear, and it has exact solutions in the form of stationary HLG modes [Eq. (3.1)] with $b = a\sqrt{2}$ and zero angular velocity, $\Omega = 0$. In good agreement with this transition, the full model predicts a very slow decrease of Ω at high powers and $k > 100$, not shown in Figure 3.2(a), i.e., solitons with larger "mass" P rotate slower.

To illustrate stable spiraling of the higher-order nonlocal beams, in Figure 3.3 the intensity and phase distributions of the tripole soliton with $\alpha = -\pi/8$ and $P = 200$ are shown. The direction of rotation is indicated by white arrows, while the spatial locations of two vortices embedded in the phase distribution are marked by white circles. Previous theoretical and experimental studies demonstrated unstable spiraling of bright solitons [32] and dark vortices [141], but this provides the first example of stable spiraling of self-trapped vortices in self-focusing nonlocal media. No mutual transformations between the different modes have been observed since such transitions are forbidden, which is partly due to the conservation of the angular momentum. In addition, as it is demonstrated in the next section, energy bands corresponding to the different tripole solitons never cross or coincide, and this has a great impact on the stability properties of the beams.

Tracing the spatial positions of the vortex cores, in Figure 3.4 it is possible to reconstruct a double helix formed by the braided nodal lines. Note that an analogous effect in free propagation in linear media can be observed by perturbing a specific superposition of nondiffracting Bessel beams with a plane wave [143].

In summary, tripole-like beams have been studied in nonlocal nonlinear media with a gaussian response. The propagation dynamics of the higher-order solitons carrying a pair of vortices have thus been analyzed in detail and the general approach developed here will be useful for analyzing other types of singular self-trapped beams, i.e., the beams with nonzero angular momentum carrying optical vortices that can describe knots and links of vortices [144] in nonlocal nonlinear media [see Section 3.4].

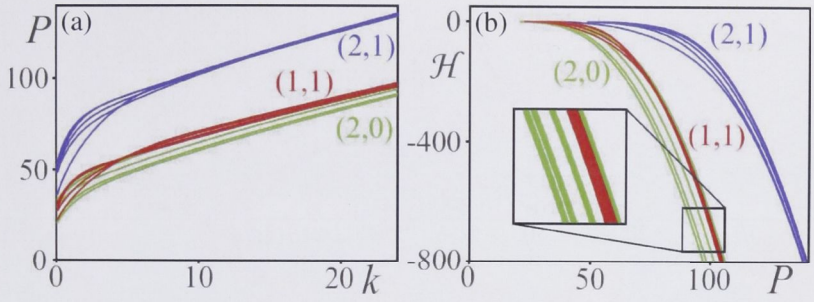

Figure 3.6: (a) Power P vs. k for $\alpha = 0, \pi/16, \pi/8, 3\pi/16$ and $\pi/4$, different families are denoted by indices next to the curves. (b) Hamiltonian vs. P. Bands belonging to the GN_{11} states are shown to emphasize the difference in the structures. Inset shows an enhancement of a small section of the bands belonging to GN_{11} and GN_{20}.

3.3 Spiraling accompanied by transformations

In the following the generalized 3×2 matrix solitons GN_{21} are considered. As before direct simulation of the beam propagation is performed with the fast-Fourier-transform splitstep algorithm, using variational solutions as input profiles. Again varying both α and power P numerous simulations are executed to investigate the dynamics and stability properties of these higher-order generalized beams.

The family of the generalized 3×2 multipole matrix consists of the U_{21} modes given by

$$\begin{aligned} U_{21}(x,y;\alpha) = &-2\,\mathrm{i}A\exp(-(x^2+y^2)/2a^2) \\ &\times\Big[y\left(b^2+x^2-y^2\right)\cos\alpha + y\left(-3b^2+3x^2+y^2\right)\cos 3\alpha \\ &+2\mathrm{i}x\left(-2b^2+x^2+y^2+\left(-3b^2+x^2+3y^2\right)\cos 2\alpha\right)\sin\alpha\Big]/b^3. \end{aligned} \tag{3.4}$$

Using Eq. (3.4) and varying α from 0 to $\pi/4$ produces the astigmatic transformation from the 3×2 matrix to a double ring single charge necklace mode, [see Figure 3.5]. Recall that this transformation was observed numerically, by investigating the instability-induced evolution of a perturbed double-ring single-charge vortex soliton [100].

By numerically deriving variational solutions, the resulting beam profiles and their pertaining phase distributions are shown in Figures 3.5(a)– 3.5(j). This reveals a deformation from the pure 3×2 matrix with zero topological charge through highly complex profiles, note in particular the 7 separate vortices enclosed in the phase distributions. Finally, at $\alpha = \pi/4$ a single charge double vortex ring emerge. Note also that a total topological index of 1 is conserved for all $0 < \alpha \leq \pi/4$. Due to a nonzero angular momentum resulting from a nonzero topological index, in [100] it was demonstrated that the beams rotate during propagation.

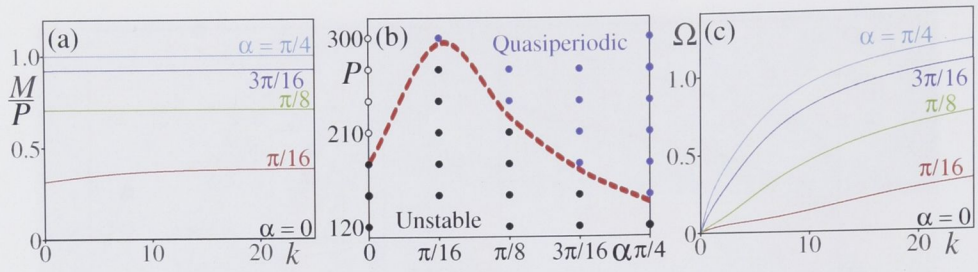

Figure 3.7: (a) Ratio of Angular momentum M and power P vs. k of various $\mathrm{GN}_{21}(x, y; \alpha)$. (b) Stability domain in the parameter plane (α, P). Circles denote stable propagation while black and blue dots signify unstable and quasi-periodic propagation respectively. (c) Angular velocity Ω of $\mathrm{GN}_{21}(x, y; \alpha)$.

Next, direct simulations of Eq. (1.22) are carried out and they reveal several different phenomena. In spite of substantial differences in structure, propagation dynamics and stability scenarios of the $\mathrm{GN}_{21}(x, y; \alpha)$ modes are remarkably similar to those of the $\mathrm{GN}_{11}(x, y; \alpha)$, with the obvious deviations manifested by the rotation of the $\mathrm{GN}_{21}(x, y; 0 < a)$ and different power thresholds. Hence it is found that at low beam power, reminiscent of a local medium, the beams become unstable and break, where at higher power the propagation of the beams is significantly altered and become quasi-periodic for $0 < \alpha \leq \pi/4$. However, similarly to the pure quadrupole $\mathrm{GN}_{11}(x, y; 0)$ the pure 3×2 matrix soliton $\mathrm{GN}_{21}(x, y; 0)$ also becomes fully stable.

In Section 3.2 propagation of the generalized rotating tripole was studied and it was found that at a given power threshold the solitons became stable regardless of α. This dynamics is in sharp contrast with the dynamics reported here and this deviation becomes more evident by comparing the two diagrams in Figures 3.6(a) and 3.6(b). Here bands of $P(k)$ and $\mathcal{H}(P)$ formed by three soliton families are shown and it clearly demonstrates how the bands for different α of the generalized tripole i.e., GN_{20} never cross or coincide even for high powers, not shown here. Therefore due to the structure of the energy bands for various α transitions from one symmetry to another do not occur. In clear contrast different bands within the families GN_{11} and GN_{21} cross and even coincide, and the beams experience mutual transformations accordingly.

Interestingly, variational solutions for the GN_{21} at different values of α and k demonstrate that the ratio of angular momentum and beam power M/P increases with α, see Figure 3.7(a). Evidently however, this does not prevent mutual transformations between different states, and in addition simulations demonstrate that M/P is conserved throughout propagation, not shown here. The resulting stability domain in the (α, P) plane is shown in Figure 3.7(b), where, similar to the rotating dipole and tripole, the threshold reaches a minimum for $\alpha = \pi/4$.

Due to a nonzero angular momentum M for all $0 < \alpha \leq \pi/4$, nontrivial transformations of the $\mathrm{GN}_{21}(x, y; \alpha)$ are accompanied by spiraling of the beams. This is clearly demonstrated in Figure 3.8 which shows quasi-periodic propagation and

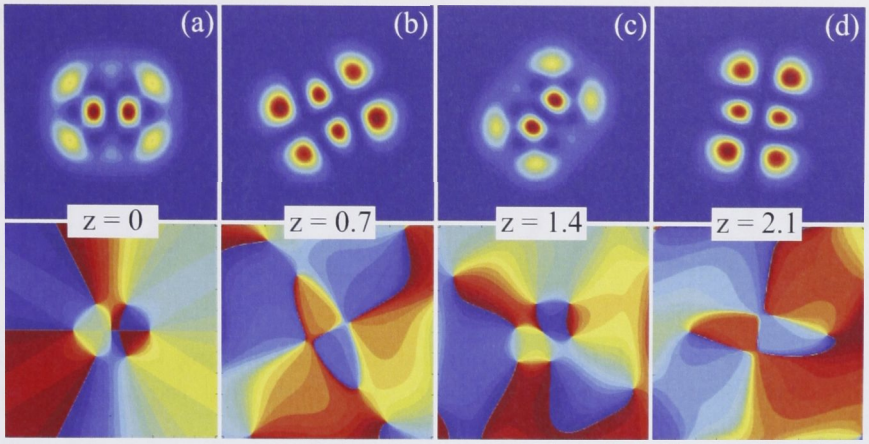

Figure 3.8: Quasi-periodic propagation accompanied with spiraling of the $\mathrm{GN}_{21}(x, y; \alpha = \pi/8)$ mode with power $P = 275$.

rotation of the $\mathrm{GN}_{21}(x, y; \pi/8)$ mode at $P = 275$. In other words since the beam is not structurally stable, at certain distances throughout propagation the beam transforms into a 3×2-like structure with subsequent revivals of the initial state. In fact, for all values of $\alpha > 0$ the beams evolve into the 3×2-like structure, whereas transitions into the circular symmetric mode $\mathrm{GN}_{21}(x, y; \pi/4)$ do not occur.

Note that for $0 < \alpha < \pi/4$ the beams initially consist of rather complex phase structures carrying seven distinguishable vortices and by tracing the spatial locations of the vortices a nodal thread is constructed. This structure is similar to the double helix obtained in Section 3.2, only this time with no less than seven nodal lines forming the thread.

To summarize the family of the generalized 3×2 multipole has been studied. Through extensive numerical investigations it was found that propagation of the generalized multipole soliton GN_{21} with $\alpha > 0$ involves both spiraling and quasi-periodic mutual transitions of different states. Given the complex structures, spiraling of the beams gives rise to twisted nodal threads formed by the self-trapped vortices embedded in the phase distributions.

3.4 Links and knots of vortices

In previous works [36] it was theoretically predicted and experimentally confirmed [144] that a specific superposition of optical beams in linear media led to formations of vortex links and knots. In addition these complex nodal line structures were threaded by braids of vortices consisting of two and three nodal lines respectively. Observing that, similarly to [144], the structure of the double helix in Section 3.2 traced out by the two vortices embedded in the phase of the tripole beams consists of exactly two braided nodal lines, the natural question is to ask if this results in the formation of vortex links in a nonlocal nonlinear medium.

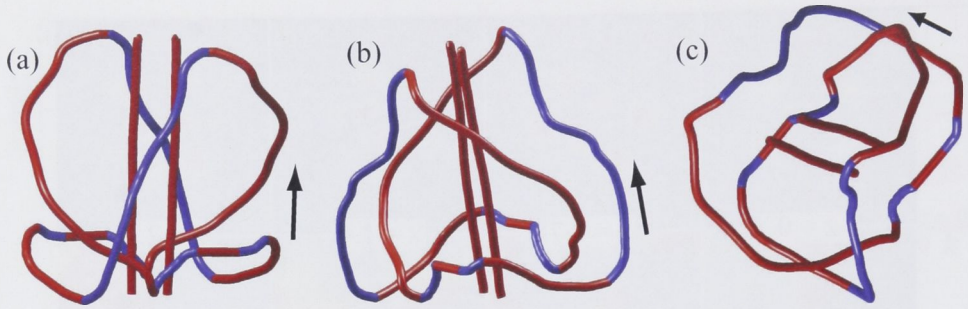

Figure 3.9: Vortex link formed by nodal lines surrounding the double helix braid. Arrows indicate propagation direction. Note that red and blue lines indicate topological index 1 and -1 respectively.

Therefore, recall the generalized family of the rotating tripole solition [see Section 3.2] which exhibited stable propagation over hundreds of soliton periods above a given power threshold. In Figure 3.1 the variationally obtained stationary solutions are depicted and except for the state with $\alpha = 0$ they all carry two vortices of the same charge in the phase distributions. Thus the propagation of these beams is accompanied by rotation as well as oscillation of the intensity profile.

In the following, the spatial locations of vortices are then traced in the entire computational window which extends well beyond the beam, and that enables to literally obtaining a forest of nodal lines weaving highly complex patterns as the beam propagates. Nevertheless at certain propagation distances several distinguishable vortex links surrounding the nodal braid are indeed detected [see Figure 3.9]. Note that the propagation direction coincides with the direction of the nodal braid threading the link.

Motivated by these findings and from [36], the idea then is that the extended case, i.e., the nodal thread consisting of seven nodal lines constructed from the $\mathrm{GN}_{21}(x, y; \alpha)$ modes with $\alpha = \pi/16; \pi/8$ and $3\pi/16$ will correspondingly lead to formations of more complex topological structures such as vortex knots.

By performing identical investigations this is indeed confirmed and the resulting vortex knot is shown in Figure 3.10. Note again that the propagation direction coincides with the direction of the nodal lines in this case threading the knot. Interestingly, the knots for $\mathrm{GN}_{21}(x, y; \pi/16)$, $\mathrm{GN}_{21}(x, y; \pi/8)$, and $\mathrm{GN}_{21}(x, y; 3\pi/16)$ were found only above a certain power threshold.

Explaining and predicting the formation of such complicated structures as vortex links and knots represents a highly complicated problem, however in Figure 3.7(c) it is noticed that the angular velocity and hence the pitch of the nodal lines threading the knots increases with k and α. It is therefore expected that formations of links and knots depend crucially on the pitch of the thread and the angular velocity of the beam as a whole.

In summary, propagation of the generalized multipole solitons, here exemplified by the two modes GN_{20} and GN_{21}, involves spiraling of the beams. Due to the

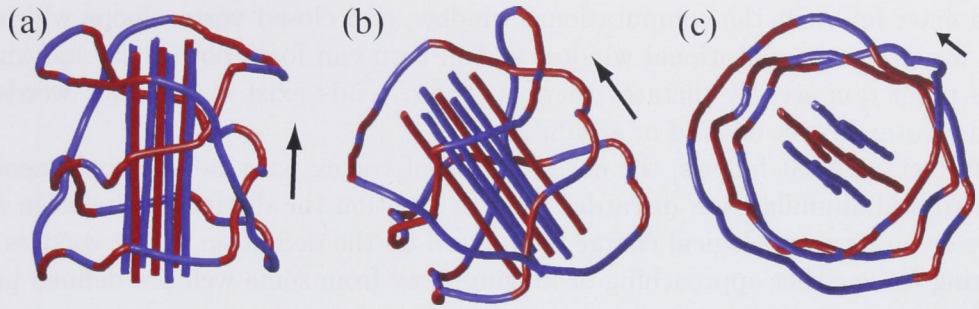

Figure 3.10: Vortex knot formed by nodal lines surrounding a multi nodal thread. Arrows indicate propagation direction. Red and blue lines indicate topological index 1 and -1 respectively.

complex structures of the solitons this gives rise to twisted nodal threads formed by the self-trapped vortices embedded in the phase distributions. As it turns out, the combined effect of spiraling and oscillations of the beams leads to formations of intricate topological distributions in form of links and knots which are studied in more detail in the next section.

3.5 Vortex loops, links and knots in nonlinear media

In this section, our main focus is aimed at exploring more elaborately the intricate dynamics responsible for the formation of various complex topological nodal line structures such as vortex loops, links and knots [36, 144]. In order to fully appreciate these highly complicated phenomena, the following analysis is based on the fundamental soliton propagating in a local saturable medium. This obviously represents a far more simple example as compared to the highly involved beam structures propagating in a nonlocal nonlinear medium, which were considered in the preceding sections.

As such, it allows for a semi-analytical investigation based on the variational approach, supplemented by extensive numerical simulations of both the variationally obtained stationary state corresponding to the fundamental soliton and a deformed fundamental soliton obtained by adding various perturbations and modulations to both the intensity and the phase distribution of the beam. As will be shown, the investigations clearly demonstrate that even in this relatively simple case, vortex loops, links, and knots are formed.

The nature of the investigations obviously necessitate the ability to both detect and trace effectively and accurately the singularities appearing in the phase distributions of the propagating beams. Therefore, it should be noted that in order to perform such involved computations, a sophisticated approach has been developed, which is mainly based on the assumption that in general only two types of nodal lines are possible. More specifically, these are global vortex lines, i.e., lines that

both enter and exit the computational window, and closed vortex loops which reside inside the computational window and in turn can form both links and knots. This prediction strictly dictates that no "loose" ends exist or in other words no single vortex is ever created or annihilated.

In fact, in what follows, the entire notion of vortex pairs being simultaneously created and annihilated is discarded, and in addition the distinction between negative or positive topological charge is replaced by the definition of the vortices appearing to be either approaching or moving away from some well pre-defined point of view.

Due to the exact balancing of spatial diffraction and self-focusing effects the phase front of a propagating soliton is shown to be flat [2, 3] and invariable, however even small perturbations in the intensity profile can cause the beam to oscillate. This alters the phase distribution and in some cases intricate singularities i.e., the appearances of zeros in the intensity as well as the phase [see Section 1.2] arise which occasionally form vortex loops surrounding the beam. The loops are geometrically orientated parallel to the transverse plane and the spatial extent or the size of the loops apparently depends on a number of various factors, such as beam power and amplitude of oscillations.

Presumably the formation of the loops occurs at or in the vicinity of the interface between nonlinear and linear regions, i.e., regions of high and negligible intensity. It is thus determined by the competition between the two distinct beam profiles, namely the fast decaying nonlinear Gaussian-like profile and the slower decaying exponential profile of the small amplitude beam tail.

It follows that whenever a fundamental soliton undergoes continuous oscillations of the intensity profile during propagation but otherwise remains stationary and structurally stable, it should be expected that vortex loops are created throughout the entire propagation length. Moreover, due to the symmetry of the current physical system, a more or less regular periodicity is assumed to appear in the formations, sizes, and locations of the loops.

Clearly the formation of vortex loops is not limited to the case of a propagating fundamental soliton and the following analysis holds for beam propagation in nonlinear media in general as well as for different beam topologies, however with the important constraint being that the beams are structurally stable.

As mentioned, here the stable propagation of a fundamental soliton in a local nonlinear saturable medium is considered. Numerous simulations are conducted with the main purpose of investigating in detail the dependence of formation and properties of nodal line structures on various adjustable parameters such as beam widths, power, and different types of perturbations added to the variationally obtained stationary solutions. Note that, as in the preceding sections, the variational solutions do not represent exact solutions and the beams are found to oscillate regardless of which input profile is being launched.

Similar to the nonlocal Gaussian model variational solutions are derived using the standard Ritz minimization procedure with the Lagrangian given by

$$\mathcal{L} = \int \frac{\mathrm{i}}{2}\left(E^*\frac{\partial E}{\partial z} - E\frac{\partial E^*}{\partial z}\right)\mathrm{d}\mathbf{r} - \mathcal{H}, \tag{3.5}$$

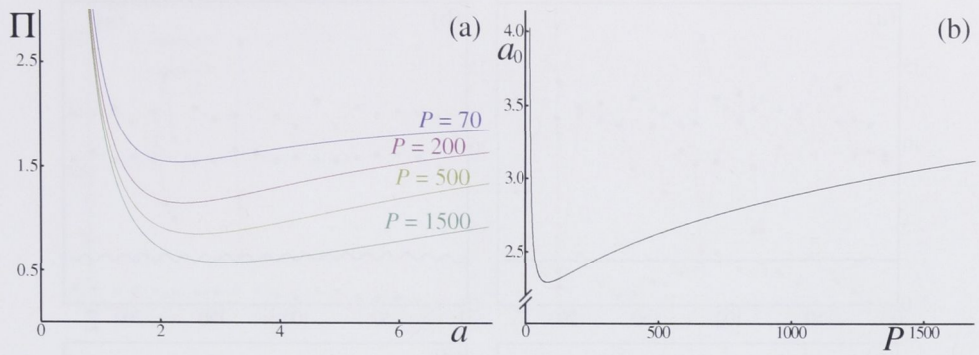

Figure 3.11: (a) Self-induced potentials for several beam powers P. Beam width a_0 of the variational stationary solutions correspond to the points on the curves where $\mathrm{d}\Pi/\mathrm{d}a = 0$. (b) Beam width a_0 of the stationary solutions vs. beam power P. Note that at approximately $P \simeq 80$ a_0 attains a minimum and hence there are no stationary solutions with beam widths smaller than some threshold value ~ 2.3.

where the Hamiltonian $\mathcal{H}$ represents an integral of motion and for a saturable medium is given by

$$\mathcal{H} = \int |\nabla E|^2 - |E|^2 + \ln(1 + |E|^2)\mathrm{d}\mathbf{r}. \tag{3.6}$$

As a solution to the nonlinear problem a Gaussian ansatz for the fundamental soliton is employed

$$E = A(z)\exp[-\frac{x^2 + y^2}{2a(z)^2} + \mathrm{i}\beta(z)(x^2 + y^2) + \mathrm{i}\varphi(z)], \tag{3.7}$$

where variational parameters A, a, β, and φ in general depend on the propagation distance z. Note that, for the truly stationary state with a flat phase front $\beta(z) = 0$, and in that case the free phase parameter φ depends linearly on z, i.e., $\varphi = kz$, with k being the propagation constant.

By deriving the variational equations the following expression for the second derivative of the beam width a is obtained

$$\frac{\mathrm{d}^2 a}{\mathrm{d}z^2} = \frac{4}{a^3} + \frac{4\pi a}{P}\ln(1 + A^2) + \frac{4\pi a}{P}\sum_{n=1}^{\infty}(-P/a^2\pi)^n/n^2, \tag{3.8}$$

and as expected it depends on the amplitude A and power P, note that $P = A^2 a^2 \pi$.

By using the fact that

$$\frac{\mathrm{d}^2 a}{\mathrm{d}z^2} = \frac{1}{2}\frac{\mathrm{d}}{\mathrm{d}a}\left(\frac{\mathrm{d}a}{\mathrm{d}z}\right)^2 \tag{3.9}$$

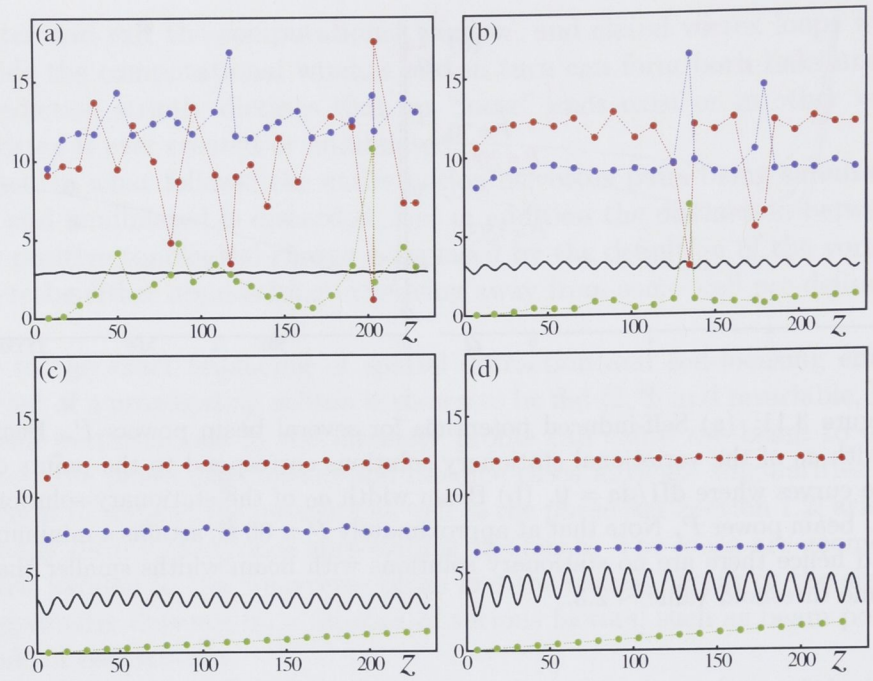

Figure 3.12: Different properties of the formed loops for $P = 200$ and different values of the perturbation parameter p. In particular in (a) $p = 1$, (b) $p = 1.05$, (c) $p = 1.1$, and (d) $p = 1.2$. Here black curves depict the amplitude of the oscillations of the beams, while blue, red, and green curves show the widths of the loops, the distances between adjacent loops, and the thickness of the individual loops respectively. Note that each dot on the colored curves indicates the formation of a vortex loop.

and substituting this expression into Eq. (3.8), integration on the left hand side yields

$$\frac{1}{2}\left(\frac{\mathrm{d}a}{\mathrm{d}z}\right)^2 = \frac{2}{a^2} - \frac{2a^2\pi}{P}\sum_{n=1}^{\infty}(-P/a^2\pi)^n/n^2 + E_0, \tag{3.10}$$

where the first expression on the right hand side is in fact the negative potential in which the soliton self-traps, henceforth denoted $\Pi(a)$, i.e.,

$$\Pi(a) = -\frac{2}{a^2} + \frac{2a^2\pi}{P}\sum_{n=1}^{\infty}(-P/a^2\pi)^n/n^2 \tag{3.11}$$

and E_0 denotes the constant of integration, in this case given by $-\Pi(a_0)$, where a_0 is the beam width of the stationary solution.

In Figure 3.11(a) several different potentials for various beam powers are plotted and beam widths of the stationary variational solutions correspond to the points on the curves where the derivative of the potential with respect to a vanishes, i.e., $\left.\frac{\mathrm{d}\Pi}{\mathrm{d}a}\right|_{a_0} = 0$.

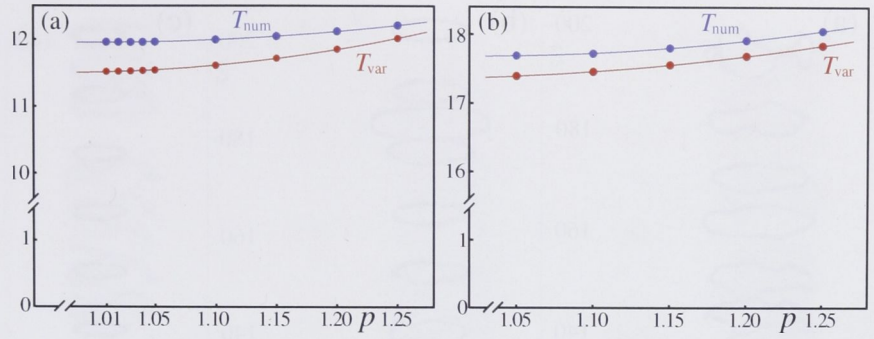

Figure 3.13: Comparison of the period of oscillations for different p as predicted by variational approach T_{var} and numerical simulations T_{num}. (a) $P = 200$. (b) $P = 1500$.

In Figure 3.11(b) the different beam widths are plotted against the beam powers and it demonstrates that the width attains a minimum value at $P \simeq 80$, or in other words there are no stationary variational solutions with beam widths smaller than some threshold value ~ 2.3.

Next, extensive numerical simulations are performed for several different powers and with small perturbations in the form of modulated beam widths. These are obtained by multiplying the stationary solution a_0 by some small parameter p, where in particular $1.01 \leq p \leq 1.25$. The results are summarized in Figure 3.12, which depicts the oscillations (black curves) of the beams during propagation for $P = 200$.

In particular, Figures 3.12(a)– 3.12(d) thus correspond to different increasing perturbations, note that because the solutions are not exact, the variationally found stationary states oscillate slightly during propagation [see Figure 3.12(a)].

The previous equation [Eq. (3.10)] allows to estimate the period T of oscillations of the various perturbed states and by considering the two extremum points a_1 and a_2 between which the beam width oscillates, T is given by

$$\int_0^{T/2} \mathrm{d}z = \int_{a_1}^{a_2} \frac{\mathrm{d}a}{\sqrt{2(E_0 - \Pi(a))}} \tag{3.12}$$

Hence it is possible to perform a comparison between the semi-analytical results and the exact numeric solutions, and in Figure 3.13 the dependence of the period T on perturbation p is depicted for both variational T_{var} and numerical T_{num} solutions for powers (a) $P = 200$ and (b) $P = 1500$ respectively.

Generally the results in the two cases show a reasonably good agreement to within a few percent difference and with both solutions exhibiting similar tendencies to increase with perturbations, as is obviously expected. The variational solutions underestimate the periods of oscillations which is probably due to the fact that the exact numerical solution differ significantly from the Gaussian profile.

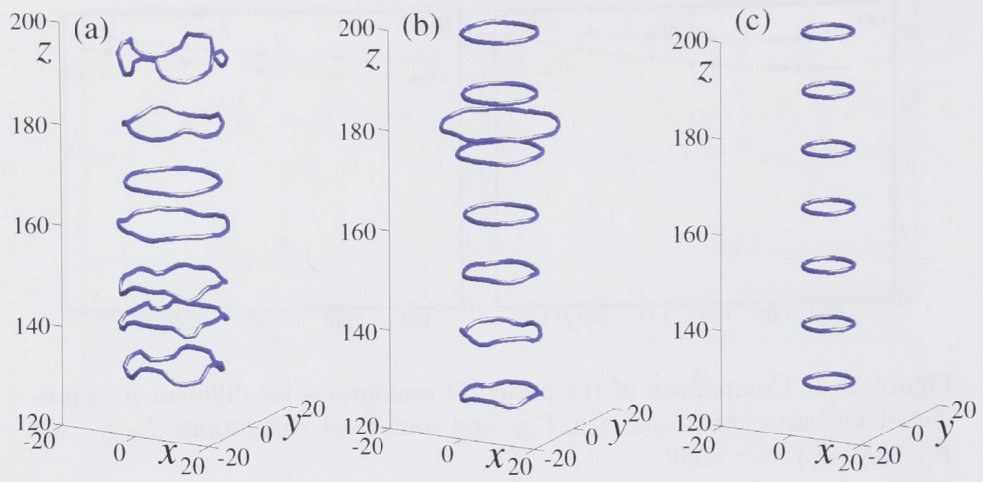

Figure 3.14: 3D plot of the formed loops for $P = 200$ and three different values of p, i.e., (a) $p = 1$, (b) $p = 1.05$, and (c) $p = 1.2$.

As mentioned, the oscillations are presumably what cause singularities to appear in the phase distributions and remarkably at certain distances the singularities combine to attain the form of vortex rings or loops which surround the beam. These rings vary in both thickness (i.e., spatial extent in the propagation direction) and size (width), and in addition, as can clearly be seen in Figure 3.12, the magnitude of the fluctuations depend strongly on the amplitude of the oscillations, and hence the perturbation of the beam widths. Note that in both red, blue, and green lines each large dot indicates the formation of a vortex loop.

Interestingly, in Figures 3.12(b)– 3.12(d) the periodicity of the appearance of the loops, i.e., the distance between neighboring loops is more or less constant and appear to be in sync with the minima of the beam oscillations. Moreover, the loops apparently become less distorted and thereby increasingly smooth and regular as the oscillations become stronger. Finally the widths of the loops decrease while on the other hand the thickness shows an almost linear dependence on z. On the other hand, when launching the stationary solution [see Figure 3.12(a)], which undergoes very small oscillations, the loops become highly irregular and distorted. Note that for all cases, the spatial extent of the oscillations never overlaps with the spatial location of the vortex loops.

In Figure 3.14 the formed vortex loops are depicted for three different values of the perturbation parameter p. By comparing Figures 3.14(a)– 3.14(c) it immediately becomes evident that the loops indeed show a clear tendency to evolve from strongly distorted and irregular entities to highly ordered structures exhibiting a remarkable uniformity. Note that in excellent agreement with Figure 3.12 (blue lines) the widths of the loops clearly decrease with stronger perturbations, while the distance between the loops remain almost constant thus keeping the loops well separated spatially.

At substantially higher beam power, not shown, the dynamics and properties

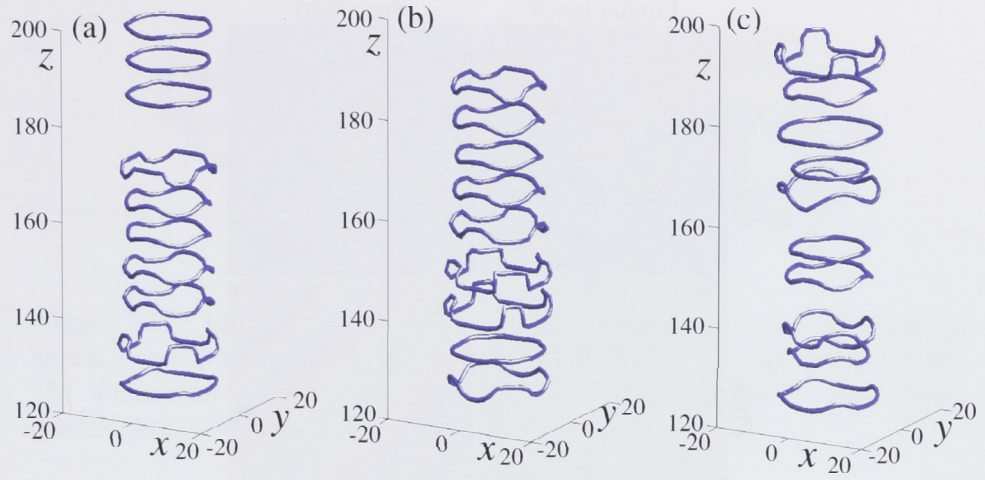

Figure 3.15: 3D plot of the formed loops at a substantially higher power, namely $P = 1500$ for three different values of p, i.e., (a) $p = 1$, (b) $p = 1.05$, and (c) $p = 1.2$.

of the loops change dramatically. Both the amplitude A and beam width a are increased and opposite to the previous case [see Figure 3.12] both the loop width and the distance between loops show a distinct tendency to experience a growth in their fluctuations with stronger perturbations. It follows that rather than damping the fluctuating behavior of the loops, i.e., both widths, thickness, and mutual distances, the spatial magnitude of the beam oscillations eventually overlap with the spatial region in which the loops reside, which triggers a strong interaction between the soliton and the singularities. In addition, the number of loops is increased which suggests that a slower oscillating beam causes additional loops to form during the oscillations.

The vortex rings depicted in Figure 3.15 are both wider and appear slightly more deformed than the loops in Figure 3.14, and the distance between the loops is markedly decreased. In this case the width is more or less constant. Note the distinct spatial periodicity with which the loops, in groups of two, appear to have arranged themselves.

The idea now is that whenever the distance between neighboring loops becomes sufficiently small, or alternatively the thickness of the loops is comparable with the spatial separation of the loops, it will cause neighboring loops to interact and cause them to recombine into nontrivial nodal line structures such as links and knots. It is however expected that this necessitates a certain twisting and deformation of the rings, which can be realized by launching an elliptical beam rather than the radially symmetric beam considered above. In addition, rotation of the beam structure as a whole, causing the loops to rotate along with the beam, is assumed to be essential to the formation of such complex topological compositions.

In the following, a different beam structure based on the fundamental soliton

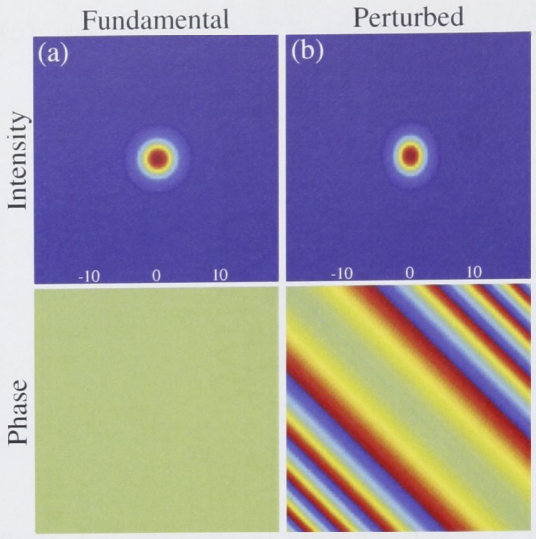

Figure 3.16: (top) Intensity profiles for (a) fundamental soliton and (b) perturbed beam. (bottom) Corresponding phase distributions. As before the colors for intensity are mapped from zero (blue) to maximal value (red), while phase is scaled from $-\pi$ to π.

is therefore considered. The parameter p is now multiplied only with the beam width in one transverse direction which gives the beam its elliptical shape and a different phase distribution is imposed on the original flat phase of the soliton. The perturbed beam E_{pert} thus takes the form

$$E_{pert} = A \exp\left\{ -\frac{x^2}{2a^2} - \frac{y^2}{2pa^2} + \mathrm{i}k(x\cos\alpha + y\sin\alpha)^2 \right\} \tag{3.13}$$

where the free parameters k and α in combination with power P determine the angular momentum and hence the angular velocity or pitch of the rotating soliton.

In Figure 3.16 a comparison between the unperturbed fundamental soliton with a flat phase front and a perturbed beam with a complicated phase distribution is depicted.

Here $\alpha = \pi/4$ has been chosen and by simple trial and error, numerical simulations revealed that very low values of k correspondingly have very little effect on the beam propagation as well as properties and structures of the loops. On the contrary, high values of k cause the beam to experience such strong modulations that it eventually becomes unstable and breaks, which obviously has similar destructive effects on the loops as well. As a result the value of k is found to lie within a relatively narrow range of $0.01 \leq k \leq 0.05$ for the desired effects to transpire.

As previously, the investigations involve numerous numerical simulations with several beam powers and different values of the modulation parameters, p and k. In good agreement with the considerations above, links and knots were never observed

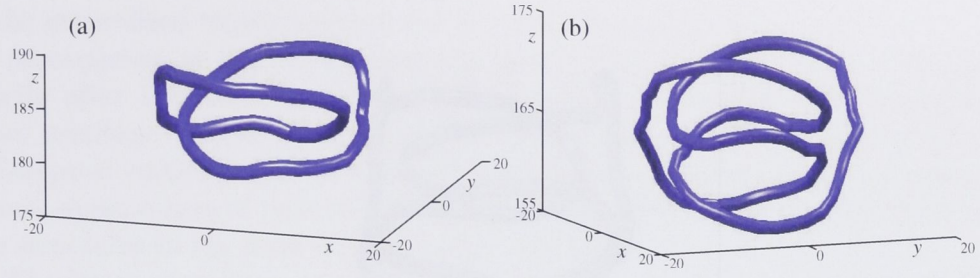

Figure 3.17: (a) Vortex link formed by two spatially overlapping spiraling nodal loops. Parameters here are $P = 1500$, $\alpha = \pi/4$, $p = 1.2$, and $k = 0.02$. (b) Vortex knot formed by three modulated spiraling nodal loops. Same parameters as in the case of the link.

to form for $P = 200$. Specifically, this apparent absence of both links and knots is mainly due to the relatively large distance between neighboring loops, i.e., even at strong deformations the spatial extent of the individual loops never reach or overlap the spatial regions of adjacent vortex rings.

This picture is radically altered however when considering a significantly higher power, namely $P = 1500$. As noted in Figure 3.15 the loops here are situated markedly closer to one another and hence a spatial overlap of adjacent loops is much more likely to occur. This is clearly demonstrated by the formations of vortex links in a great range of parameter values, and as an example in Figure 3.17(a) one such link is shown. Here the individual loops have been deformed and twisted to such a degree that they eventually occupy the same spatial region, which causes them to form a pair of vortex rings linked together.

Intriguingly, a somewhat more complex topological composition is also possible in which three deformed spiraling loops can occupy the same spatial region and combine to form a vortex knot [see Figure 3.17(b)].

Note an important difference between links and knots manifested by the fact that the vortex link clearly consists of two distinct loops which remain self-similar, while the knot, on the other hand, appears as just one loop which, through intricate twists and turns, eventually folds into itself and "bites" its own tail.

It should be stressed here that both the vortex link and the vortex knot depicted in Figures 3.17(a) and 3.17(b) respectively are obtained for power $P = 1500$ with $p = 1.2$, $\alpha = \pi/4$, and $k = 0.02$. At the same values of parameters P, p, and α, but a slightly smaller value of k, namely $k = 0.018$ no less than five loops are found to merge and form the knot depicted in Figure 3.18.

In summary, in the above analysis propagation of the fundamental soliton in a local saturable medium was investigated. Stationary solutions were subsequently derived be employing the well-known variational approach with a Gaussian profile serving as the trial function. By varying the beam width and simultaneously keeping the power constant numerous numerical simulations were conducted. Due to the fact that the beams exhibited periodic oscillations of the intensity profile during

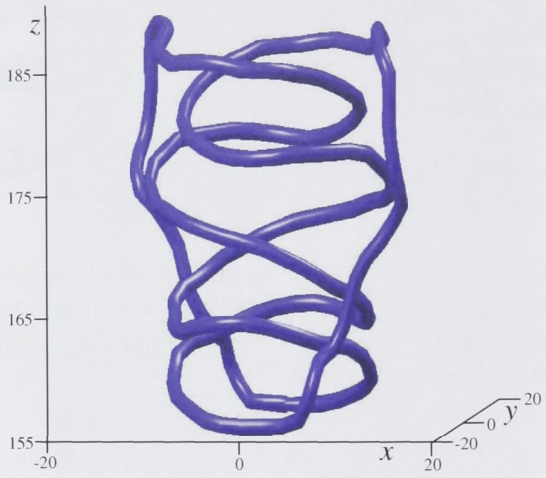

Figure 3.18: Vortex knot this time formed by no less than five modulated spiraling nodal loops. Same parameters as above except for the slightly smaller value of k, namely $k = 0.018$.

propagation, intricate singularity distributions emerged, and special attention was given to the formation of vortex rings surrounding the beam.

Simulations clearly demonstrated a strong dependence of these structures on both amplitude of the oscillations and beam power. In addition the distance between adjacent loops was found to monotonically decrease with power and consequently above a certain power threshold highly complicated nodal line structures emerged, created by the interaction and recombination of several deformed and spiraling vortex loops.

The above results, as mentioned, are not limited to propagation of the fundamental beam, but are rather generic in the sense that the essential requirement of the appearance of singularities is represented by the oscillations of the beam and that the beam remains structurally stable over large propagation distances.

Given the fact that nonlocality on one hand is shown to allow for stable propagation of optical solitons and in addition supports formation and propagation of a substantially greater variety of optical beams, these considerations are in excellent agreement with the observations of similar phenomena in a nonlocal medium as demonstrated in Section 3.4.

3.6 Summary

To summarize, in the first part of this chapter evolution of two distinct families of higher-order nonlocal GN solitons was investigated in detail through extensive numerical simulations. In particular the studies involved the propagation dynamics

of the generalized tripole solitons and 3×2 matrix solitons.

As expected, at low beam power the beams were all unstable and disintegrated shortly after launching, however above a certain power threshold depending on beam topology, various novel phenomena were uncovered in the form of spiraling self-trapped vortices, quasi-periodic transformations accompanied by rotation of the beams, appearances of twisted vortex trajectories, and formations of intricate nodal line structures in the form of vortex links and knots.

The latter were later studied in more detail by considering a perturbed fundamental soliton in a local nonlinear saturable medium. It was shown that oscillations of the beam triggered the creation of vortex loops surrounding the beam, and they appeared more or less periodically.

By perturbing the fundamental soliton even further, the beam attained an elliptical shape and an angular momentum, and combination of this asymmetry as well as spiraling of the beam paved the way for the creation of both vortex links and knots.

The model used for the construction and propagation of the solitons in the first part of this chapter as well as in the preceding chapter was based on the phenomenological Gaussian nonlocal response function which is very instructive and generic in the sense that similar results will be observable in more realistic models, however it does not as yet represent a known physical system.

In the next chapter a more realistic nonlocal thermal model will therefore be considered and the particular reason for that is two-fold. In particular, it is investigated to what extend such a nonlocal medium supports stable propagation of several types of higher-order optical solitons and moreover whether similar transformation dynamics are observable in a thermal medium, which could eventually lead to the experimental observation of such transitions.

Finally boundary effects on soliton propagation is considered and to that end different sample geometries are investigated, supplemented by launching the solitons at different transverse spatial locations in the thermal sample.

CHAPTER 4

Solitons in thermal nonlocal media

4.1 Introduction

The nonlocal nonlinear responses generally appear as a consequence of several different physical processes, [see Section 1.3], and they are therefore present in a large variety of physical systems. The study of the effects determined by the nonlocal nonlinear response has experienced a growing interest recently, both theoretically and experimentally, due to properties that include arrest of catastrophic collapse [65], significant suppression of modulational instability [68], and the ability to support the formation of higher-order solitons [75, 93, 94].

In order to investigate to what extend nonlocality supports stable propagation of various higher-order modes, in Chapter 2 the higher-order solitons were constructed that extended the well-known HG, LG and HLG linear modes to the case of nonlinear media with the Gaussian nonlocal response. Thus the nonlocal HN, LN, and GN were realized and the propagation of these beams, varying both the modulation parameter p for the LN modes and α for the GN modes, was studied for several power levels and beam symmetries.

Extensive numerical simulations revealed fundamental differences in their propagation dynamics depending on both beam topology and degree of nonlocality. Indeed, in the local limit all higher order nonlinear modes were found to be unstable, but at some threshold which varied depending on the structure of the solitons they would either become stable or exhibit highly nontrivial mutual transformations between seemingly disparate beam structures of radial and rectangular symmetries.

In addition, it has been shown recently that nonlocal media enable stable propagation of the rotating soliton complexes, the so-called azimuthons [100, 101]. Recall that azimuthons were originally proposed in the context of local nonlinear media [64] and they are azimuthal modulated beams with nontrivial phase structures exhibiting steady angular rotation in propagation.

The above mentioned works, however, employed the so-called Gaussian model for describing the nonlocal response of the media. While being very instructive and

useful, in particular, in applying the analytical approach to study the dynamics of solitons, this model serves only as a phenomenological model of nonlocality and does not describe the nonlocal optical response of any known specific physical system.

The aim of this chapter is to explore the interaction and propagation dynamics of different beams in a more realistic thermal medium which represents a real system with nonlocal nonlinearity. Unlike weakly nonlocal systems and the systems with the Gaussian response where the degree of nonlocality is finite, in the systems with thermal response the spatial scale of nonlocality is always as large as the physical dimensions of the material sample. This is because the thermal response is determined by the details of heat transfer at the boundaries. As a consequence, the sample geometry may have a profound effect on the structure of the formed solitons, their stability and mutual interaction [116, 125, 145]. In particular, recent experiments [116] have shown that, when a circularly symmetric beam is launched in a sample with rectangular boundaries, it evolves into an elliptically shaped output beam. Moreover, numerical simulations [125] have demonstrated that a thermal sample of rectangular cross section with the appropriate dimensions stabilizes nonrotating dipole solitons, which are unstable in a square sample. In the same work it was also noted that all higher order solitons, e.g., tripoles, quadrupoles and necklaces, are unstable regardless of the sample geometry.

Note that this behavior is in sharp contrast to the results in [100] and Chapter 3, showing that both the rotating and nonrotating dipoles and tripoles are stable in a nonlinear media with a nonlocal Gaussian response, provided the degree of nonlocality is sufficiently high.

Propagation of the rotating dipole and a necklace beam is therefore studied and, similar to the results in [100], it is observed that above a certain power threshold the dipole solitons propagate stably for several tens of soliton periods. In addition, an example of a semi-stable rotating necklace-type soliton is demonstrated. These results, when compared with the results from the preceding chapter, strongly suggest that the stabilization mechanism is a generic property of a spatial nonlocal nonlinear response independent of its particular functional form.

However, the thermal response is determined by the details of heat transfer at the boundaries, and the sample geometry has a profound effect on the propagation dynamics as a whole [116, 125]. This effect is demonstrated by launching several beam symmetries in samples of different geometries and at different transverse positions in the sample. As a consequence, the beams undergo different transitions depending on the ratio of the sample. In a different case they experience a strong modulation of the input profile induced at an earlier stage of propagation due to a correspondingly stronger force resulting from the soliton being launched closer to the boundary. Moreover, the solitons exhibit transverse motion across the sample due to the induced difference in the gradient of the transverse profile of the response.

In a thermal medium the intensity of the optical beam acts as a heat source. As a consequence the nonlinearity stems from a local heating of the medium which effectively alters the refractive index via the thermo-optic coupling. Through diffusion the heat is transported to regions of lower temperature which in effect renders the response nonlocal. In thermal media the steady-state temperature and the re-

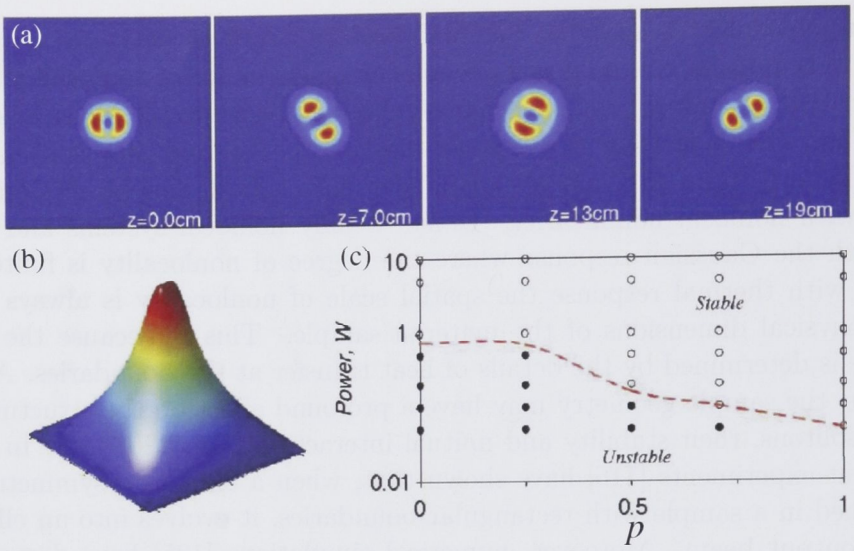

Figure 4.1: (a) Example of a stable rotating dipole soliton in a thermal nonlocal nonlinear medium. (b) Spatial profile of the refractive index change induced by a dipole soliton with the contrast parameter $p = 0.7$ and input power $5W$. (c) Stability domain for the rotating dipole solitons for the parameters (p, P).

fractive index distributions are determined not only by the intensity of the beam but also by the boundary conditions [146]. In the following we therefore adopt the Dirichlet boundary condition corresponding to thermally connecting the boundaries to a heat sink at a fixed temperature T_c.

Propagation of optical beams is governed by the paraxial NLS [Eq. (1.2)] with the nonlinear response $\mathcal{F}(I)$ of the thermal medium, which can be either focusing or defocusing, described by the heat equation, which in the steady state has the following form

$$\frac{\partial^2 \mathcal{F}(I)}{\partial x^2} + \frac{\partial^2 \mathcal{F}(I)}{\partial y^2} = -\gamma I, \tag{4.1}$$

where γ depends on the material parameters such as thermal diffusion constant, linear absorption, and thermo-optic coefficient.

In the following, the split-step beam propagation method based on the fast Fourier transform algorithm is employed to simulate beam propagation in a thermal sample, and at each propagation step the spatial profile of the refractive index is evaluated by solving iteratively the heat equation [Eq. (4.1)] with the corresponding light intensity distribution as a heat source.

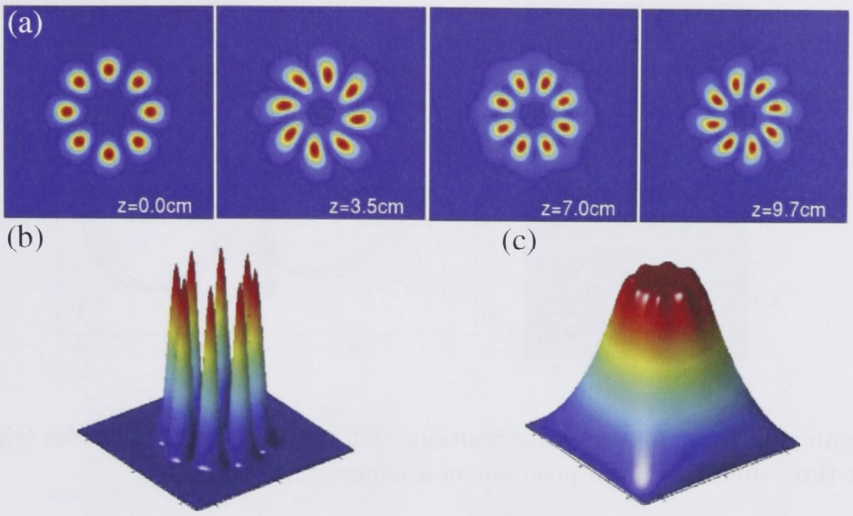

Figure 4.2: (a) Example of a stable rotating necklace soliton in a thermal nonlocal medium with input power $5W$. (b,c) Surface plots of the intensity and refractive index profile, respectively.

4.2 Spiraling dipole and multipole solitons

In this section, propagation dynamics and stability of rotating two-soliton bound states and higher-order necklace solitons in nonlocal nonlinear media are investigated and compared for two different nonlocal models. This serves two distinct purposes, namely first by comparing the results from two different nonlocal models, i.e., phenomenological versus more realistic model, a more detailed insight into the generic properties of nonlocality is naturally obtained. Secondly, investigations involving a more realistic model promise to determine more accurately the prospect of experimentally realizing and observing various interesting effects in thermal nonlinear media.

The Gaussian model employed in Ref. [100] serves as a phenomenological example of a nonlocal nonlinear medium. This is a very useful model for the theoretical analysis, but it does not, as mentioned, describe a specific physical system of a nonlocal optical response. For comparison, the properties of the rotating solitons in a thermal medium, which represents a real system with nonlocal nonlinearity, are studied. In both models it is demonstrated that the rotating two-soliton bound states and higher-order necklace solitons can be stabilized for sufficiently high degree of nonlocality. The results indicate that such rotating dipole solitons and higher-order necklace solitons should be observed experimentally in thermal nonlinear media.

As with the Gaussian response, an ansatz similar to Eq. (2.5) with $n = 0$, $m = 1$ and different values of the modulation depth p is used to define the initial amplitude of the beam. With various input conditions, evolution of the beams over

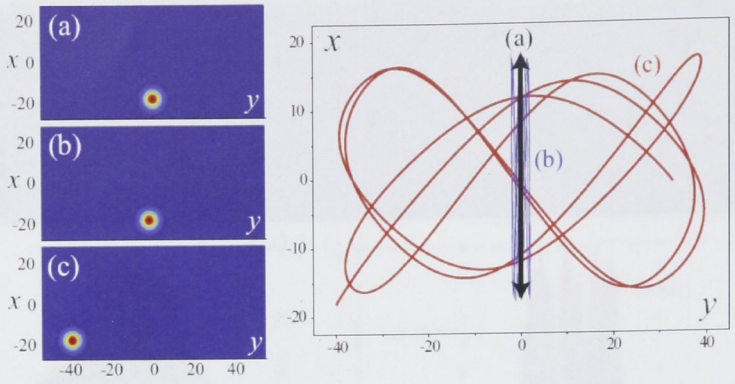

Figure 4.3: (a–c) Intensity distributions (left) and soliton trajectories (right) for three different initial positions of a Gaussian input beam.

the distance of tens of the diffraction lengths are numerically investigated.

In physical units, this corresponds to a distance of more than $20cm$ for beams of tens of micrometers in diameter. In order to link the simulations to real physical systems, the material parameters of lead glasses from [116] are considered. The thermally induced maximum index change then is of the order of 10^{-4} for the beam power in the range of a few watts.

In Figure 4.1, stable propagation of a rotating dipole soliton is demonstrated, similar to the results shown in Ref. [100]. In this particular case, the initial modulation parameter is $p = 0.7$, and the beam power is taken as $5W$. To demonstrate the unique long-range character of thermal nonlocality, in Figure 4.1(b) the spatial distribution of the refractive index change is shown. It is clear that while the dipole soliton itself occupies only a finite region, the steady-state refractive index profile extends over the whole computational window.

In order to characterize the stability properties of the rotating dipole solitons, additional extensive numerical simulations of the soliton propagation are conducted by varying the initial modulation p as well as input power. The results of these simulations are summarized in Figure 4.1(c) which is analogous to that in the case of the Gaussian nonlocal nonlinear model [100]. Each point of this graph represents a rotating dipole soliton with the specific set of parameters, and its stability is determined numerically by the study of the propagation dynamics. The investigation is restricted to a physically reasonable region of the input powers up to $10W$. In this region, the only relevant instability scenario involves the breakup of the dipole-soliton structure. However, because of a finite size of the computational window and an infinite extent of nonlocality, the complete breakup was never observed. Even if the splinters separate initially, this process is slowed down later by the index gradient in the vicinity of the boundaries. As a result, the dashed line in Figure 4.1(c) represents a qualitative transition between the stable and unstable regimes. Its position was determined from the dependence of separation between

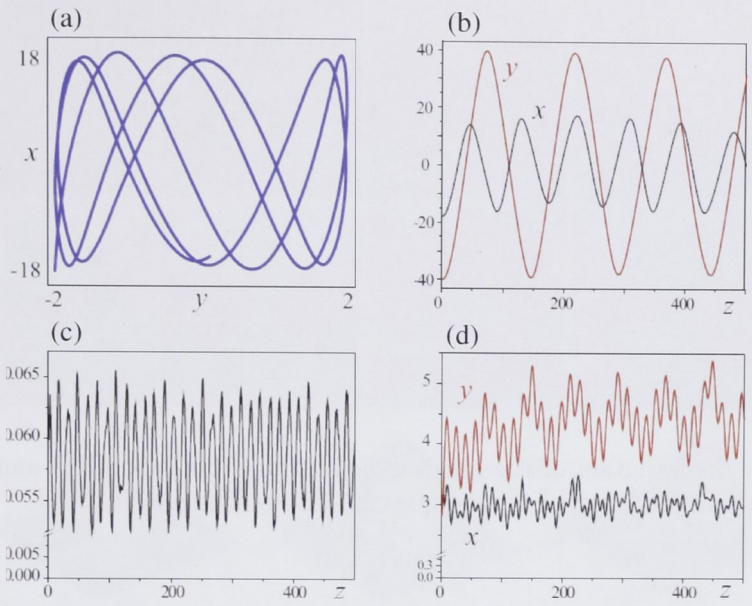

Figure 4.4: (a) Magnified trajectory of the blue trajectory (b) in Figure 4.3. (b) Coordinates, (c) amplitude, and (d) widths of the soliton on the red trajectory (c) in Figure 4.3; red lines: y-direction, black lines: x-direction.

the fragments of the dipole soliton as a function of the input power.

It should be mentioned that in recent studies [115, 125] the stability of non-rotating dipole solitons in thermal media has been investigated, and it was found that all such dipoles are in principle unstable when the thermal sample in which they propagate has a square geometry as is the case in this study. With higher optical power they experience collapse and simulations performed here (not shown) confirm that scenario. However, since the growth rate for this type of instability is very low and collapse becomes important only for very high input powers, for typical experimental conditions these dipole solitons are physically stable.

The stabilizing character of nonlocal nonlinearity suggests that nonlocal media should be able to support higher-order rotating soliton structures [see Chapter 3]. In Figure 4.2 an example of the stable rotating necklace-type soliton is depicted. The initial spin is imposed onto the structure by an initial helical phase modulation. Visible focusing is caused by the fact that the initial intensity pattern does not represent a stationary solution of the nonlinear model.

In conclusion, it has been demonstrated numerically that a Kerr-type nonlinear optical medium with a Gaussian nonlocal nonlinear response supports the formation of stable rotating dipole solitons, i.e., dipole azimuthons for sufficiently high degree of nonlocality. Similar rotating dipole solitons and higher-order localized structures have been shown to exist in another, more realistic optical medium with thermal nonlinearity. Numerical simulations have demonstrated that nonlocality provides an effective stabilization mechanism for such rotating dipole structures as

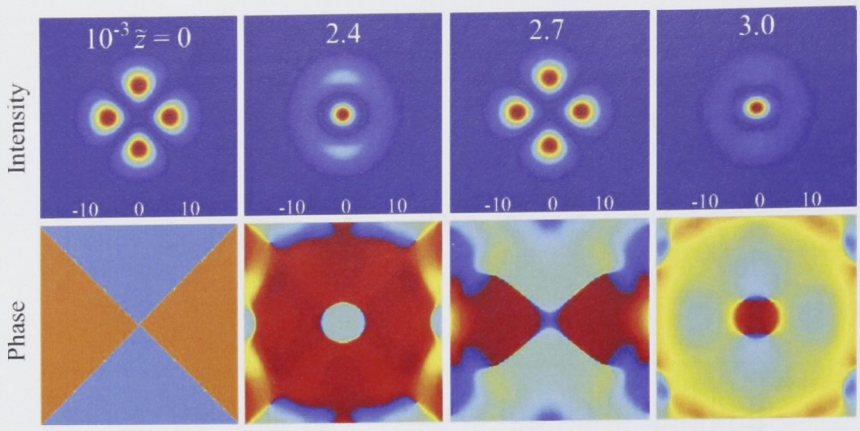

Figure 4.5: Evolution of the quadrupole soliton. Intensity (top) and phase (bottom) distributions of input beam and intermediate states.

well as higher-order localized structures such as soliton necklaces against azimuthal modulational instability.

4.3 Boundary effects on propagation dynamics

The aim in this section is to explore the effect of the sample geometry on beam propagation in a realistic thermal medium and to that end several beam symmetries are considered. It is highly expected that boundaries play a major role in the dynamics displayed by the solitons, so to uncover a substantial variety of novel effects a comprehensive study is undertaken which involve numerous beam symmetries, different sample geometries, and varying input conditions.

Initially, the fundamental soliton is launched in a rectangular shaped sample from three different positions resulting in transverse motions across the sample. Specifically, the trajectories of a fundamental soliton in a rectangular shaped sample with aspect ratio two for three different cases are considered, i.e. the soliton is launched from three different positions (x_0, y_0). In all cases the beam is launched adjacent to the elongated boundary keeping $y_0 = 18$, [see Figure 4.3(a)–(c)], with various positions in the horizontal direction, $x_0 = 0$, -2, and -40.

In the case where the beam is placed in the center of the cell $x_0 = 0$, as shown in Figure 4.3(a), the induced refractive index profile is symmetric in one x-direction and thus the effective forces from opposite x-boundaries compensate each-other. However, due to the induced asymmetry [106, 145] in the gradient of the transverse profile of the response in y-direction, the beam is repelled by the boundary and the soliton moves in the vertical y-direction, periodically bouncing from one side of the sample to the other as it propagates.

This behavior changes remarkably, however, when the input beam is shifted slightly off the center, $x_0 = -2$ in Figure 4.3(b). As a consequence of the displace-

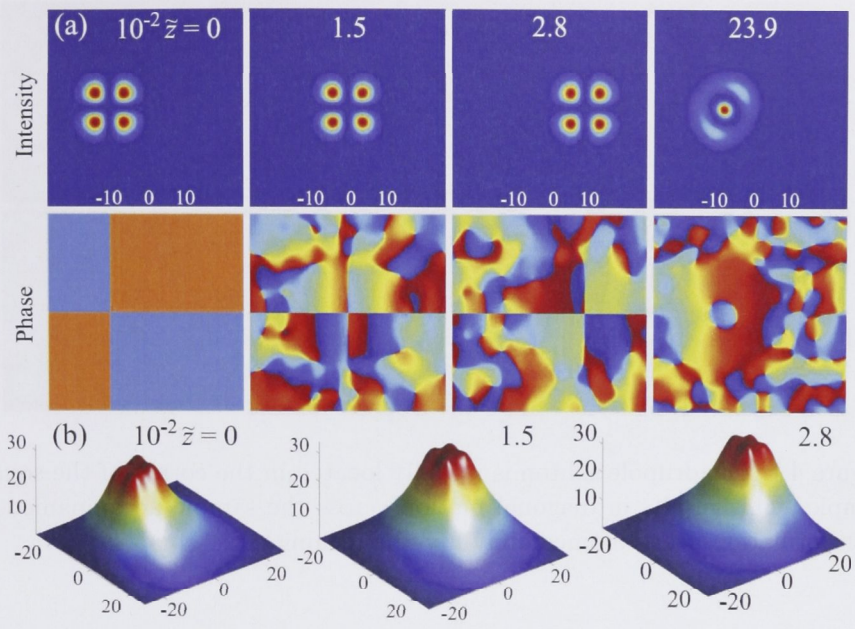

Figure 4.6: (a) Evolution of the quadrupole when launched closer to the boundary. During propagation the beam clearly exhibits back and forth motion. (b) Refractive index profile at three propagation distances.

ment, the induced potential well or the refractive index distribution, is now both horizontally and vertically asymmetric and exerts a net force in both transverse directions. The force exerted by the further away vertical boundary is correspondingly smaller and the velocity of the soliton is therefore much higher in the vertical direction. This causes the soliton to follow a steep trajectory, the blue line in Figure 4.3(b) and the corresponding magnified trajectory in Figure 4.4(a), which clearly show that despite being launched very near the center, the soliton in fact reaches and bounces off the upper horizontal boundary before the middle of the cell is reached.

Lastly, the soliton was launched near the corner of the sample [see Figure 4.3(c)] and here the repelling effect of the vertical boundary is correspondingly stronger. In contrast to the previous case, the soliton actually crosses the center of the cell before the opposite horizontal boundary is reached. The dynamics of the beam in this case is further demonstrated in Figures 4.4(b)– 4.4(d), where the beam amplitude is plotted (b), two spatial positions (c) in x (red line) and y (black line) directions, and two full soliton widths (d) in both directions (x, red, and y, black). Note that the degree of ellipticity of the beam is comparable with the ratio of lengths of the cell boundaries.

Thus, for both non-symmetric launch conditions it appears that once the soliton crosses the middle of the cell it slows down and eventually turns around due to the repelling force of the opposite boundary. This repulsion is a direct consequence of

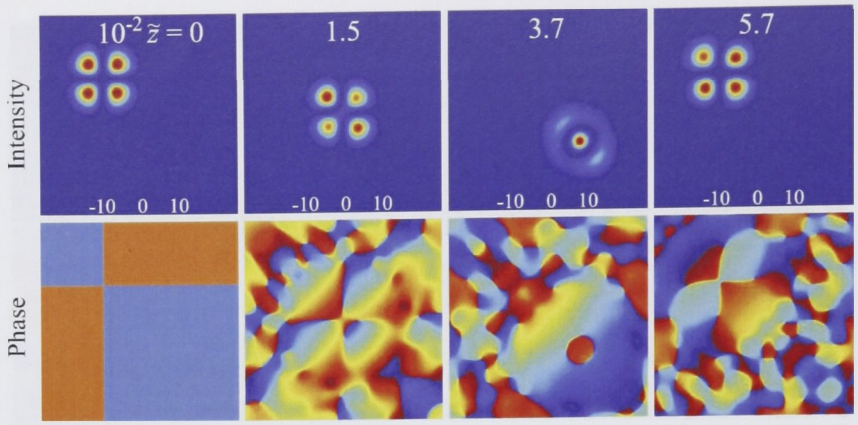

Figure 4.7: Quadrupole soliton is initially located in the corner of the square sample. This results in diagonal motion across the sample accompanied by transformation nearly immediately upon launching.

the nonlocal nature of the thermal response, combined with the intricate dependence of the response on the specific properties of the boundaries. In general, boundaries affect not only the position, but also the internal dynamics of more complex solitons of different symmetries.

Next, more complex higher-order beam structures are launched in order to investigate whether a thermal nonlocal medium allows for the self-induced soliton transformations observed previously in the Gaussian model in Chapters 2 and 3. Therefore, two illustrative examples are considered, namely quadrupole and double-ring vortex solitons. The role of rectangular boundaries on transformation dynamics and evolution of multi-soliton structures is demonstrated by (i) changing the initial location of a quadrupole soliton in a square sample and (ii) changing the aspect ratio of the transverse dimensions of a rectangular sample with double-ring vortex soliton. In general, any asymmetry facilitates the development of soliton transformations; however, for ring structures in rectangular samples novel transformations with no analogy in the free-boundary model are observed.

As the first case, the propagation of a quadrupole beam, i.e., an optical necklace is studied, which consists of four out-of-phase petals and the (normalized) field distribution given by

$$U(x,y) = Axy\exp(-x^2/2w^2 - y^2/2w^2)/w^2 \tag{4.2}$$

The results of numerical simulations in a thermal sample with square cross section are shown in Figure 4.5.

In the simulations the following parameters were used: $A = 9$, $w = 4$ and $\gamma \simeq 10^{-2}$. In full agreement with the results of Chapter 2 mutual transformations between two modes of different symmetries are observed, namely the intermediate states resemble a single-ring fundamental soliton. Shortly after the second transition the dynamics however become increasingly disordered and eventually neither of the

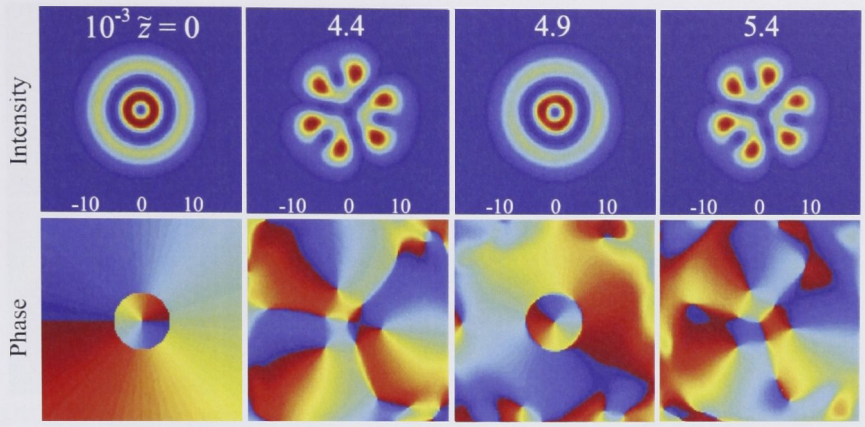

Figure 4.8: Evolution of the single-charge double-ring vortex soliton in square sample. Propagation dynamics entails transitions into a complex multihump ring-like structure consisting of six discernible humps.

two different symmetries will be distinguishable (not shown). The fact that the quadrupole is unstable agrees well with the predictions in [125]. However, the beam remains localized during propagation due to the strong confinement from the induced refractive index potential well. This confinement is a direct consequence of the fact that, in a nonlocal thermal system, unbound states or rather radiation waves do not exist [130].

Substantially different dynamics appear when an identical beam is launched asymmetrically, i.e., closer to one of the boundaries [see Figure 4.6].

Due to the induced difference in the gradient of the transverse profile of the response, in Figure 4.6(b) the beam is repelled by the boundary and moves periodically during propagation back and forth from one side of the sample to the other before experiencing nontrivial transitions at $\tilde{z} \simeq 2.4 \times 10^3$, the same as in Figure 4.5. Note that this repulsion of the quadrupole beam leads to similar behavior as the dynamics depicted in Figure 4.3.

Another example of the asymmetric launching of the beam, namely at the corner of the sample, is shown in Figure 4.7. The beam moves diagonally across the sample and transformation to the same fundamental mode with a single ring as in Figure 4.5 is observed. However, the combined influence of two boundaries is considerably stronger and causes instabilities to initiate the transitions at a much earlier stage, cf. $\tilde{z} = 1.5 \times 10^2$ in Figure 4.7 and $\tilde{z} = 2.4 \times 10^3$ in Figure 4.5. At the later stage (not shown) the beam loses its symmetries and exhibits unstable propagation.

Next the evolution of a double-ring single-charge vortex beam is considered. The beam is obtained as

$$U(x,y) = A(x+\mathrm{i}y)(2w^2 - x^2 - y^2)\exp(-x^2/2w^2 - y^2/2w^2)/w^3 \qquad (4.3)$$

and simulations shown are done using the following parameters: $A = 9$, $w = 4$ and $\gamma \simeq 4 \times 10^{-3}$. Recall from the results of [100] that the instability-induced mod-

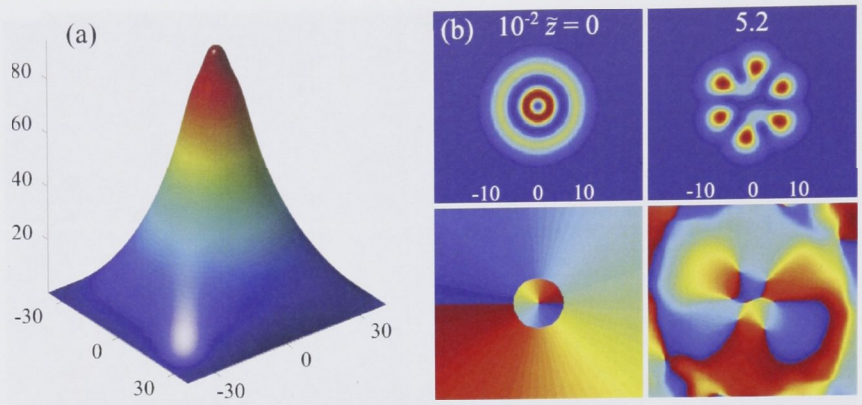

Figure 4.9: (a) Spatial refractive index profile in a rectangular geometry with ratio 1.1. (b) Evolution of the same mode as in Figure 4.8 showing very similar features at much smaller propagation distances.

ifications of this structure result in several appearances of a rectangularly shaped 3×2 soliton matrix, followed by subsequent revivals of the original beam. On the other hand, as a consequence of the fact that the geometry of the thermal sample imposes limitations on the permitted beam structure [116, 125], in a square sample the transformations into the 3×2 soliton matrix are forbidden. Nevertheless, different transitions occur and the vortex beam attains a rather complex structure consisting of six discernible humps arranged in a ring-like azimuthally modulated structure [see Figure 4.8].

The question then arises whether a rectangular cross section will be able to support the formation of a beam of similar geometry (3×2 soliton matrix), and by considering different samples of various ratios (a ratio of one being a square sample) it is observed that this is indeed the case. In particular, several different geometries are investigated which reveal that the solitons exhibit different dynamics depending on the ratio. At nearly square cross section (ratio of 1.1) the dynamics is very similar to the square case and, as seen in Figure 4.9(b) at $\tilde{z} = 5.2 \times 10^2$, the modulational instability causes the beam to attain a structure that only slightly deviates from the one in Figure 4.8 at $\tilde{z} = 4.4 \times 10^3$. Note a major difference in the distance at which the first transformation occurs; it is an order of magnitude smaller.

Increasing further the ratio eventually leads to the formation of a 3×2 multihump structure as seen in Figure 4.10 depicting propagation in a rectangular sample of ratio 1.5.

Note also that the distance of first transition is further decreased. As it turns out, this distance decreases monotonically with increase in the sample ratio, although showing a tendency to saturate. By comparing Figures 4.9 and 4.10 it is also noted that, due to the larger sample in the latter case, the refractive index profile is correspondingly larger or, in other words, the depth of the induced poten-

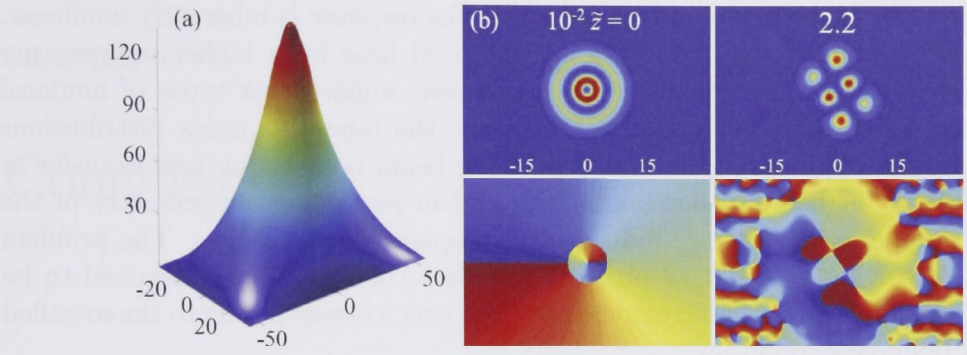

Figure 4.10: (a) Spatial refractive index profile in a rectangular geometry with ratio 1.5. (b) Due to increased ratio of the sample cross-section dimensions the formation of a rectangular multihump beam is possible: note that the distance is further decreased.

tial well is proportional to the sample size [130]. In all cases, i.e. regardless of the sample cross section, the modes are unstable and eventually undergo random oscillations accompanied by appearances of various unrecognizable structures, while still remaining strongly self-trapped and unable to escape the induced potential well.

In conclusion, the propagation of both the fundamental and higher-order two-dimensional spatial solitons in media with a nonlocal thermal nonlinear response has been studied numerically. It has thus been demonstrated that the solitons exhibit rather complicated dynamics strongly influenced by the boundaries, including mutual transformations between solitons of different geometries. The results suggest that mutual transitions between seemingly different beam structures is a generic feature of higher-order nonlinear modes belonging to the same general family of modes [see Chapter 2] which can be approximated, for example, by the so-called Hermite Laguerre generalized beams [128]. In addition, this remarkable property may pave the way for the observation of such highly nontrivial and intriguing dynamics experimentally, e.g., in lead glass samples. On the other hand, such observations are drastically limited, among other factors, by the topology of the beams and the actual shape of the sample.

4.4 Summary

In summary in this chapter the nonlocal beam propagation in a thermal nonlinear medium has been investigated. To this end a thermal nonlocal model has been introduced, which represents a more realistic nonlocal model than its phenomenological counterpart [Eq. (1.22)].

In such a thermal medium the physical process accounting for the nonlinearity is a local heating of the medium induced by a propagating light beam, and through the thermo-optic effect the refractive index changes with a magnitude depending

on the intensity of the beam and consequently the response is inherently nonlinear. The nonlocality arises due to diffusion of induced heat from higher temperature regions into areas of lower temperature. However, unlike other types of nonlocal media, the steady-state temperature and hence the refractive index distributions are determined not only by the intensity of the beam but also by heat transfer at the boundaries, indicating that boundaries and in particular the geometry of the thermal sample exhibit strong influence on propagation dynamics. The problem amounts to solving a boundary problem and here the sample was assumed to be thermally connected to a fixed temperature heat sink, corresponding to the so-called Dirichlet boundary condition.

The problem was studied numerically by solving simultaneously the NLS equation [Eq. (1.2)] governing nonlinear beam propagation and the Poisson equation [Eq. (4.1)] governing the evolution of the steady-state temperature with the intensity acting as the heat source.

In the first section of this chapter, the stability properties of the rotating dipole solitons were characterized by conducting extensive numerical simulations of the soliton propagation varying the modulation parameter and input power. The results of these simulations were analogous to the case of the Gaussian nonlocal nonlinear model. In addition higher-order localized structures in the form of necklace solitons were also shown to exist in optical media with thermal nonlinearity.

In the following section an extensive investigation of the boundary effects on beam propagation was undertaken. To that end several scenarios were studied numerically and the general conclusion was that (i) the boundaries exerted repulsive forces on the propagating beams, thereby causing an asymmetrically launched beam to follow complicated trajectories in the transverse plane, (ii) in general, any asymmetry facilitated the evolution of mutual transitions between complex higher-order beam structures similar to the transformations observed previously in the Gaussian model [see Chapter 2], and (iii) the geometry of the cross-section imposed strong constraints on the permitted beam structure in the thermal sample.

In conclusion, although several intriguing effects can be correctly stated to be largely generic to nonlocal nonlinear media, it appears that especially stabilizing effects as well as certain propagation dynamics cannot be readily generalized from one nonlocal model to another.

Indeed, certain stability properties do depend on the particular realization of the nonlocal nonlinear response [76] clearly illustrated, for instance, by the existence of an upper limit on the allowed topological charge for vortex solitons in thermal media, namely $m \leq 2$ [146], while in Gaussian media no such constraint is known to exist. Moreover, by comparing numerical results from the preceding chapters it is clear that both soliton interactions and propagation dynamics obtained by considering different models, although in general pointing to similar behavior, in fact differ significantly in certain cases.

Therefore it should be stressed that various problems need to be modeled differently depending obviously on the physical system being studied but, indeed, also on the level of accuracy needed and the particular significance attributed to the numerical results.

CHAPTER 5

Conclusions

In this thesis the propagation dynamics of higher-order nonlocal spatial solitons has been thoroughly investigated theoretically. Main purpose has been to explore in detail the existence and stabilization of a great variety of multihump modes which have no analogies in local nonlinear media.

To that end, novel classes of higher-order spatial optical solitons were introduced in the form of the soliton necklaces and soliton matrices stabilized by the nonlocal nonlinearity. These higher-order solitons represented a generalization of the well-known Laguerre-Gaussian and Hermite-Gaussian linear modes to the case of nonlinear media.

A rich variety of the stationary states found both analytically and numerically allowed for nontrivial mutual transformations induced by modulational instability when the soliton powers became close or coincided. These soliton transformations were manifested as periodic robust oscillations between two or more spatially localized states with distinctly different symmetries.

At intermediate stages during the transitions the states resembling generalized Hermite-Laguerre-Gaussian linear modes appeared which motivated the construction of generalized nonlocal solitons. Numerous families of higher-order solitons were obtained consisting of complicated beam symmetries with several vortices located in their phase topologies.

One distinct feature divided the solitons into two classes, namely nonrotating and rotating. In the nonrotating case, beams exhibited quasi-periodic breather-like behavior for hundreds of soliton periods and transitions between beating modes appeared as frequency shifts in the adhering Fourier spectrum. On the other hand, when the solitons exhibited a nonzero angular momentum, the combination of oscillations and spiraling of the beams triggered the formation of intricate nodal line structures and both vortex links and knots were demonstrated.

Intriguingly, such complicated vortex distributions also appeared in a local nonlinear medium and it followed that the main requirement of the formation of vortex loops, links and knots is structurally stable propagation, in which the beams re-

main self-similar, accompanied by oscillations of the intensity distribution as well as spiraling of the beam as a whole.

In the study above a phenomenological model was considered, in which the refractive index change was assumed to be represented by a nonlocal Gaussian response function. By rescaling the governing equation different degrees of nonlocality, ranging from the purely local case to the highly nonlocal regime, could be considered simply by varying the propagation constant or equivalently the beam power.

For comparison, investigations were conducted which involved a realistic thermal nonlocal model. Here the nature of the nonlocality, i.e., thermal diffusion, prompted a different approach in which a coupled set of equations was solved simultaneously.

Simulations revealed that solitons in thermal media exhibit rather complicated dynamics strongly influenced by the boundaries, including mutual transformations between solitons of different geometries. These results suggest the generic nature of mutual transitions of nonlinear modes coexisting energetically and this remarkable property may pave the way for the experimental realization, e.g., in lead glass samples. Such observations rely heavily on the topology of the beams and the actual shape of the thermal sample.

In conclusion, higher-order solitons in media with a thermal nonlocal nonlinear response differ from their counterparts in the phenomenological model and it follows that predictions regarding the stability of the complicated beam structures in one particular system cannot be readily generalized to other nonlocal models. Various stability properties depend crucially on the actual form of the nonlocal nonlinear response.

Bibliography

[1] Y. S. Kivshar and G. P. Agrawal, *Optical Solitons: From Fibers to Photonic Crystals* (Academic Press, San Diego, 2003).

[2] G. I. Stegeman and M. Segev, "Optical Spatial Solitons and their Interactions: Universality and Diversity," Science **286**, 1518–1523 (1999).

[3] G. I. Stegeman, D. N. Christodoulides, and M. Segev, "Optical Spatial Solitons: Historical Perspectives," IEEE Journal on selected Topics in Quantum Electronics **6**, 1419–1427 (2000).

[4] Y. R. Shen, *The Principles of Nonlinear Optics* (John Wiley and Sons, New York, 1984).

[5] P. N. Butcher and D. Cotter, *The Elements of Nonlinear Optics* (Cambridge, UK, 1992).

[6] R. W. Boyd, *Nonlinear Optics* (Academic Press, San Diego, 1992).

[7] V. E. Zakharov and A. M. Shabat, "Interaction between solitons in a stable medium," Zh. Eksp. Teor. Fiz. **64**, 1627-1639 (1973) (in russian) [English translation: Sov. Phys. JETP **37**, 823–828 (1973)].

[8] Y. S. Kivshar and B. Luther-Davies, "Optical Dark Solitons: Physics and Applications," Phys. Rep. **298**, 81–197 (1998).

[9] M. Hercher, "Laser-induced damage in transparent media," J. Opt. Soc. Am. **54**, 563 (1964).

[10] P. Lallemand and N. Bloembergen, "Self-focusing of laser beams and stimulated Raman gain in liquids," Phys. Rev. Lett. **15**, 1010–1012 (1965).

[11] G. A. Askar'yan, "Effects of the gradient of a strong electromagnetic beam on electrons and atoms," Sov. Phys. JETP **15**, 1088 (1962).

[12] R. Y. Chiao, E. Garmire, and C. H. Townes, "Self-trapping of optical beams," Phys. Rev. Lett. **13**, 479–482 (1964).

[13] N. J. Zabusky and M. D. Kruskal, "Interaction of "solitons" in a collisionless plasma and the recurrence of initial states," Phys. Rev. Lett. **15**, 240–243 (1965).

[14] V. E. Zakharov and A. B. Shabat, "Exact theory of two-dimensional self-focusing and one-dimensional self-modulation of waves in nonlinear media," Zh. Eksp. Teor. Fiz. **61**, 118–134 (1971) (in russian) [English translation: Sov. Phys. JETP **34**, 62–69 (1972)].

[15] J. S. Aitchison, A. M. Weiner, Y. Silberberg, D. E. Leaird, M. K. Oliver, J. L. Jackel, and P. W. E. Smith, "Experimental observation of spatial soliton interactions," Opt. Lett. **16**, 15–17 (1991).

[16] A. Y. Wong and P. Y. Cheung, "Three-Dimensional Self-Collapse of Langmuir Waves," Phys. Rev. Lett. **52**, 1222–1225 (1984).

[17] E. Garmire, R. Y. Chiao, and C. H. Townes, "Dynamics and Characteristics of the Self-Trapping of Intense Light Beams," Phys. Rev. Lett. **16**, 347–349 (1966).

[18] C. A. Sackett, J. M. Gerton, M. Welling, and R. G. Hulet, "Measurements of Collective Collapse in a Bose-Einstein Condensate with Attractive Interactions," Phys. Rev. Lett. **82**, 876–879 (1999).

[19] T. B. Benjamin and J. E. Feir, "The disintegration of wave trains on deep water Part 1. Theory," J. Fluid Mech. **27**, 417–430 (1967).

[20] A. Hasegawa, *Plasma Instabilities and Nonlinear Effects* (Springer, Berlin, 1975).

[21] L. A. Ostrovskii, "Propagation of Wave Packets and Space-time Self-focusing in a Nonlinear Medium," Zh. Eksp. Teor. Flz. **51**, 1189–1194 (1966) (in russian) [English translation: Sov. Phys. JETP **24**, 797–800 (1967)].

[22] V. E. Zakharov and A. M. Rubenchik, "Instability of waveguides and solitons in nonlinear media," Zh. Eksp. Teor. Fiz. **65**, 997–1002 (1973) (in russian) [English translation: Sov. Phys. JETP **38**, 494–500 (1974)].

[23] P. L. Kelley, "Self-Focusing of Optical Beams," Phys. Rev. Lett. **15**, 1005–1008 (1965).

[24] E. L. Dawes and J. H. Marburger, "Computer Studies in Self-focusing," Phys. Rev. **179**, 862–868 (1969).

[25] J. E. Bjorkholm and A. Ashkin, "cw Self-Focusing and Self-Trapping of Light in Sodium Vapor," Phys. Rev. Lett. **32**, 129–132 (1974).

[26] G. A. Swartzlander, Jr., D. R. Andersen, J. J. Regan, H. Yin, and A. E. Kaplan, "Spatial dark-soliton stripes and grids in self-defocusing materials," Phys. Rev. Lett. **66**, 1583–1586 (1991).

[27] G. R. Allan, S. R. Skinner, D. R. Andersen, and A. L. Smirl, "Observation of fundamental dark spatial solitons in semiconductors using picosecond pulses," Opt. Lett. **16**, 156–158 (1991).

[28] G. A. Swartzlander, Jr. and C. T. Law, "Optical vortex solitons observed in Kerr nonlinear media," Phys. Rev. Lett. **69**, 2503–2506 (1992).

[29] A. V. Mamaev, M. Saffman, and A. A. Zozulya, "Vortex evolution and bound pair formation in anisotropic nonlinear optical media," Phys. Rev. Lett. **77**, 4544–4547 (1996).

[30] Z. Chen, M. Segev, D. W. Wilson, R. E. Muller, and P. D. Maker, "Self-trapping of an optical vortex by use of the bulk photovoltaic effect," Phys. Rev. Lett. **78**, 2948–2951 (1997).

[31] Y. S. Kivshar and E. A. Ostrovskaya, "Optical vortices: folding and twisting waves of light," Opt. Photon. News **12**, 26–31 (2001).

[32] A. S. Desyatnikov, Y. S. Kivshar, and L. Torner, "Optical vortices and Vortex Solitons," Prog. Optics **47**, 291-391 (2005).

[33] J. F. Nye and M. V. Berry, "Dislocations in wave trains," Proc. R. Soc. London Ser. A-Math. Phys. Eng. Sci. **336**, 165–190 (1974).

[34] M. Vasnetsov and K. Staliunas (eds.), *Optical Vortices*, volume **228** of *Horizons in World Physics*, (Nova Sciences Publishers, New York, 1999).

[35] M. S. Soskin and M. V. Vasnetsov, "Singular optics," Prog. Optics **42**, 219–276 (2001).

[36] M. V. Berry and M. R. Dennis, "Knotted and linked phase singularities in monochromatic waves," Proc. R. Soc. Lond. A **457**, 2251–2263 (2001).

[37] H. A. Haus, "Higher Order Trapped Light Beam Solutions," Appl. Phys. Lett. **8**, 128–129 (1966).

[38] Z. K. Yankauskas, Sov. Radiophys. **9**, 261 (1966).

[39] J. M. Soto-Crespo, D. R. Heatley, E. M. Wright, and N. N. Akhmediev, "Stability of the higher-bound states in a saturable self-focusing medium," Phys. Rev. A **44**, 636–644 (1991).

[40] D. E. Edmundson, "Unstable higher modes of a three-dimensional nonlinear Schrodinger equation," Phys. Rev. E **55**, 7636–7644 (1997).

[41] D. V. Skryabin and W. J. Firth, "Dynamics of self-trapped beams with phase dislocation in saturable Kerr and quadratic nonlinear media," Phys. Rev. E **58**, 3916–3930 (1998).

[42] V. I. Kruglov and R. A. Vlasov, "Spiral self-trapping propagation of optical beams in media with cubic nonlinearity," Phys. Lett. A **111**, 401–404 (1985).

[43] V. I. Kruglov, Y. A. Logvin, and V. M. Volkov, "The theory of spiral laser-beams in nonlinear media," J. Mod. Opt. **39**, 2277–2291 (1992).

[44] J. Atai, Y. J. Chen, and J. M. Soto-Crespo, "Stability of 3-dimensional self-trapped beams with a dark spot surrounded by bright rings of varying intensity," Phys. Rev. A **49**, R3170–R3173 (1994).

[45] V. V. Afanasjev, "Rotating ring-shaped bright solitons," Phys. Rev. E **52**, 3153–3158 (1995).

[46] L. Allen, "Introduction to the atoms and angular momentum of light special issue," J. Opt. B: Quantum Semicl. Opt. **4**, S1–S6 (2002).

[47] M. Berry, M. R. Dennis, and M. Soskin, "The plurality of optical singularities," J. Opt. A-Pure Appl. Opt. **6**, S155–S156 (2004).

[48] M. Padgett, J. Courtial, and L. Allen, "Light's orbital angular momentum," Phys. Today **57**, 35–40 (2004).

[49] N. G. Vakhitov and A. A. Kolokolov, "Stationary solutions of the wave equation in the medium with nonlinearity saturation," Izv. Vyssh. Uchebn. Zaved. Radioz. **16**, 1020–1028 (in Russian) (1973) [English translation: Radiophys. Quantum Electron. **16**, 783–789 (1973)].

[50] J. M. Soto-Crespo, E. M. Wright, and N. N. Akhmediev, "Recurrence and azimuthal-symmetry breaking of a cylindrical Gaussian beam in a saturable self-focusing medium," Phys. Rev. A **45**, 3168–3175 (1992).

[51] W. J. Firth and D. V. Skryabin, "Optical solitons carrying orbital angular momentum," Phys. Rev. Lett. **79**, 2450–2453 (1997).

[52] J. P. Torres, J. M. Soto-Crespo, L. Torner, and D. V. Petrov, "Solitary-wave vortices in quadratic nonlinear media," J. Opt. Soc. Am. B **15**, 625–627 (1998).

[53] V. Tikhonenko, J. Christou, and B. Luther-Davies, "Spiraling bright spatial solitons formed by the breakup of an optical vortex in a saturable self-focusing medium," J. Opt. Soc. Am. B **12**, 2046–2052 (1995).

[54] V. Tikhonenko, J. Christou, and B. Luther-Davies, "Three dimensional bright spatial soliton collision and fusion in a saturable nonlinear medium," Phys. Rev. Lett. **76**, 2698–2701 (1996).

[55] M. S. Bigelow, P. Zerom, and R. W. Boyd, "Breakup of ring beams carrying orbital angular momentum in sodium vapor," Phys. Rev. Lett. **92**, 083902–4 (2004).

[56] A. Barthelemy, C. Froehly, M. Shalaby, P. Donnat, J. Paye, and A. Migus, in *Ultrafast Phenomena VIII*, edited by J. J. Martin et al. (Springer, Berlin), pp. 299–305 (1993).

[57] A. Barthelemy, C. Froehly, and M. Shalaby, "Nonlinear propagation of picosecond tubular beams: self phase modulation and induced refraction," in *Proc. SPIE Int. Soc. Opt. Eng.*, volume **2041**, p. 104–113 (1994).

[58] M. Soljacic, S. Sears, and M. Segev, "Self-trapping of "necklace" beams in self-focusing Kerr media," Phys. Rev. Lett. **81**, 4851–4854 (1998).

[59] M. Soljacic and M. Segev, "Self-trapping of "necklace-ring" beams in self-focusing Kerr media," Phys. Rev. E **62**, 2810–2820 (2000).

[60] A. S. Desyatnikov and Y. S. Kivshar, "Spatial optical solitons and soliton clusters carrying an angular momentum," J. Opt. B: Quantum Semicl. Opt. **4**, S58–S65 (2002).

[61] M. Soljacic and M. Segev, "Integer and fractional angular momentum borne on self-trapped necklace-ring beams," Phys. Rev. Lett. **86**, 420–423 (2001).

[62] A. S. Desyatnikov and Y. S. Kivshar, "Rotating optical soliton clusters," Phys. Rev. Lett. **88**, 053901–4 (2002).

[63] A. S. Desyatnikov, C. Denz, and Y. S. Kivshar, "Nonlinear optical beams carrying phase dislocations," J. Opt. A-Pure Appl. Opt. **6**, S209–S212 (2004).

[64] A. S. Desyatnikov, A. A. Sukhorukov, and Y. S. Kivshar, "Azimuthons: Spatially Modulated Vortex Solitons," Phys. Rev. Lett. **95**, 203904–4 (2005).

[65] O. Bang, W. Krolikowski, J. Wyller, and J. J. Rasmussen, "Collapse arrest and soliton stabilization in nonlocal nonlinear media," Phys. Rev. E. **66**, 046619–5 (2002).

[66] W. Krolikowski, O. Bang, J. J. Rasmussen, and J. Wyller, "Modulational instability in nonlocal nonlinear Kerr media," Phys. Rev. E **64**, 016612–7 (2001).

[67] A. Dreischuh, G. G. Paulus, F. Zacher, F. Grasbon, and H. Walther, "Generation of multiple-charged optical vortex solitons in a saturable nonlinear medium," Phys. Rev. E **60**, 6111–6117 (1999).

[68] W. Krolikowski, O. Bang, N. I. Nikolov, D. Neshev, J. Wyller, J. J. Rasmussen, and D. Edmundson, "Modulational instability, solitons and beam propagation in spatially nonlocal nonlinear media," J. Opt. B: Quantum Semiclass. Opt. **6**, S288–S294 (2004).

[69] G. F. Calvo, F. Agullo-Lopez, M. Carrascosa, M. R. Belic, and W. Krolikowski, "Locality vs. nonlocality of (2+1)-dimensional light-induced space-charge field in photorefractive crystals," Europhysics Letters **60**, 847–853 (2002).

[70] D. Suter and T. Blasberg , "Stabilization of transverse solitary waves by a nonlocal response of the nonlinear medium," Phys. Rev. A **48**, 4583–4587 (1993).

[71] F. W. Dabby and J. B. Whinnery, "Thermal Self-focusing of Laser Beams in Lead Glasses," Appl. Phys. Lett. **13**, 284–286 (1968).

[72] G. Assanto and M. Peccianti, "Spatial solitons in nematic liquid crystals," IEEE J. Quantum Electron. **39**, 13–21 (2003).

[73] F. Dalfovo, S. Giorgini, L. P. Pitaevski, and S. Stringari, "Theory of Bose-Einstein condensation in trapped gases," Rev. Mod. Phys. **71**, 463–512 (1999).

[74] J. Stuhler, A. Griesmaier, T. Koch, M. Fattori, T. Pfau, S. Giovanazzi, P. Pedri, and L. Santos, "Observation of Dipole-Dipole Interaction in a Degenerate Quantum Gas," Phys. Rev. Lett. **95**, 150406–4 (2005).

[75] D. Briedis, D. E. Petersen, D. Edmundson, W. Krolikowski, and O. Bang, "Ring vortex solitons in nonlocal non-linear media," Opt. Express **13** 435–443 (2005).

[76] S. Skupin, M. Grech, and W. Krolikowski, "Rotating soliton solutions in nonlocal nonlinear media," Opt. Express **16**, 9118–9131 (2008).

[77] T. A. Davydova and A. I. Fishchuk, "Upper hybrid nonlinear wave structures," Ukr. J. Phys. **40**, 487–494 (1995).

[78] W. Krolikowski and O. Bang, "Solitons in nonlocal nonlinear media: Exact solutions," Phys. Rev. E **63**, 016610–6 (2000).

[79] A. Snyder and J. Mitchell, "Accesible Solitons," Science **276**, 1538–1541 (1997).

[80] D. Deng, Q. Guo, and W. Hu, "Complex-variable-function Gaussian beam in strongly nonlocal nonlinear media," Phys. Rev. A **79**, 023803–6 (2009).

[81] Y. J. He, B. A. Malomed, D. Mihalache, and H. Z. Wang, "Spinning bearing-shaped solitons in strongly nonlocal nonlinear media," Phys. Rev. A **77**, 043826–5 (2008).

[82] Y. J. He, B. A. Malomed, D. Mihalache, and H. Z. Wang, "Crescent vortex solitons in strongly nonlocal nonlinear media," Phys. Rev. A **78**, 023824–5 (2008).

[83] D. Lu, W. Hu, Y. Zheng, Y. Liang, L. Cao, S. Lan, and Q. Guo, "Self-induced fractional Fourier transform and revivable higher-order spatial solitons in strongly nonlocal nonlinear media," Phys. Rev. A **78**, 043815–4 (2008).

[84] D. Deng and Q. Guo, "Ince-Gaussian beams in strongly nonlocal nonlinear media," J. Phys. B: At. Mol. Opt. Phys. **41**, 1–7 (2008).

[85] W. Hu, S. Ouyang, P. Yang, Q. Guo, and S. Lan, "Short-range interactions between strongly nonlocal spatial solitons," Phys. Rev. A **77**, 033842–6 (2008).

[86] W.-P. Zhong, L. Yi, R.-H. Xie, M. Belić, and G. Chen, "Robust three-dimensional spatial soliton clusters in strongly nonlocal media," J. Phys. B: At. Mol. Opt. Phys. **41**, 1–6 (2008).

[87] W.-P. Zhong and L. Yi, "Two-dimensional Laguerre-Gaussian soliton family in strongly nonlocal nonlinear media," Phys. Rev. A **75**, 061801–4 (2007).

[88] M. Shen, Q. Wang, and J. Shi, "Elliptic incoherent accessible solitons in strongly nonlocal media," Opt. Commun. **270**, 384–390 (2007).

[89] D. Deng, X. Zhao, Q. Guo, and S. Lan, "Hermite-Gaussian breathers and solitons in strongly nonlocal nonlinear media," J. Opt. Soc. Am. B **24**, 2537–2544 (2007).

[90] M. Shen, J. Shi, Q. Wang, "Incoherent accessible white-light solitons in strongly nonlocal Kerr media," Phys. Rev. E **74**, 027601–4 (2006)

[91] J. Wyller, W. Krolikowski, O. Bang, and J. J. Rasmussen, "Generic features of modulational instability in nonlocal Kerr media," Phys. Rev. E **66**, 066615–13 (2002).

[92] S. K. Turitsyn, "Spatial Dispersion of Nonlinearity and Stability of Multidimensionally Solitons," translated from Teor. Mat. Fiz. **64**, 226–232 (1985).

[93] X. Hutsebaut, C. Cambournac, M. Haelterman, A. Adamski, and K. Neyts, "Single-component higher-order mode solitons in liquid crystals," Opt. Commun. **233**, 211–217 (2004).

[94] Z. Xu, Y. V. Kartashov, and L. Torner, "Upper threshold for stability of multipole-mode solitons in nonlocal nonlinear media," Opt. Lett. **30**, 3171–3173 (2005).

[95] D. Mihalache, D. Mazilu, F. Lederer, L.-C. Crasovan, Y. V. Kartashov, L. Torner, and B. A. Malomed, "Stable solitons of even and odd parities supported by competing nonlocal nonlinearities," Phys. Rev. E **74**, 066614–6 (2006).

[96] B. A. Malomed, D. Mihalache, F. Wise, and L. Torner, "Spatiotemporal optical solitons," J. Opt. B: Quantum Semicl. Opt. **7**, R53–R72 (2005).

[97] D. Mihalache, D. Mazilu, F. Lederer, B. A. Malomed, Y. V. Kartashov, L.-C. Crasovan, and L. Torner, "Three-dimensional spatiotemporal optical solitons in nonlocal nonlinear media," Phys. Rev. E **73**, 025601–4 (2006).

[98] A. I. Yakimenko, Y. A. Zaliznyak, and Y. S. Kivshar, "Stable vortex solitons in nonlocal self-focusing nonlinear media," Phys. Rev. E **71**, 065603–4 (2005).

[99] S. Skupin, O. Bang, D. Edmundson, and W. Krolikowski, "Stability of two-dimensional spatial solitons in nonlocal nonlinear media," Phys. Rev. E **73**, 066603–8 (2006).

[100] S. Lopez-Aguayo, A. S. Desyatnikov, Y. S. Kivshar, S. Skupin, W. Krolikowski, and O. Bang, "Stable rotating dipole solitons in nonlocal optical media," Opt. Lett. **8**, 1100–1102 (2006).

[101] S. Lopez-Aguayo, A. S. Desyatnikov, and Y. S. Kivshar, "Azimuthons in nonlocal nonlinear media," Opt. Express **14**, 7903–7908 (2006).

[102] S. Skupin, M. Saffman, and W. Krolikowski, "Nonlocal Stabilization of Nonlinear Beams in a Self-Focusing Atomic Vapor," Phys. Rev. Lett. **98**, 263902–4 (2007).

[103] C. Conti, M. Peccianti, and G. Assanto, "Route to Nonlocality and Observation of Accessible Solitons," Phys. Rev. Lett. **91**, 073901–4 (2003).

[104] M. Peccianti, C. Conti, G. Assanto, A. De Luca, and C. Umeton, "Routing of anisotropic spatial solitons and modulational instability in liquid crystals," Nature **432**, 733–737 (2004).

[105] M. Peccianti, A. Fratalocchi, and G. Assanto, "Transverse dynamics of nematicons," Opt. Express **12**, 6524–6529 (2004).

[106] A. Alberucci, M. Peccianti, and G. Assanto, "Nonlinear bouncing of nonlocal spatial solitons at the boundaries," Opt. Lett. **32**, 2795–2797 (2007).

[107] C. Conti, M. Peccianti, and G. Assanto, "Observation of Optical Spatial Solitons in a Highly Nonlocal Medium," Phys. Rev. Lett. **92**, 113902-4 (2004).

[108] M. Peccianti, A. Dyadyusha, M. Kaczmarek, and G. Assanto, "Tunable refraction and reflection of self-confined light beams," Nature Physics **2**, 737–742 (2006).

[109] W. Hu, T. Zhang, Q. Guo, L. Xuan, and S. Lan, "Nonlocality-controlled interaction of spatial solitons in nematic liquid crystals," Appl. Phys. Lett. **89** 071111–3 (2006).

[110] G. Assanto, A. Fratalocchi, and M. Peccianti, "Spatial solitons in nematic liquid crystals: from bulk to discrete ," Opt. Express **15** 5248–5259 (2007).

[111] G. Assanto, N. F. Smyth, and A. L. Worthy, "Two-color, nonlocal vector solitary waves with angular momentum in nematic liquid crystals," Phys. Rev. A **78**, 013832–8 (2008)

[112] C. G. Reimbert, A. A. Minzoni, T. R. Marchant, N. F. Smyth, and A. L. Worthy, "Dipole soliton formation in a nematic liquid crystal in the nonlocal limit," Physica D **237**, 1088–1102 (2008).

[113] A. A. Minzoni, N. F. Smyth, A. L. Worthy, and Y. S. Kivshar, "Stabilization of vortex solitons in nonlocal nonlinear media," Phys. Rev. A **76**, 063803–6 (2007).

[114] A. A. Minzoni, N. F. Smyth, and A. L. Worthy, "Modulation solutions for nematicon propagation in nonlocal liquid crystals," J. Opt. Soc. Am. B **24**, 1549–1556 (2007).

[115] C. Rotschild, M. Segev, Z. Xu, Y. V. Kartashov, L. Torner, and O. Cohen, "Two-dimensional multipole solitons in nonlocal nonlinear media," Opt. Lett. **31**, 3312–3314 (2006).

[116] C. Rotschild, O. Cohen, O. Manela, M. Segev, and T. Carmon, "Solitons in Nonlinear Media with an Infinite Range of Nonlocality: First Observation of Coherent Elliptic Solitons and of Vortex-Ring Solitons," Phys. Rev. Lett. **95**, 213904–4 (2005).

[117] C. Rotschild, B. Alfassi, O. Cohen, and M. Segev, "Long-range interactions between optical solitons," Nature Physics **2**, 769–774 (2006).

[118] A. Dreischuh, D. N. Neshev, D. E. Petersen, O. Bang, and W. Krolikowski, "Observation of Attraction between Dark Solitons," Phys. Rev. Lett. **96**, 043901–4 (2006).

[119] A. V. Mamaev, A. A. Zozulya, V. K. Mezentsev, D. Z. Anderson, and M. Saffman, "Bound dipole solitary solutions in anisotropic nonlocal self-focusing media," Phys. Rev. A **56**, R1110–R1113 (1997).

[120] A. V. Mamaev, M. Saffman, and A. A. Zozulya, "Decay of High Order Optical Vortices in Anisotropic Nonlinear Optical Media," Phys. Rev. Lett. **78**, 2108–2111 (1997).

[121] W. Krolikowski, M. Saffman, B. Luther-Davies, and C. Denz, "Anomalous Interaction of Spatial Solitons in Photorefractive Media," Phys. rev. Lett. **80**, 3240–3243 (1998).

[122] A. A. Zozulya, D. Z. Anderson, A. V. Mamaev, and M. Saffman, "Solitary attractors and low-order filamentation in anisotropic self-focusing media," Phys. Rev. A 57, 522–534 (1998).

[123] A. A. Zozulya, D. Z. Anderson, A. V. Mamaev, and M. Saffman, "Self-focusing and soliton formation in media with anisotropic nonlocal material response," Europhysics Letters **36**, 419–424 (1996).

[124] V. M. Lashkin, A. I. Yakimenko, and O. O. Prikhodko, "Two-dimensional nonlocal multisolitons," Phys. Lett. A **366**, 422–427 (2007).

[125] F. Ye, Y. V. Kartashov, and L. Torner, "Stabilization of dipole solitons in nonlocal nonlinear media," Phys. Rev. A **77**, 043821–7 (2008).

[126] M. Peccianti, K. A. Brzdakiewicz, and G. Assanto, "Nonlocal spatial soliton interactions in nematic liquid crystals," Opt. Lett. **27**, 1460–1462 (2002).

[127] N. I. Nikolov, D. Neshev, W. Krolikowski, O. Bang, J. J. Rasmussen, and P. L. Christiansen, "Attraction of nonlocal dark optical solitons," Opt. Lett. **29**, 286–288 (2004).

[128] E. G. Abramochkin and V. G. Volostnikov, "Generalized Gaussian beams," J. Opt. A: Pure Appl. Opt. **6**, S157–S161 (2004).

[129] V. A. Mironov, A. M. Sergeev, and E. M. Sher, "Multidimensional bound solitons in nonlinear field equations," Sov. Phys. Dokl. **26**, 861–862 (1981).

[130] I. Kaminer, C. Rotschild, O. Manela, and M. Segev, "Periodic solitons in nonlocal nonlinear media," Opt. Lett. **32**, 3209–3211 (2007).

[131] M. Peccianti and G. Assanto, "Nematicons across interfaces: anomalous refraction and reflection of solitons in liquid crystals," Opt. Express **15**, 8021–8028 (2007).

[132] B. A. Malomed, "Variational methods in nonlinear fiber optics and related fields," Prog. Optics **43**, 71–193 (2002).

[133] J. J. García-Ripoll and V. Peŕez-García, "Optimizing Schrödinger Functionals Using Sobolev Gradients: Applications to Quantum Mechanics and Nonlinear Optics," SIAM J. Sci. Comput. **23**, 1316–1334 (2001).

[134] Y. S. Kivshar, T. J. Alexander, and S. K. Turitsyn, "Nonlinear modes of a macroscopic quantum oscillator," Phys. Lett. A **278**, 225–230 (2001).

[135] A. I. Yakimenko, V. M. Lashkin, and O. O. Prikhodko, "Dynamics of two-dimensional coherent structures in nonlocal nonlinear media," Phys. Rev. E **73**, 066605–9 (2006).

[136] D. Deng and Q. Guo, "Propagation of Laguerre-Gaussian beams in nonlocal nonlinear media," J. Opt. A. Pure. Appl. Opt. **10**, 035101–7 (2008).

[137] Y. V. Kartashov, L. Torner, V. A. Vysloukh, and D. Mihalache, "Multipole vector solitons in nonlocal nonlinear media," Opt. Lett. **31**, 1483–1485 (2006).

[138] M. Peccianti, C. Conti, G. Assanto, A. D. Luca, and C. Umeton, "All-optical switching and logic gating with spatial solitons in liquid crystals," Appl. Phys. Lett. **81**, 3335– 3337 (2002).

[139] G. Assanto, M. Peccianti, and C. Conti, "Nematicons: Optical Spatial Solitons in Nematic Liquid Crystals," Optics & Photonics News **14**, 44–48 (2003).

[140] N. N. Rozanov, "On the Translational and Rotational Motion of Nonlinear Optical Structures as a Whole," Opt. Spectrosc. **96**, 405-408 (2004).

[141] D. Rozas and G. A. Swartzlander, Jr. "Observed rotational enhancement of nonlinear optical vortices," Opt. Lett. **25**, 126–128 (2000).

[142] D. Rozas, Z. S. Sacks, and G. A. Swartzlander, Jr. "Experimental Observation of Fluidlike Motion of Optical Vortices," Phys. Rev. Lett. **79**, 3399–3402 (1997).

[143] M. R. Dennis, "Braided nodal lines in wave superpositions," New J. Phys. **5**, 134.1–134.8 (2003).

[144] J. Leach, M. R. Dennis, J. Courtial, and M. J. Padgett, "Knotted threads of darkness," Nature **432**, 165–166 (2004).

[145] A. Alberucci and G. Assanto,"Propagation of optical spatial solitons in finite-size media: interplay between nonlocality and boundary conditions," J. Opt. Soc. Am. B **24**, 2314–20 (2007).

[146] Y. V. Kartashov, V. A. Vysloukh, and L. Torner, "Stability of vortex solitons in thermal nonlinear media with cylindrical symmetry," Opt. Express **15**, 9378–9384 (2007).